MODIFICATION OF THE NEAR-INFRARED SIGNATURE OF TEXTILE FABRICS VIA COLLOIDAL SELF-ASSEMBLY

A Thesis

Presented to the Faculty of the Graduate School

of Cornell University

In Partial Fulfillment of the Requirements for the Degree of

Master of Science

by

Christina Michelle Diaz

May 2009

ABSTRACT

This thesis presents a novel method to modify the near-infrared (NIR) reflectance of textile fabrics using colloidal self-assembly of polystyrene (PS) particles via electrostatic and convective forces. This work studies the effect of particle coating on a textile fabric where the size of the particle is of same order of magnitude as the incident wavelength of light, which has not been studied for textiles.

Sulfate functionalized PS particles were deposited on cationic cotton, poly(allylamine hydrochloride) (PAH) coated nylon-cotton, and cationic cellophane film. The nylon-cotton fabric was obtained from the Army Camouflage Uniform (ACU) and contained three colors. Spherical particles of 0.2, 0.5, and 1.0 μm in diameter and a non-spherical, mushroom cap shaped particle, 1.2 μm in diameter, were used. The PS particles were deposited onto the substrates using aqueous suspensions.

Scanning electron microscopy (SEM) was used to assess particle deposition on fibers. SEM revealed that the particles were able to conformally coat both nylon and cotton fibers despite their small radius of curvature. Micrographs showed two smaller particles had longer range, single layer coverage of particles on the fibers, while the larger particles were prone to agglomerate.

The NIR reflectance of the PS particle coatings textiles materials was assessed using the testing method specified in the US Army standard MIL-DTL-44436A. NIR reflectance data was collected with a spectrophotometer equipped with an integrating sphere to collect diffuse light scatter. The effect of the particle coating on the NIR reflectance was assessed using average

reflectance spectra and principal component analysis (PCA). The spectra analysis showed that the change in reflectance on fabric substrates ranged from 0 to 6 units. The PCA effects test was used to confirm that the particle coatings significantly changed the reflectance of the substrates. The analysis also revealed that the particle size influenced the reflectance of the fabrics and that the mushroom cap particle behaved more similarly to the smaller spherical particle than the 1.0 μm particle. The PCA results also confirmed the dyes on the nylon-cotton substrate significantly altered the reflectance behavior. Potential improvements to the deposition procedure and particle selection for altering the reflectance of fabrics are also proposed.

BIOGRAPHICAL SKETCH

Christina Diaz was born August 4, 1983 in Fort Bragg, North Carolina at Womack Army Medical Center. Her mother is Jeanne A. Diaz from Mount Holly, New Jersey. Her father is US Army Retired Staff Sergeant Carlos Miguel Diaz from Ponce, Puerto Rico. Christina grew up in Cary, NC with her four siblings Bonnie, Michael, Rebecca, and David. She grew up playing basketball and soccer. She attended Cary High School where she graduated in 2001.

In July 2001 Christina began courses at North Carolina State University (NCSU) through the Minority Engineering Program's Summer Transition Program. She received the Edward E. Hood, Jr. and BASF Prestige Merit Scholarships from NCSU. While at NCSU, Christina was actively involved in the student chapters of the Society of Hispanic Professional Engineers (SHPE) and the National Society of Black Engineers (NSBE). In the Spring of 2003, she was part of the founding pledge class of the Rho Chapter of Latinas Promoviendo Comunidad/Lambda Pi Chi Sorority, Inc., the first Latino Greek lettered organization at NCSU's campus. Christina completed her Bachelor of Science in Textile Engineering and Bachelor of Sociology magna cum laude in May 2006.

In August 2006 Christina moved to Ithaca, New York to attend Cornell University to pursue her Masters and PhD in Fiber Science. She received a GEM Consortium Master Fellowship and a NY State Diversity Fellowship for her Master's studies.

To the countless men and women who serve this country, particularly those who serve in silence

ACKNOWLEDGMENTS

I would like to acknowledge my research advisor and mentor, Dr. Juan Hinestroza. His love of science and pride in his research is remarkable and inspiring.

I would also like to thank my committee member, Dr. Chekesha Liddell, for her guidance and support during the process. In addition, I would like to thank her graduate student, Ian Hosein, for his advice and providing the mushroom cap particles.

I would like to thank my fellow graduate students and group members, Alejandra Andere, Camila Flor, Yan “Vivian” Li, Dr. Laura McJilton, Karmann Mills, Anna Paola Soliani, and Dr. Huaning Zhu. Their support has been tremendous during my graduate school experience.

I would like to thank the National Textile Center for funding this project. I would also like to thank the Cornell Center for Materials Research for the use of their facilities.

Finally, I would like to thank my friends and family. I would like to thank my NSBE family for constantly providing encouragement. I would like to thank my siblings and parents for their support.

TABLE OF CONTENTS

LIST OF FIGURES

LIST OF TABLES

Chapter 1. Introduction

1.1. Purpose

The goal of this project was to modify the near-infrared (NIR) signature of textile fabrics via deposition of self-assembling colloidal particles of polystyrene (PS). Cotton and nylon-cotton blend fabrics were used as the substrates. A cellulosic film was used as a control substrate. Both spherical and non-spherical PS particles were used as coatings for the substrates. The spherical particles were 0.2, 0.5, and 1.0 micrometers in diameter. The non-spherical particles were mushroom cap shaped and measured 1.2 micrometers in diameter. The deposition method utilized both electrostatic and convective forces. The substrates were treated to have positive charges and the particles were negatively charged.

Polystyrene submicron sized particles were selected because they are the same order of magnitude as the wavelength of incident light of interest. This size characteristic has interesting optical properties, which have been explored in photonic device research [1-8]; however, no known research exists regarding applications for textile fabrics.

1.2. Need

Modifying the NIR signature is of interest for improving military camouflage performance against night vision devices (NVDs). The nylon-cotton substrate used was obtained from the Army Combat Uniform (ACU) camouflage fabric. The need for increased protection against NVDs has resulted from an increase in availability of NVDs due to their decreased cost and the increase in night time military activity [9, 10].

1.3. Challenges

From prospective of particle deposition, fabric and fiber substrates present a challenge for the convective assembly method due to their 3-D, non-planar structure [8, 11, 12]. Cotton fibers and yarns are highly twisted and have a non-spherical cross-section. In order to evaluate the particle deposition and particle size effects on the coating a scanning electron microscope (SEM) was used.

An additional challenge presented by the structure of the fabric is its diffuse scatter of light. For reflectivity measurements, a spectrophotometer equipped with an integrating sphere was used to collect the diffusely scattered light and not just the spectral reflectance.

1.4. Research Objectives

The basic objective of this project is to modify the NIR reflectance of fabrics by the deposition of PS particles using colloidal self-assembly. SEM was used to assess deposition and the effects of particle size on deposited layer structures. The NIR reflectance was measured using method provided in Army Detail Specification MIL-DTL-44436A for camouflage patterns [13]. Specific objectives of the work include:

1. Determine the effect of PS particle coatings on the near-infrared reflectance of fabrics;
2. Determine the effect of particle size on the reflectance of the modified fabrics;
3. Determine the effect of particle shape on reflectance, particularly whether the non-spherical particle coatings behaves like the spherical particle coatings of similar diameter; and

4. Determine the effect of dye on the NIR signature of the particle coated nylon-cotton fabrics.

Chapter 2. Literature Review

2.1. Motivation

Prior to the second half of the twentieth century, the U.S. Army was heavily dependent on cotton as a material for uniforms and tents [14]. Since the 1960's fibers composed of nylon, Kevlar, and other synthetic materials have replaced cotton in many applications because synthetic fibers are lighter, stronger, and more versatile [15]. One concern of military uniforms and equipment is the minimization of added weight [14, 16, 17], which has led to the development of thin protective layers for clothing.

While the threat of detection by night vision devices (NVDs) was a moderate concern in the 1950s [14], NVDs create greater apprehension now due to the decrease in price of such technology allowing more enemy forces access to NVDs. In addition to an increase in NVD availability there has been an increase in night time activity of enemy forces [10]. Due to the increased use of NVDs by enemy combatants, the Army has developed an initiative to improve protection against detection by NVDs [9]. The new Army Combat Uniform (ACU) was introduced in 2004 [18] to address issues associated with detection by NVDs [9].

NVDs detect near-infrared (NIR, 700 – 1300 nm) and mid-infrared (mid-IR, 1300 – 3000 nm) wavelengths of light. In order to improve the camouflage the reflectance signatures of the colors in the ACU design seeks to emulate the reflectance signature of things found in nature such as soil, sand, and bark [9]. The ACU has a tri-color digitally printed design. The new uniform does not contain black and seeks to perform well in all environments. The previous Battle Dress Uniforms (BDUs) had different color patterns for different environments such as for desert, city, or jungle operations and contained black

which was easily detectable by NVDs [14, 18]. Although, the Army has specified a reflectance range for current uniform fabric for wavelengths of 600 – 860 nm [13], shown in Figure 1, this range does not include the majority of the NIR light, which extends to 1300 nm. Recently, the Army has begun testing the effectiveness of uniforms against NVDs at the Camouflage Evaluation Facility. The Camouflage Evaluation Facility at the Soldier Systems Center in Natick, Massachusetts tests the performance capabilities of camouflage designs in different environments and light conditions [19].

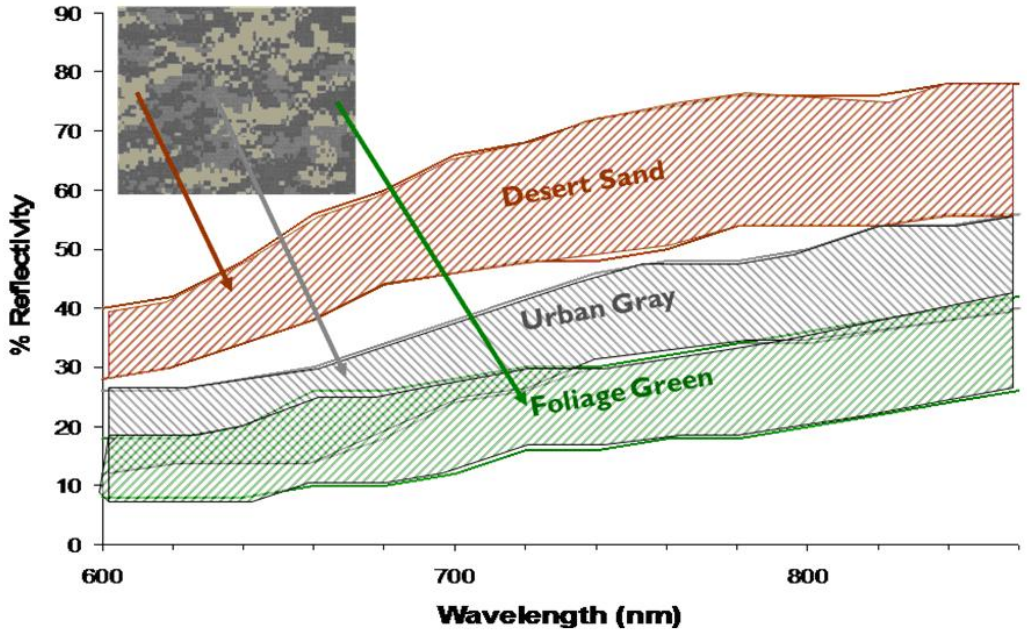

Figure 1. Specified reflectance ranges for (from top to bottom) Desert Sand, Urban Gray, and Foliage Green for Army Camouflage; inset: Army Universal Camouflage design.

It is important to further reduce the reflectance into the NIR range due to the increased use of NVDs in combat situations. Untreated cotton and nylon fabric, which are used in the ACU, naturally reflect more than 80 percent of light in the NIR range [9]; thus finding a means to mask or modify the natural

signature of such fibers is necessary to reduce the reflectance in the NIR range and improve protection against NVDs.

The goal of this project is to modify the NIR signature of textile fabrics via deposition of self-assembling colloidal particles of polystyrene. To minimize added weight of the protective coating, thin layers of colloidal particles are used. The project will look at effect of fiber type, dye, and surface structure by using cotton, dyed nylon/cotton blend, and a model smooth surface of cellulose film.

As background an overview is given on the current state of art of textile modification. Next, a review is given on the interaction of NIR light with fibers and particles, particularly, submicron particles. These particles can exhibit special behavior because they are of the same magnitude as the wavelength of light to which they are exposed.

2.2. Fiber Modification

Fibers and fabrics are commonly modified to improve aspects of the material based on their intended end use. There are several methods that can be used to modify the optical properties of fibers and fabrics. These include physical modification, surface modification, and modification by additives [20].

Physical modification of fibers includes changes of cross-sectional shape and changes to the supramolecular structure through the spinning and drawing processes [20]. It is well documented that changing the cross-sectional shape of a fiber can alter its interaction with light and its luster properties [20].

Surface modification can be used to alter various properties of fibers and fabrics, in addition to their desired effects they may create undesired changes to mechanical properties or alter the color of the fabrics. Wrinkle-free

treatments are a popular surface modification and often use dimethyloldihydroxylethylene urea (DMDHEU) as the crosslinking agent to prevent wrinkling [21, 22].

More recently colloidal, nanoparticle, and nanolayer treatments have been used on fabrics to modify the fiber surfaces [23-26]. Silver has antibacterial properties and nanoparticles have been used to coat textile fabrics and fibers [23, 24]. Nanolayers of polyelectrolytes have been deposited on cotton [25], nylon [26], and silk [26] by extending Gero Decher's layer-by-layer (LbL) method [27] to textiles. The LbL method uses opposing surface charges to deposit the polyelectrolytes on the fabric surface. The deposition of polyelectrolyte nanolayers on fabrics has opened the door for the use of LbL method for deposition of other charged nano- and colloidal particles onto textiles [27].

The inclusion of additives into the fiber or fiber system is another method of modification. Typical additives include dyes, pigments, and addition of particles into polymer melt. Dyes and pigments can be added either during fiber formation for synthetic fibers or after fiber or fabric production. Dyes and pigments are used to alter the interaction of visible light with the fabric. Recently, there has been work to develop dyes which interact with long wavelengths of light, particular near-infrared light [28-33].

2.3. Near Infrared Dyes

Although most of the NIR absorbing dyes are not currently used in textile applications, they are researched in the medical field for tissue repair and fluorescent markers as well as in the electronics field for optical storage devices [28, 29, 34, 35]. Current challenges with creating suitable NIR absorbing dyes include reducing aggregation of dye particles, reducing the

effects of photobleaching, and extending the absorbance peaks to longer wavelengths [28-30]. The majority of the research is focused on shifting the absorbance of current dyes to longer wavelength, called a bathochromic shift; methods to achieve this shift include adding strong electron donating and accepting groups to dye molecules [28], increasing the rigidity of dye molecules [30], and extending the π-conjugation of dye molecules [31-33].

2.3.1. Dyes with Strong Donor and Acceptor Groups

Dye molecules typically contain a chromophore connected to an electron donating or accepting groups. NIR absorbing dyes based on the donor/acceptor model, Do—π—A—π—Do, can be achieved by incorporating a strong acceptor (A) and strong donor (Do) groups into the molecule [28]. The donor and acceptor groups are linked together through conjugated π bonds. The carbenium ion and mesoionic unit, shown in Figure 2, both act as super accepting groups. These acceptor groups have been incorporated

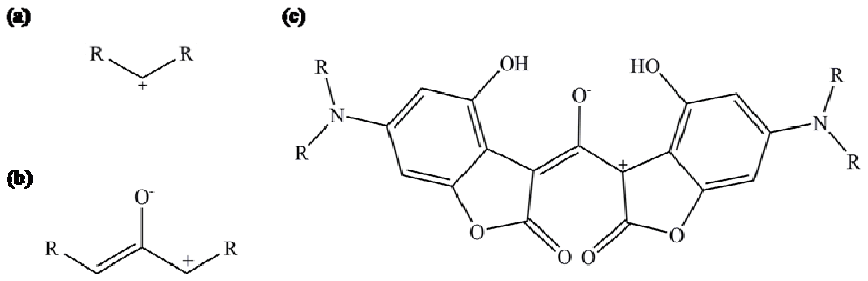

Figure 2. Super Acceptor groups, (a) carbenium ion, (b) mesoionic unit; and (c) NIR absorbing dye with mesoionic unit acceptor group (redrawn from [28]).

into dyes by Langhals [28]. The dye, pictured in Figure 2c, can be synthesized with various groups in the R position; however, the yield tends to be low. When the R substitute group is $(CH_3)_2CHCH_2$ the absorbance peak occurs at

1100 nm; the absorbance in NIR range rather than visible is surprising given the small size of the molecule [28]. The use of super acceptor group exhibits shifts in absorbance peaks into the NIR range that can be achieved without large extended π-conjugated systems. One limitation of the strong acceptor/donor model is that solvent systems must be carefully chosen since the ion groups are extremely sensitive to pH and presence of ions.

A bathochromic shift can be achieved by altering the nature and position of the substituted groups. A group of dyes was created by modifying quinone disperse dyes. These NIR absorbing semiquinone dyes, shown in Figure 3, vary the chemistry of the substituted and position of substituted group. The

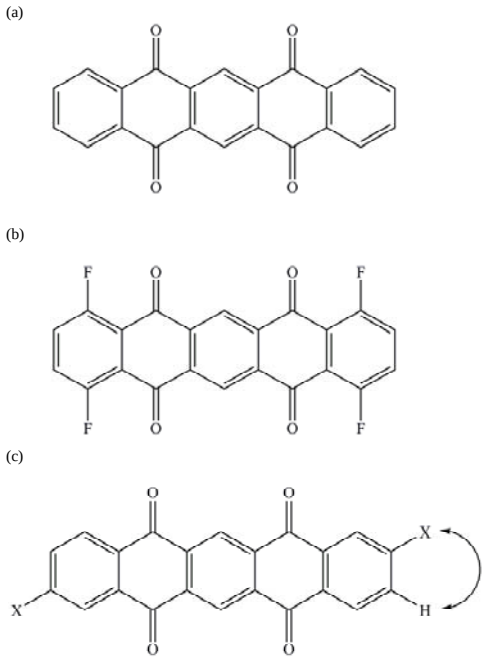

Figure 3. NIR Absorbing Semiquinone Dyes. Substitution of electron-withdrawing groups in (b) and (c) causes absorption shift toward higher wavelengths. Substituted group X in dye (C) can be Cl or F. (adapted from [36])

pentacenediquinone dye, Figure 3a, absorbs at 1335 nm. If electron withdrawing groups, such as fluorine, are substituted for hydrogen on the outside benzene rings to form dye 3(b), as shown in Figure 3b absorbs at 1335 nm. If electron withdrawing groups, such as fluorine, are substituted for hydrogen on the outside benzene rings to form dye 3(b), as shown in Figure 3b, there will be a bathochromic shift in absorbance wavelength toward 1500 nm [36].

By changing the hydrogens which are substituted, thus changing the position of the substituted groups, the bathocromic shift can be reduced. Dye 3(c), as shown in Figure 3c, has different position of substituted groups than dye 3(b) and has absorbance at a shorter wavelength. The semiquinone dyes show promise for creating dyes with absorbance up into the mid-IR range.

2.3.2. Dyes with Conformational Restrictions

A second method used to create bathochromic shifts—longer wavelength of absorbance—from a parent molecule is by restricting its molecular movement. This can be achieved by imposing rigidity [30] or by restricting movement through steric hindrance [29]. Zhao and Carreira developed a NIR absorbing dye by connecting two pyrroles and restricting their rotation by introducing a heterocyclic ring between the pyrroles. The absorbance of the dye has a bathochromic shift from the known dye, Figure 4b, has been restricted by introducing two additional six member rings to form a new dye, Figure 4a. The new restricted aza-bodipy dye, Figure 4a, has a sharp absorbance peak at 740 nm, seen in Figure 5, and can be produced in high yields. The new dye also shows good solvent- and photo-stability as compared to a standard indocyanine green dye [30].

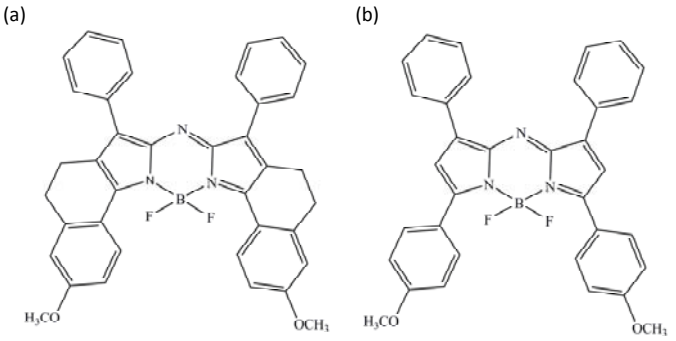

Figure 4. (a) Conformationally restricted Aza-Bodipy dye, (b) known dye used as a comparison (adapted from [30]).

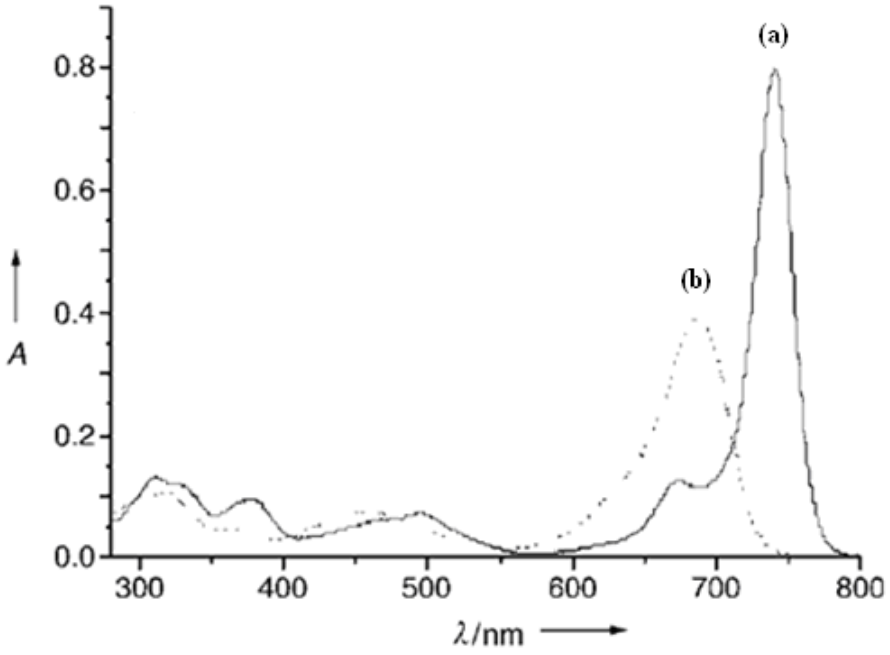

Figure 5. Absorbance data of Aza-Bodipy dye (a) and known dye(b) from Figure 4 (modified from [30])

Figure 6 shows a naphthoquinone methide dye molecule whose absorbance can be shifted further into NIR range by changing the R1 group from H to CH_3 the, as seen in Table 1 and Figure 7. Also, by changing R2 group from H to CH_3 to an acetylamino group interesting absorbance shifts are observed. The steric hindrance in dyes 1b and 1c leads to the bathochromic

shift from dye 1a, as seen in Table 1. The substitution of the acetylamino group, in dye 1d, had a shorter bathochromic shift than 1c due to the ability of the molecule to overcome the steric hindrance to form a planar ring [29]. This extension of the π-conjugated system led to an increased intensity of absorbance as compared to dyes 1a, 1b, and 1c, as seen in Figure 7.

Table 1. Absorption Band wavelengths for Naphthoquinone Methide Dyes shown in Figure 6 (table adapted from [29]).

Dye	R^1	R^2	λ_{max}/nm (ε_{max}) (C_6H_6)	$\Delta\lambda$
1a	H	H	711 (25,200)	
1b	H	CH_3	731 (27,100)	20
1c	CH_3	CH_3	791 (7,700)	80
1d	H	NHAc	756 (51,200)	45

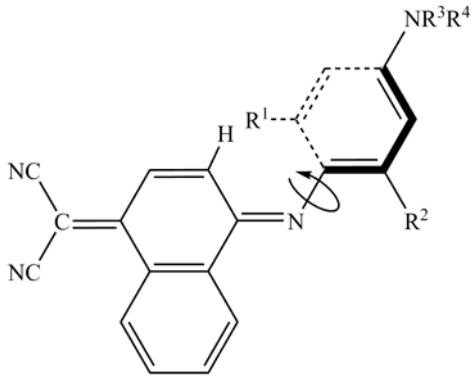

Figure 6. Naphthoquinone Methide Dyes. Absorbance wavelength can be changed by changing the substituted group R (adapted from [29]).

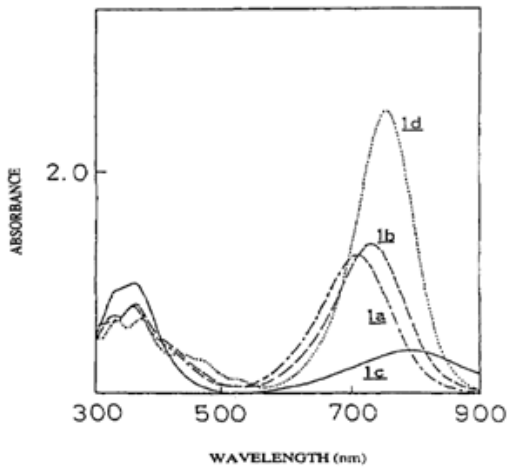

Figure 7. Comparison of Absorbance intensity of Naphthoquinone Methide Dyes with different R substitute groups (R groups are defined in Table 1).

2.3.3. Dyes with Extended π-Conjugated Systems

The primary means to create NIR absorbing dyes is by extending the conjugated π-system of molecules. Extension of the π-conjugation has an effect on the energy level of the lowest unoccupied molecular orbital (LUMO) and the highest occupied molecular orbital (HOMO) [31-33]. The π-conjugation can be extended in the direction of the major axis or in the direction of the minor axis. Adachi et al. found that bathochromic shifts occurred with extension in the major axis direction of polynaphthalenetetracarboxylic dianhydride diimide based dyes, but not with extension in the minor axis direction [32]. Computer based modeling has been used to analyze the HOMO and LUMO energy levels of polynaphthalenetetracarboxylic dianhydride diimide dyes, shown in Figure 8, to determine the greatest contributor in creating bathochromic shift [32]. The reduction of the band gap between the LUMO and the HOMO is responsible for the NIR absorption and bathochromic shift in absorbance from PTCAI to TTCAI to QTCAI. The reduction in the energy gap is primarily due to the

increase in the HOMO energy level, as seen in Figure 9. The extension in the π-conjugation in the major axis direction is responsible for the increase in the HOMO energy level [32].

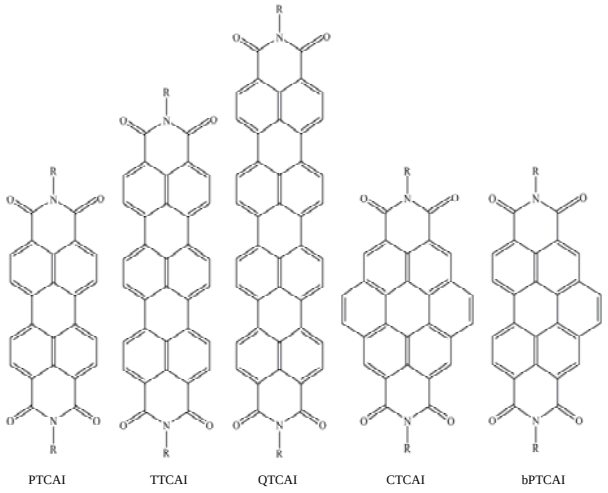

Figure 8. Polynaphthalenetetracarboxylic dianhydride diimide dyes π-conjugation extended in major axis direction (TTCAI, QTCAI) and in the minor axis direction (CTCAI, bPTCAI) [32].

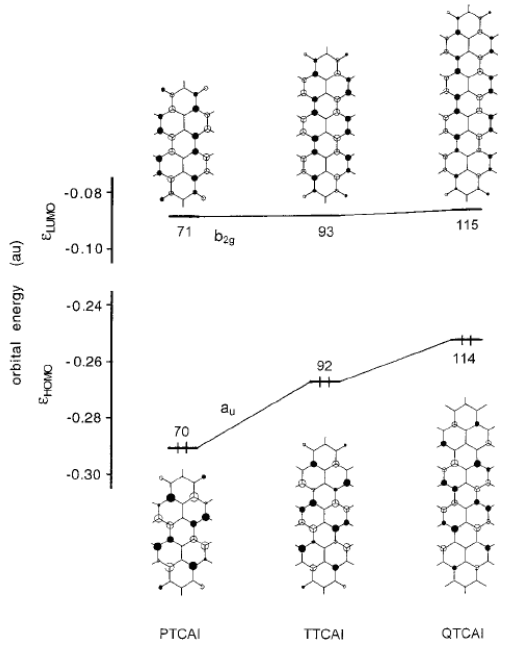

Figure 9. Reduction of energy band gap due to extension of π-conjugation in major axis direction [32].

Extension of the π-conjugation in dibenzopentarylenebis(dicarboximide) dyes has been studied by Avlasevich and Müllen [33]. Their work suggests that conjugation in the minor axis direction can contribute to bathochromic shifts as exhibited in the dye system in Figure 10. Dye 10(b) absorbs at a wavelength higher than that of dye 10(a). Furthermore, larger bathochromic shifts, on the order of 500 nm, can be achieved by extending the conjugation of the rylene based dyes in the major axis direction. As seen in Figure 11, the absorbance of dye 11(b) is shifted 500 nm from that of its precursor 11(a). As seen in the absorption data in Figure 11c, the rylene dye 11(b) has absorbance peaks in both the visible and NIR regions. The multi-absorbance peak dye could be used to both impart color and to reduce the reflection of NIR light from fabrics.

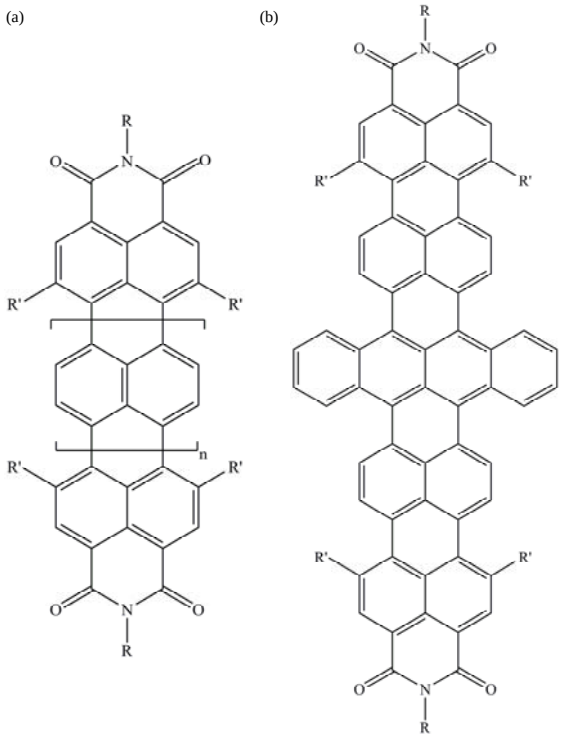

Figure 10. Extension of π-conjugation in minor axis direction leading to bathochromic shift in absorbance between dye (a) and dye (b) [33].

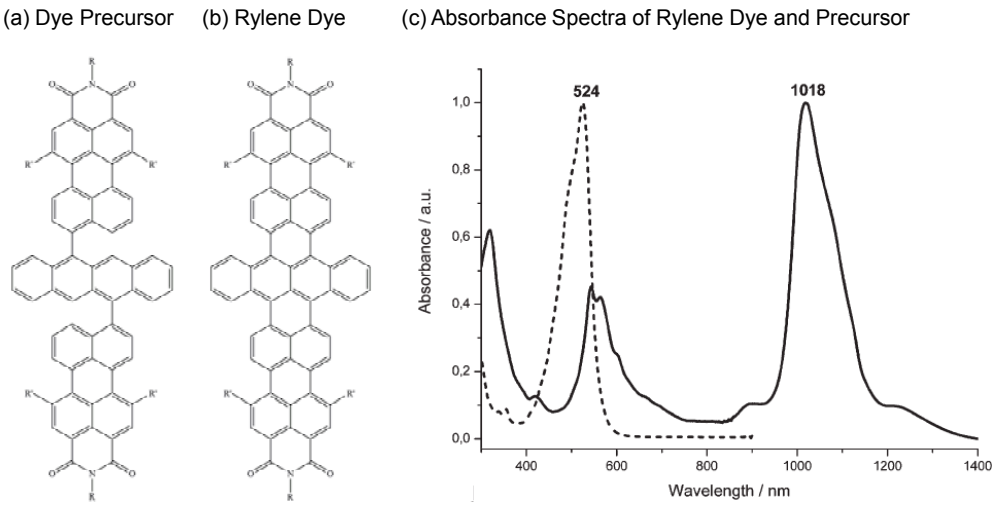

Figure 11. Large bathochromic shift achieved from extension of π-conjugation in major axis direction of dye precursor (a) to Rylene dye (b), where R' is Hydrogen; and shown in absorbance spectra (c) of precursor (dashed line) and Rylene dye (solid line). (modified from [33])

NIR absorbing dyes with broad absorption peaks can be synthesized by extending the π-conjugation in polysquaraine dyes. The broadness of the peak is determined by the groups substituted for R and R', as seen in Figure 12. The peaks can be narrowed by substituting a longer alkyl chain in the R and R' positions [31]. NIR dyes with broad absorbing peaks show promise since they can absorb a large range of NIR light, thus increasing its usefulness as protection against NVDs.

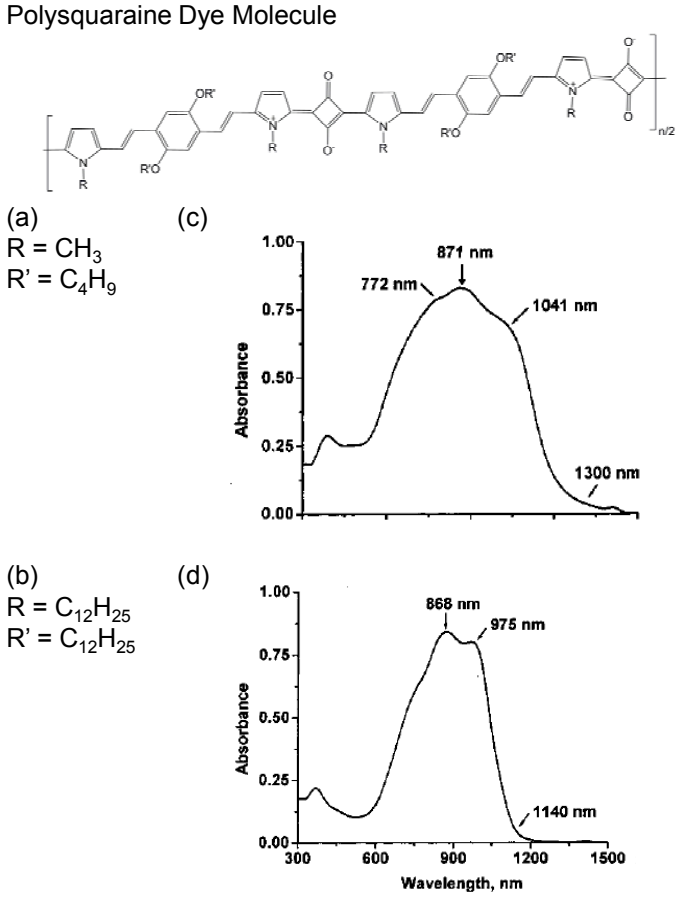

Figure 12. Broad NIR absorption peak for Polysquaraine Dyes. Absorbance of dye molecules with R and R' substituents given in (a) has broad absorbance peak (c); dye with (b) substitution gives narrower absorbance peak (d). (Modified from [31])

2.3.4. NIR Reflectance and Dyes Used by US Army

Currently the US Army uses traditional acid and vat dyes for nylon and cotton, respectively. The Army wants better color fastness properties and better sustainability during laundering. A concern with the new NIR absorbing dyes is that they are not likely to be durable enough for textiles, particularly military uniforms. [37]

2.4. Reflectance

The manner in which a material reflects, transmits, and absorbs electromagnetic waves in the ultraviolet, visible and infrared ranges affects its optical and radiative properties. The reflectance of a material is influenced both by its refractive index [38]; chemical composition [39, 40]; surface shape [41], size [42, 43], and roughness [42, 43]; and presence of interfaces between media [38, 44-46].

2.4.1. Chemical Composition

The chemical composition of a material plays a significant role in the reflectance of electromagnetic waves, particularly in the visible and infrared regions. For most dyed textile materials the primary consideration is reflectance in the visible region. However, the reflectance in the infrared range is important in camouflage applications. The chemical composition and structure affects the reflectance properties in NIR and mid-IR energy ranges. The chemical bonds in the material have particular wavelengths at which they vibrate and create absorption bands in the NIR and mid-IR region. Particular bonds have characteristic frequencies at which they vibrate in the mid-IR energy region; the absorbance bands in the NIR range are overtones of the characteristic frequencies [39, 40].

The NIR and mid-IR absorbance and reflectance of polymers and fibers commonly used in textile products have been studied extensively [39, 40, 47, 48]. The earliest study by Greenler and O'Neil was focused on relating reflectance to heat transfer properties of fabrics [48]. This study was focused on reflectance changes caused by the dyes used and only explored wavelengths from 400 to 1000 nm. Later studies were mainly concerned with creating methods to characterize polymers and fibers so that the information

can be used to identify unknown fiber samples. The study by Papini examined cotton, wool, polyamide, polyester and polypropylene [39]. The article lacks physical characterization of the natural fibers and the polyester; and while presenting a comparison of particle sizes and fiber diameters of polypropylene and their effect on reflectance, the authors neglect to address the fiber characteristics of the other materials but still compare them directly to one another. The author uses principle component analysis (PCA) to compare the polymers and summarizes the variation into three principle components (PC) which explain 98.1% of the variation in the NIR range. The author reports that the first PC explains 86.1% of the variation and is generally related to particle size; while the other PCs are related to differences in the chemical composition of the polymers [39]. The work of Jasper and Kovacs presents the use of neural networks as an alternative to PCA and other mathematical methods for comparing NIR spectra of fibers. The method reduces the number of samples needed in the library to achieve a good match identification of fiber type. However, large variations in cotton and similarity of its NIR signature to other cellulosic fibers; led the method to achieve a lower confidence match.

2.4.2. Size, Shape, and Roughness

The optical properties of fibers and spherical particles have been studied. The analysis of the optical properties of fibers typically treats the fibers as infinitely long cylinders. Kerker presents an analysis of the scattering of light by infinite cylinders for both perpendicular and oblique incidence beams [38]. The geometry shown in Figure 13a depicts the fiber in the cylindrical coordinate system with coordinates z, r, θ, in which the fiber is aligned in the z-direction. When the incident beam is perpendicular to the z direction, the light

scatters as a cylindrical wave. However, when the incident light travels at an angle, Φ, the cylinder scatters the light and it propagates along the surface of a cone, as seen in Figure 13b [38, 42]. The scattering efficiency is a function of the refractive index, the size parameter, and the angle of incidence [38]. The size parameter, χ, equals $\pi d/\lambda$, where d is the diameter of the fiber and λ is the wavelength of the incident light. The inclusion of the size parameter makes the efficiency equations universal since the interaction is dependent on the ratio of the size of the fiber to the wavelength of light.

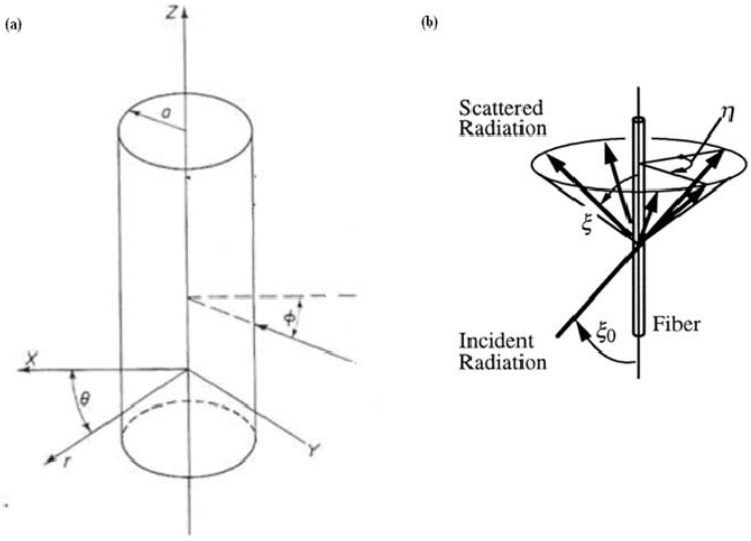

Figure 13. Light Scatter by Infinitely Long Cylinder. (a) Geometry of infinitely long cylinder and coordinate system (from [38]); and (b) scatter of light by fiber based on infinitely long cylinder model (from [42])

There are some limitations for using the infinite cylinder to represent the scatter of light by fibers. The analogy with monofilament yarn is much better than for yarn made of staple fibers due to the twist needed to make spun yarn [49]. As a result twisted spun yarn have a rougher surface compared to a circular cross-section monofilament. For the cylindrical model to work, the roughness of the yarn would have to be much smaller than the wavelength of

light being studied. Another limitation of this model results from the variation in refractive index along the yarn length. Studies of the optical diffraction of fibers, both synthetic and natural, by Lynch and Thomas revealed that there is significant variation in the diffractive pattern at different spots along the length of synthetic fibers [50]. Since the optical properties are dependent on the refractive index, then the scatter of light of a yarn would be dependent on the location on the fiber where the testing occurred. Furthermore, as the size parameter increases, the limits of the cylindrical model are reached, making the model insufficient for fibers with large size parameter. For size parameter greater than fifty, Yamada and Kurosaki have proposed using the rectangular aperture model instead [42]. The Yamada and Kurosaki model takes into account diffuse reflectance from the surface which is an improvement from a model proposed by Swathi and Tong that computes scattering efficient of highly absorbing cylinders [51].

The scatter of light by spheres is also of interest since spherical particles are being used to coat textiles in this project. For the case of spheres, the reflected, refracted, and internally reflected rays must be considered [38]. The interaction of the incident light with a spherical particle is shown in Figure 14. The incident light is reflected off the surface of the sphere as well as a portion of it is refracted into the sphere. The refracted ray encounters another surface in the sphere and a portion is internally reflected and a portion of the light emerges from the sphere. The internally reflected can be internally reflected again and a portion can emerge from the sphere.

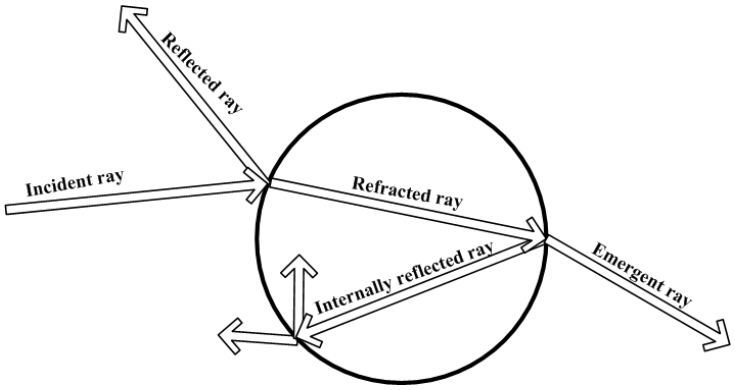

Figure 14. Sphere geometry showing geometrical optics rays (modified from [38]).

The light interactions are further complicated when the spheres are packed or on the surface of another material. In the system composed of packed spheres, a ray refracted from one sphere can emerges and strikes another sphere and can then be reflected and refracted by that sphere creating a complicated optical interaction [44, 52]. The diffuse reflectance of mid-infrared light by powders has been studied by Ventura and Papini [52]. The study examined polystyrene, calcium carbonate, glass and silver-coated glass spheres with diameters from 10 – 1800 μm. Ventura and Papini concluded that the optical properties are sensitive to particle size and that reflectance decreases with increasing particle size [52]. The work of Chan and Tien developed a model to compute radiative transfer of hollow spheres 20 – 200 μm coated with highly reflective material packed in layers [44]. The study treated the system as multilayers of thickness equal the diameter of one sphere and treated each layer as a isotropic material [44]. In the case of spherical particles coating a fiber, there are two approaches which can be taken to analyze the optical properties. The system can be treated as continuous with isotropic properties or discontinuous and composed of discrete layers. For the discontinuous model to work the particle must be

large in comparison to the wavelength of light [44], this condition may pose a problem for this study since the particles are on the order of magnitude of the wavelength of light being studied. Because this is the case it is useful to delve into the recent study of photonics and photonic crystals, since they are concerned with the interaction of light and particles of the same order of magnitude.

There are a few published studies on the effect fibers and textile coatings on their reflectance properties. One study of interest is the effect of alumina and silicon coatings on the radiative properties of silica fibers in the mid-IR range. The coating thickness ranged from 10 nm to above 200 nm and the fibers tested had radii of 0.5, 1.0 and 3.0 μm [53]. The study sought to increase the reflectance of the mid-IR light. Another study sought to assess the effect of particle size of finishing chemicals on reflectance in the visible range [21]. The study assumes that the shape of fluorocarbons and dimethyloldihydroxylethylene urea (DMDHEU), a wrinkle-free treatment, can be represented as spheres of uniform diameter. The study used the dynamic light scattering technique to determine the effective diameter, this revealed that both DMDHEU samples and one fluorocarbon samples had bi-modal size distributions and effective diameters ranging from 80 – 800 nm. The fluorocarbon treatments, whose effective diameters were smaller than the DMDHEU, reduced the reflectance of the fabrics in the visible range; however, the author states this might be attributed to difference in refractive index of the material rather than the size of the particles [21]. The results presented are useful in that compared to the other studies described, the particle size and wavelength of light studied are of the same order of magnitude.

The reflection of light by a hemispherical shell is of interest due to the use of mushroom cap shaped particles as seen in Figure 15. The shell must be treated differently than the sphere due to the changes in the location of surfaces into which the light can reflect, refract, and absorb into. As seen in Figure 16, three interfaces exist which the light encounters: air – particle interface, particle – air, and air – fiber. At each interactions at each of these interfaces affects how much radiation is reflected from the fabric system. A model for the radiative transfer by a semitransparent hemispherical shell has been developed, however, it assumes that the diameter and thickness of the shell is much greater than the wavelength of light and does not evaluate the radiative properties of the substrate [54]. These assumptions are not appropriate for this project since the particle size is on the same order of magnitude as the wavelength and the effect of the overall fabric-particle system must be considered in evaluation of the optical properties.

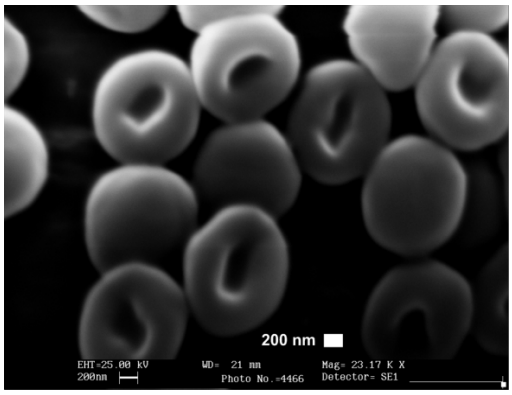

Figure 15. SEM Micrograph of polystyrene mushroom cap shaped particles, 1.2 μm in diameter

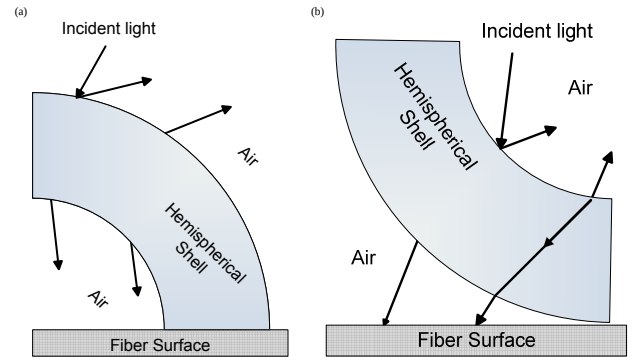

Figure 16. Interaction of light with hemispherical shell, facing down (a) and facing up (b)

2.6. Negative Refraction and Metamaterials

Metamaterials are artificial composite materials in which the characteristic length of its components are much smaller than the wavelength of light of interest [55]. Metamaterials have a negative refractive index. The refractive index, *n*, is $n = \sqrt{\varepsilon\mu}$ where ε is electric permittivity and μ is magnetic permeability. A negative refractive index results when both ε and μ are negative [55-58]. A material with a positive refractive index deflects incident light on the opposite side of the normal of the surface according to Snell's Law $\sin(\theta_1) = n \sin(\theta_2)$, as seen in Figure 17a. A negative refractive material deflects the incident light on the same side of the normal as the incident light as shown in Figure 17b. [55, 58]

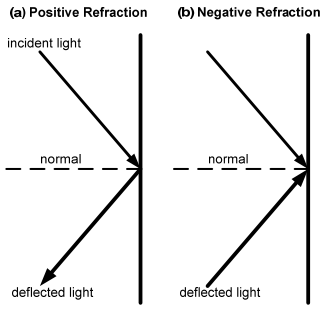

Figure 17. a) Positive refraction of light off of a flat surface and b) negative refraction of light

Negative refractive materials can be used to improve camouflage materials. Deflection of light by the material can be altered from what would typically be expected, making detection of the object difficult. Current metamaterials have been developed to interact with microwave [58], infrared [56, 59], and most recently visible [57] wavelengths of light. The fabrication of features in metamaterials must be precisely controlled in order to optimize their performance [56, 59] particularly for interactions with shorter wavelengths of light. The development of fabric metamaterial for clothing may not be practical due to deformability of the garments; however, use in more stationary fabric structures such as tenting may be a potential end use for a textile metamaterial.

2.7. Photonic Band Gaps and Photonic Crystals

Photonic crystals also offer a means to modify the interaction of light as compared to traditional materials. Research in photonic crystals began with the work of Yablonovitch and John who sought to develop materials to control radiative properties [1] and localize light [2]. The unique properties are due to juxtaposition of materials with different refractive indices [3, 4, 60]. Photonic crystals can be designed to have a complete bandgap, which is a region of frequencies of light that cannot exist within the crystal [1, 3-5]. To produce a bandgap for a particular wavelength of light, the lattice constant of the crystal must be on the same order of magnitude of the wavelength of light [3, 5, 55]. The first synthetic 3-D photonic crystals developed had a bandgap in the microwave region [5], creating a 3-D crystal for smaller wavelengths has proved challenging due to limitations of etching devices [3, 6]; however, natural 3-D photonic crystals which interact with visible and UV light can be found in nature [60].

Creating 1-D and 2-D crystals with bandgaps in the NIR [4, 61] and mid-IR [6, 61] regions has been achieved. One-dimensional crystal fibers, with diameters ranging from 175 – 500 μm, have been developed by layering poly(ether sulfone) (PES) and arsenic triselenide (Ar_2Se_3) [61]. These fibers act as omnidirectional mirrors over infrared frequency ranges [61]. Another fiber crystal has been reported by a company Crystal Fibre which is a glass fiber with hollow cylinders running through it [3]. The Crystal Fibre product resembles the 2-D structures found in setae of polychaete worm [60], these structures look like highly ordered island-in-the-sea fibers, shown in Figure 18. The current fibers act as mirror and are highly reflective. While high reflectivity on the exterior of the fiber is not desirable in this project; photonic crystals can be developed to act as wave guides and trap light by introducing defects in the crystal structures [3, 5]. The development of fibers and fabrics with light trapping capabilities would be useful in reducing the amount of near-infrared light reflected off the fabric surface.

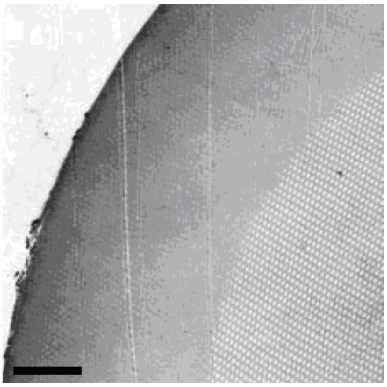

Figure 18. Image of setae of polychaete worm which resemble Crystal Fiber product and islands-in-the-sea fibers [60].

An alternative to photonic fibers is to create photonic crystal-like structures on the surface of fabrics. This technique would utilize bottom-up design

methods of photonic crystals, which offer a means to create ordered structures with nanometer range repeat elements [3]. Colloidal crystals, shown in Figure 19, offer promise in the area of bottom-up design and can be made from silica and polymeric spherical particles [62, 63]. The thickness of crystals can be controlled by particle size selection and solution concentration [62]. Colloidal crystal structures of composite particles have been developed by layer-by-layer coating PAH and PSS on polystyrene particles, by infiltrating the PAH/PSS multilayer structure with gold nanoparticles [63], and by forming core-shell [7, 64] and hollow-shell particles [7, 64, 65]. The coating thickness and composition can be controlled to alter the bandgap frequency [63]. An additional crystal structured explored has been the inverse opal crystal, shown in Figure 20, which is developed by forming a crystal of spherical particles, filling the void spaces of the crystal, and then removing the spherical particles template [66].

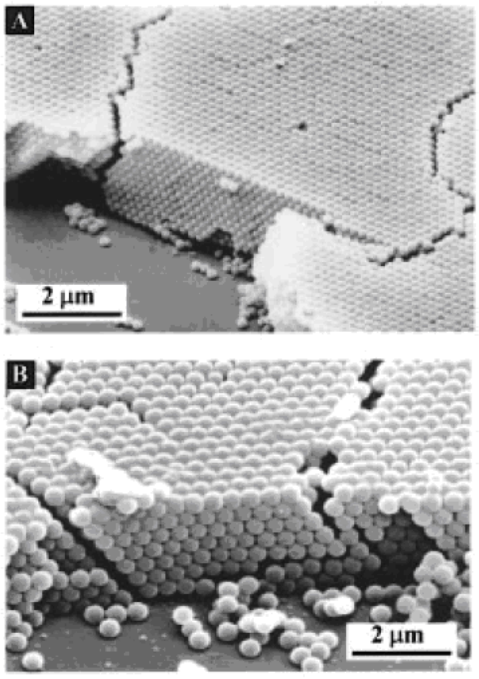

Figure 19. Multilayer colloidal crystal of spherical particles [62]

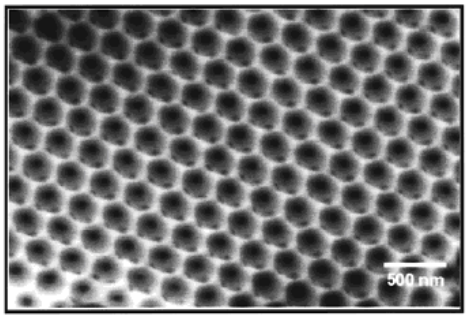

Figure 20. Inverse opal crystal made from spherical colloidal crystal template [66]

Research into non-spherical particles such as dimers [11, 67], trimers, tetramers [67], and mushroom cap [8] for colloidal crystals has also been performed. Crystal structures from polystyrene mushroom caps [8] and dimers [11] have been formed through convective assembly, as seen in Figure 21, respectively. The use of non-spherical particles in photonic crystals is predicted to create bandgaps frequencies that cannot be achieved by using spherical particle crystals [67]. Furthermore, non-spherical photonic crystal structures can be found in nature. One structure of interest can be found on arthropodal ommatidial surfaces and diurnal moth wings as seen in Figure 22 [60]. The nipple shaped structures act as anti-reflective coating and minimize surface reflectivity over a broad range of frequencies [60]. A non-spherical particle for creating an anti-reflective structure on the surface of fabrics would be useful if it can reduce reflection in the NIR range.

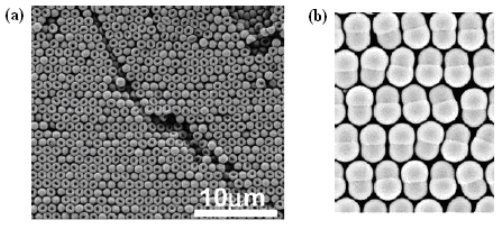

Figure 21. Colloidal crystals of non-spherical shaped particles, (a) mushroom cap shaped particles [8] and (b) dimer shaped particles [11]

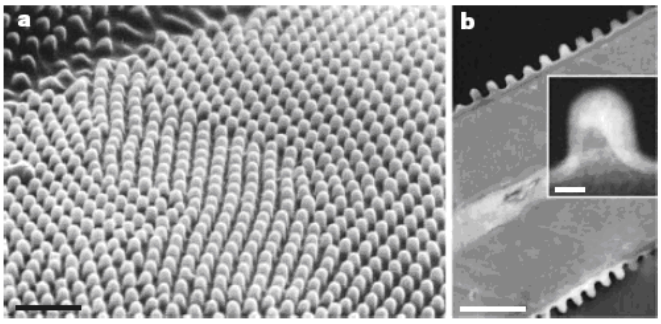

Figure 22. Anti-Reflective nipple shaped nanostructures found on (a) arthropodal ommatidial surfaces of a lepidopteran eye and (b) transparent wings of hawkmoths [60]

2.8. Summary

The primary objective of this project is to modify the NIR signature of textile fabrics via deposition of self-assembling colloidal particles of polystyrene. Polystyrene particles are being used as an alternative to NIR absorbing dyes to alter the optical properties of the fabrics. The particle deposition on fabric process is designed to make a material that could have metamaterial or photonic crystal properties. The optical properties of fibers and spherical particles have been studied separately, but there is little published work on the effect of particle coatings on optical properties of fibers. To evaluate such properties, the project will look at effect of fiber type, dye, and surface structure on fabric substrates after deposition of particles.

Chapter Three will discuss and evaluate the deposition process. Two fabrics, a cationic cotton and nylon-cotton blend, and a cationic cellophane film were used as substrates for deposition of sulfate functionalized polystyrene submicron and micron sized particles. Three spherical particles and one nonspherical particle were used to coat the fabrics via electrostatic and convective self-assembly. The effect of particle size on coverage will be evaluated using scanning electron microscopy (SEM). SEM will also be used to evaluate order in particle structure formation on the fibers.

Chapter Four will analyze the near-infrared (NIR) reflectance of the particle coated fabrics using average reflectance spectra and principal component analysis (PCA). The effects of both substrate and particle type on reflectance will be addressed. A comparison of average reflectance by particle size within each substrate type will be done. A comparison of change in percent reflectance and standard deviation will be performed within each substrate group. From the PCA results, the ability to significantly modify the NIR reflectance of fabrics using colloidal particles will be evaluated.

Chapter Five will conclude with proposed work to further the research done in this project. Additional particle compositions and modifications will be discussed. Further work in developing textile metamaterials will also be discussed.

Chapter 3. Deposition of Colloidal Nanoparticles on Textile Substrates

In this chapter, the deposition of sulfate functionalized polystyrene (PS) particles onto nylon-cotton and cotton fabric substrates will be discussed. Particles were deposited using electrostatic and convective forces. Due to sulfate groups ($–SO_3^-$) on the exterior of the PS nanoparticles, the particles are negatively charged. The fabrics were surface treated to become positively charged. The nylon-cotton sample was treated with a single poly(allylamine hydrochloride) (PAH) layer to form $–NH_3^+$ surface groups. The cotton was treated with 2,3-epoxypropyltrimethylammonium chloride to form cationic cotton with $–RN^+(CH_3)_3$ groups. The negatively charged particles were attracted to the positively charged groups of the fabrics. Spherical particles of 0.2, 0.5, and 1.0 μm and a 1.2 μm non-spherical, mushroom cap shaped particle were deposited on the fabric. A planar, cellulosic film substrate was used for a control and comparison.

SEM was used to evaluate the deposition process and particle coverage. An evaluation on the effect of particle size on coating coverage was conducted. The ability of the particles to coat the bends, twists, and sub-surface of fibers within the 3-D fabric structure was also evaluated. The single layer versus multilayer particle formation were evaluated. Long range order in layer formations was evaluated.

3.1. Nylon-Cotton Camouflage Fabric Substrates

The nylon-cotton blend fabric used in our experiments is a camouflage fabric used for the Army Combat Uniform (ACU). The ACU fabric was provided by Mr. Francisco Martinez from the Natick Soldier Center. The universal camouflage design for the ACU contains 3 colors—desert sand,

foliage green, and urban grey. Each color was treated as a separate substrate. One centimeter by three centimeter samples were judiciously cut so that only one of the three colors was primarily present.

The nylon-cotton fabric was coated with a layer of poly(allylamine hydrochloride) (PAH) using layer-by-layer electrostatic self assembly method to create a positive surface charge [25, 26]. The fabric was soaked in a deionized water bath, dipped in a 0.5 mMol aqueous PAH solution, rinsed in deionized water, and dried at 60 °C. All dip times were ten minutes.

3.2. Cellulosic Substrates

Undyed cationic cotton 3x1 twill fabric was obtained from Professor Peter Hauser of North Carolina State University (NCSU). The cationization was performed at NCSU by modification with 2,3-epoxypropyltrimethylammonium chloride [68].

A transparent cellophane film was used as a model substrate. Since the fabric substrates have a high amount of surface roughness due to the nature of fabrics made from multi-ply yarns spun from staple fibers, the film served as a more uniform cellulosic surface for comparison. A forty-two micrometer thick uncoated cellophane film was purchased from Goodfellow Corporation.

The cellophane film was cationized using the procedure described by Hauser et al. [68]. Sodium hydroxide (NaOH) solution was prepared from 97% NaOH pellets to form a 50% NaOH solution. A cationization solution was prepared using 34.7 g of 65% 3-chloro-2-hydroxyproplytrimethylammonium chloride (CR-2000 received from Dow Chemical), 25 mL of 50% NaOH solution, and 669 mL of deionized water. The film was soaked in the cationization solution for one hour. After removing from the solution, the film was dried at room temperature for twelve hours, then rinsed twice in a

deionized water bath. It was rinsed with a one (1) gram per liter aqueous acetic acid solution. The film was dried at room temperature.

3.3. Spherical Particles

2.5% wt aqueous suspensions of sulfate functionalized polystyrene (PS) spherical Polybead® colloidal particles were purchased from Polysciences, Inc. in diameters 0.2, 0.5, and 1.0 micrometers. Deposition suspensions were prepared by diluting the purchased colloidal PS suspension with deionized water to 0.016 mg PS spheres per mL of suspension.

3.4. Mushroom Cap Particles

Mushroom cap shaped particles, approximately 1.2 μm in diameter, were received from the Liddell group (Cornell University; Ithaca, NY) as an aqueous suspension. The 4.2% wt mushroom cap particle suspension was diluted with deionized water to 0.009 mg PS particle per mL of suspension.

3.5. Sample Preparation and Deposition Process

The process used to deposit the polystyrene particles onto the textiles was based on two underlying mechanisms: electrostatic and convective assembly. The electrostatic assembly method utilized the attractive forces between the opposing positively charged substrate and the negatively charged PS particles. The convective assembly method used the PS particle flow due to water evaporation to assemble the particles on the drying edge of the substrate. The schematic cartoon in Figure 23 is a simplified version of the deposition technique.

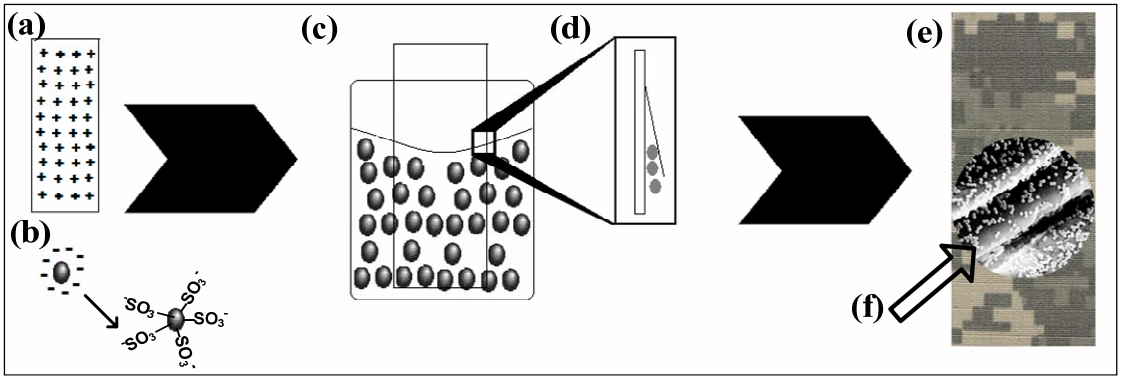

Figure 23. Particle Deposition on Fabric Substrate Schematic. This method was used to deposit PS particles on fabric and film substrates. (a) Substrate was pre-treated to create positive surface charge. (b) PS particles were negatively charged via sulfate functionalization. (c) The substrate (a) was mounted on a slide immersed in a colloidal suspension containing (b) and placed in the oven at 60 °C. The opposing electrostatic charges attracted the particles to the fabric and secured them to the surface. The second mechanism, convective assembly, is facilitated by the evaporation of the water from the suspension. The meniscus shown in blow out (d) limits the layer thickness of particles deposited. After evaporation is fully complete, (e) particle coated fabric sample was visible unchanged, yet SEM micrograph reveals successful deposition of particles on the individual fibers (f).

The cotton and cellulosic film were chemically treated to add cationic surface groups. The nylon-cotton fabric was coated with PAH. The samples were cut in 1 cm by 3 cm rectangles and mounted on half a glass slide. The samples were placed in a vial as shown in Figure 24a. The vial was filled with 8 – 10 mL of colloidal suspension to cover the sample as shown in Figure 23c and Figure 24b. The vial was placed in oven at 60 C for a minimum of twelve hours.

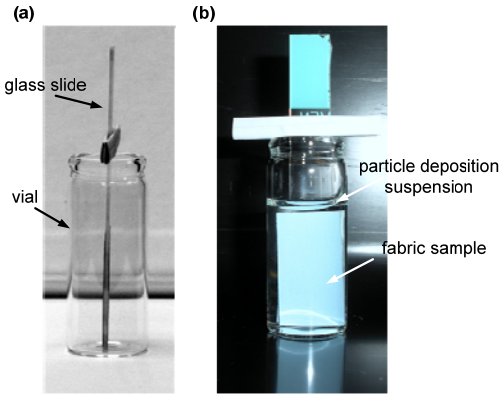

Figure 24. Sample Setup for Deposition. Substrate is secured on glass slide using double stick tape and suspended vertically in vial. Enough deposition solution is added to cover substrate. (a) shows side view of sample and (b) shows front view of sample.

As the water evaporated from the suspension, the particles assembled on the substrate via convective assembly. The meniscus formed between the substrate and liquid at the surface of the solution limited the number of layers of particles deposited as shown in Figure 23d. Smaller particles are more likely to form multilayer as shown in Figure 25. The coated fabric remained visibly unchanged after the particle deposition as shown in Figure 23e. The nylon-cotton fabric took on a whitened appearance in areas where dense crystal-like structures of particles formed. The cellulosic film once coated became slightly iridescent.

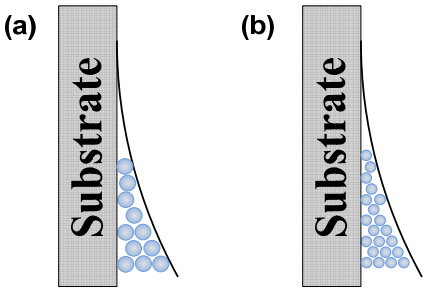

Figure 25. Size Limitation by Meniscus Area. Multilayer formation limited by particle diameter and area between substrate and meniscus. Meniscus limits multilayers of large particles in (a) as compared to smaller particles in (b).

3.6. Assessment of Surface Coverage Evaluation via SEM

SEM micrographs were taken using Leica 440 SEM with Tungsten filament at 25 kV. The sample was coated with gold/palladium or gold with sputter coater for 30 seconds.

3.6.1. Effect of PAH Coating on the Deposition of PS Particles on Nylon-Cotton Fabric

The nylon-cotton camouflage fabrics were modified using PAH to create a positively charged surface. In the absence of positive charges on the substrate, the PS particles exhibited a greater affinity for each other and preferentially formed crystal-like structures rather than depositing on the surface of the fibers. The SEM micrographs in Figure 26 illustrate this phenomena for the set of substrates not coated with PAH.

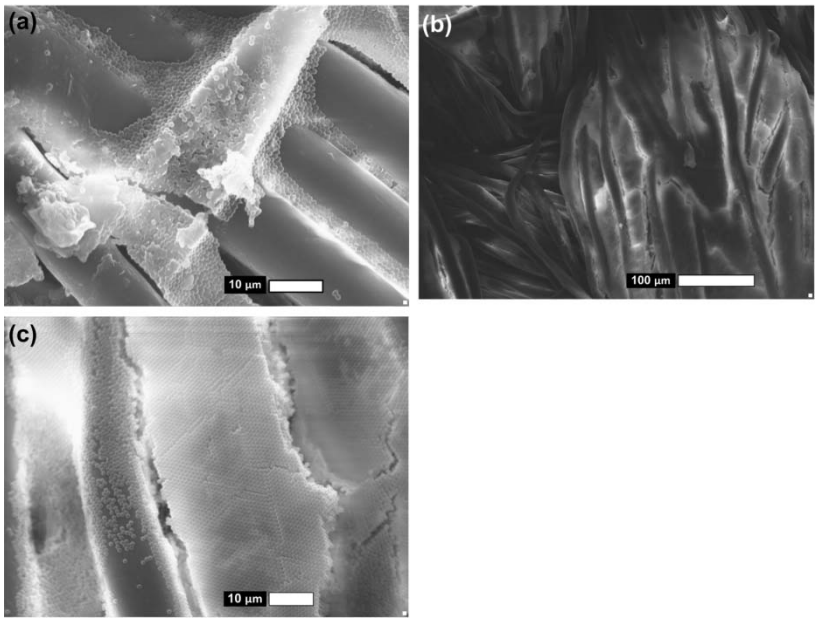

Figure 26. Nylon-Cotton camouflage fabric not surface treated with PAH and coated with 1.0 µm polystyrene spheres. (a) No affinity shown for the nylon fibers and PS beads form structures between fibers and bridges over fibers; (b) dense crystal-like structures formed between fibers of yarn by PS spheres; and (c) some affinity for fiber but particles more dense form in structures amongst themselves.

3.6.2. Deposition of Particles on Non-Planar Surface

The substrates used in this project were fabrics made of multi-ply yarns. While fabrics are often considered 2-D structures, the dimensions of the fabric and its components were orders of magnitude greater than the particles deposited, hence generating a truly 3-D structure. Coating the surface of the fabric with particles presented unique problems as compared to similar assembly processes on flat surfaces such as films and metallic substrates. Fibers have high radii of curvature. Furthermore, the cotton fabrics used had not been mercerized so the cotton fibers retained their non-spherical cross-sections. Cotton fibers are also naturally twisted along their length. SEM micrographs were used to evaluate whether the particles could conformally coat the fibers and fabric as seen in Figure 27. The 1.2 μm mushroom cap particles coated the tip of a nylon fiber as shown in Figure 27a and Figure 27b. Bends in nylon fiber were conformally coated with particles as shown in Figure 27c and Figure 27d. Bends in the cotton fibers were also conformally coated with 1.0 μm and 0.2 μm spherical particles as shown in Figure 27e and Figure 27f, respectively. The twists and contours of the cotton fibers were coated both on the interior and exterior by 1.0 μm spherical particles as shown in Figure 27g and Figure 27h.

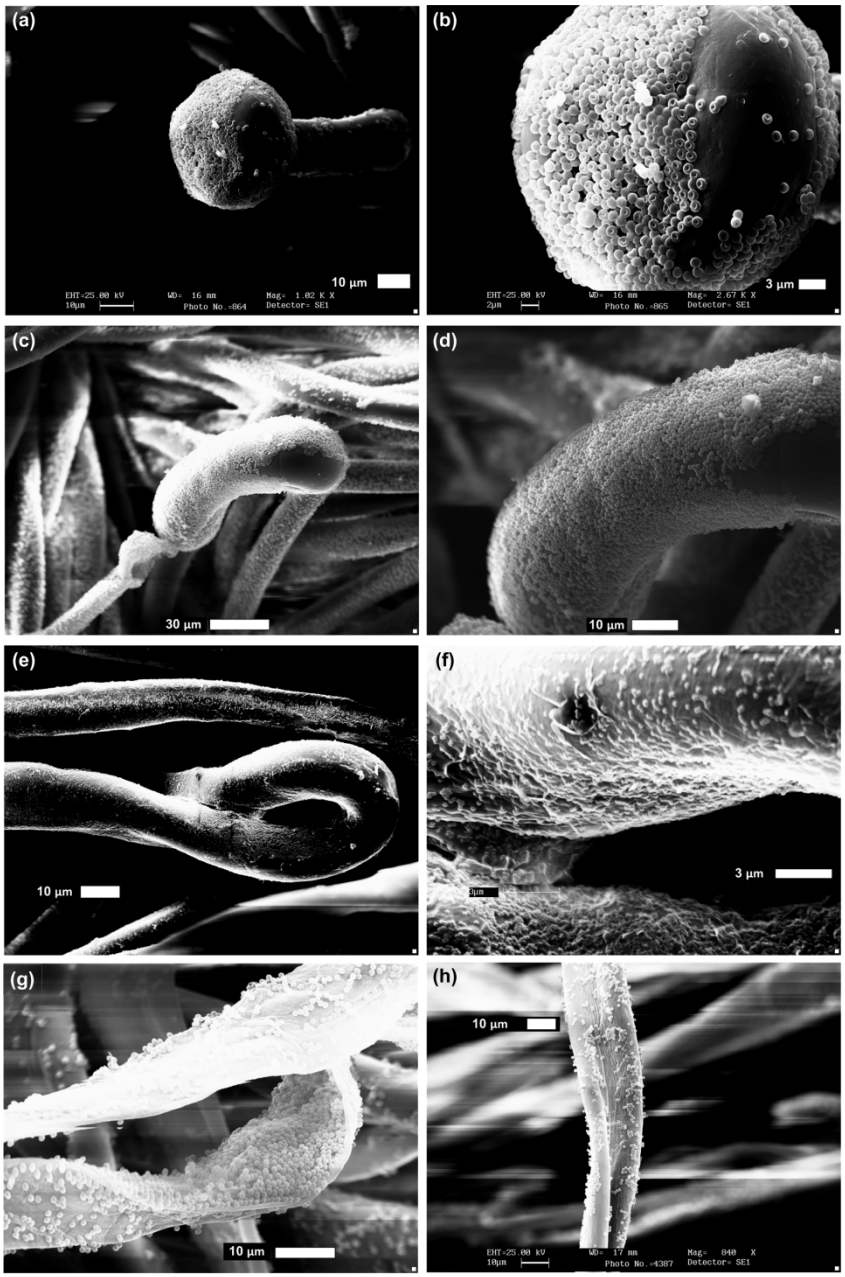

Figure 27. Conformational coating of fibers with polystyrene particles. (a) Nylon fiber tip protruding from desert sand nylon-cotton camouflage fabric coated with 1.2 µm PS mushroom caps, (b) shows (a) at higher magnification. (c) Bent nylon fiber from desert sand nylon-cotton camouflage fabric coated with 1.0 µm PS spheres with magnified image shown in (d). (e) Cotton fiber bent into a loop from foliage green nylon-cotton camouflage fabric coated with 0.2 µm PS spheres with magnified image shown in (f). (g) and (h) Twisted cationic cotton fibers coated with 1.0 µm PS spheres both on inner and outer part of twisted contoured fiber.

The deposition method used was successful at coating sub-surface fibers, as well as surface fibers, as shown in Figure 28, for both cationic cotton and nylon-cotton fabrics. The cotton fibers lying in the background were coated with particles, as well as the fibers running horizontally in the foreground, as shown in Figure 28a. Due to the 3-D nature of the fabric it is difficult to capture multiple layers of the fibers in focus using SEM, particularly those coated with the smaller particles. Several sub-surface layers of coated cotton fibers are shown in the background of Figure 28b. The cotton fibers appear less aligned in the micrographs than the nylon ones due to the fact fibers are highly twisted in the yarns. The micrographs show the fibers and not the entire yarn structure which furthers this optical illusion. The sub-surface fibers of the nylon-cotton fabric were also coated with the particles as shown in Figure 28c-e. Additionally, the sub-surface coated fibers can be seen below the bent nylon and twisted cotton fibers in Figure 27c and Figure 27g, respectively.

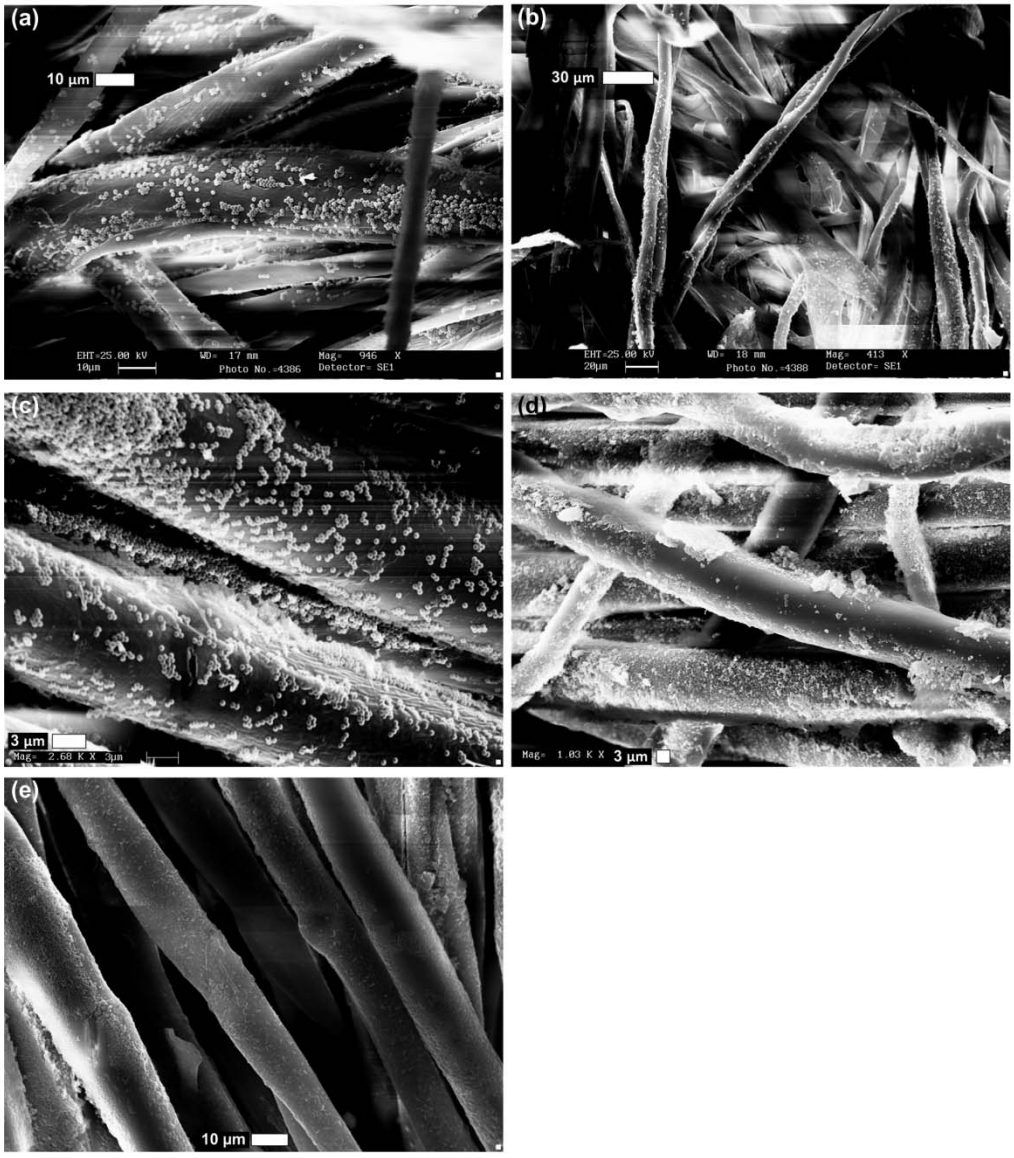

Figure 28. SEM Micrographs of Coated Non-Surface Fibers of Nylon and Cotton Fabrics with PS Particles. Cotton surface and sub-surface fibers coated with (a) 1.0 µm PS spheres and (b) 1.2 µm PS mushroom caps. Surface and sub-surface fibers in nylon-cotton camouflage fabric coated with (c) 0.5 µm and (d, e) 0.2 µm PS spheres.

3.6.3. Deposition of Particles on Planar Cellulosic Surface

Due to the aforementioned concerns regarding the use of a non-planar fabric substrate for deposition, a planar substrate was selected as a control surface and for comparison purposes. The substrate selected was a cellulose

film. The film was cationically treated using the same procedure as the one used to functionalize the cotton fabric. The cellulosic film substrate creates a bridge between deposition of particles onto non-fibrous planar material and deposition of PS microparticles onto natural and synthetic fabrics and fibers that are non-planar. SEM micrographs of the particles deposited on the cellulosic films were used to evaluate the deposition method and to gauge the method's effectiveness on coating the fabrics.

The SEM analysis of the film revealed differences in the coverage between the larger and smaller particles. The smaller particles, 0.2 and 0.5 μm spheres, more readily deposited in long range single layers or order multilayer structures, as shown in Figure 29a-d. The 0.2 μm PS spheres were deposited in a single layer on the film, Figure 29a, and in some cases multilayer, crystal-like structures formed, Figure 29b. The 0.5 μm PS spheres also deposited in single layer on the film, Figure 29c; a magnified view of the single layer coating is shown in Figure 29d. The larger particles, on the other hand, tended to not have long range single layers and were prone to agglomerate more than the smaller particles. The films coated with 1.0 μm spheres had some areas of single layers; however, there were many agglomerates present, as shown in Figure 29e. Yet, when magnified these agglomerates appeared to have order in their structures, as shown in Figure 29f. The mushroom caps behaved similarly to the 1.0 μm spheres on the film with sparse single layer coverage and the presence of particles agglomerates, as shown in Figure 29g. The mushroom caps deposited in random cap up and cap down configurations, as seen in the magnified micrograph in Figure 29h, which may lead to variation in reflectance properties.

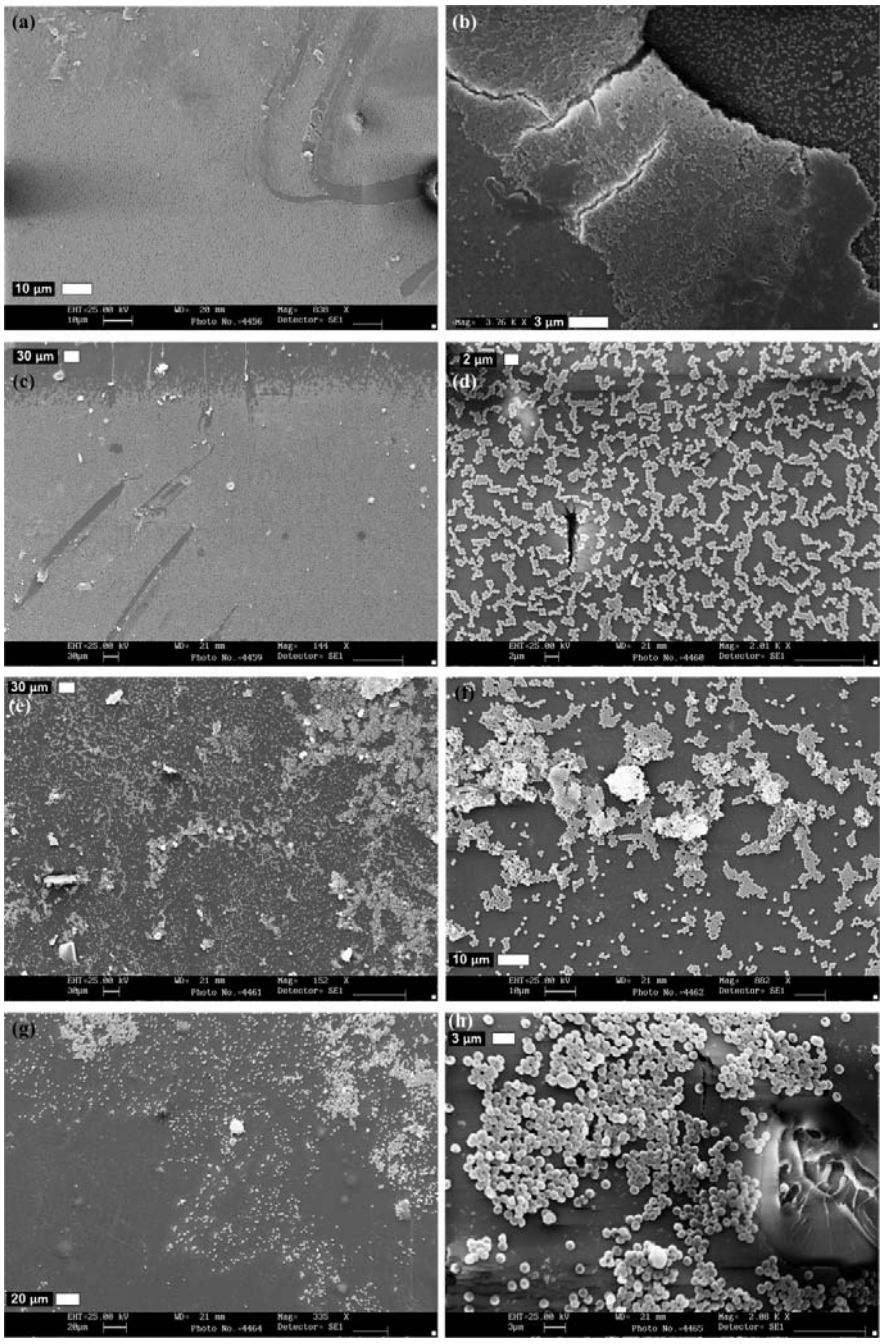

Figure 29. Deposition of Polystyrene Particles on Cationic Cellulose Films. (a) Single layer of 0.2 µm PS spheres on cellulosic film. (b) Multilayer crystal-like structure of 0.2 µm PS spheres on cellulosic film. (c) Single layer of 0.5 µm PS spheres on cellulosic film; magnified in (d). (e) Cellulosic film coated with 1.0 µm spheres, mix of single layer and agglomeration of particles; magnified in (f). (g) Cellulosic film coated with 1.2 µm mushroom cap particles, mix of single layer and agglomeration of particles; magnification of agglomerates in (h).

The analysis of the particle deposition onto the cellulose films offers information that could be applicable to the deposition on the fabric. The presence of ordered multilayered structures of the 0.2 μm spheres, shown in Figure 29b, is consistent with size limitation of the meniscus during the deposition [11]. Also the smaller particles rather than larger particles should form multilayers [11]. The agglomeration of particles versus long range single layer coating on the films presented the likelihood of variation of coatings on fabric based on particle size as well. A unique defect was present on the film substrate, likely due to both the hydrophobicity of the film and the rate of evaporation, which is not present in the fabric samples. As seen in Figure 30, a ridge-like structure formed during the deposition process of the 0.5 μm spheres on the film. This ridge-like structure is similar to coffee drop effect and the ridge is a boundary between regions where the evaporation/deposition rate varied [69]. The hydrophilicity of the fabric is likely to prevent this effect from occurring in the fabric.

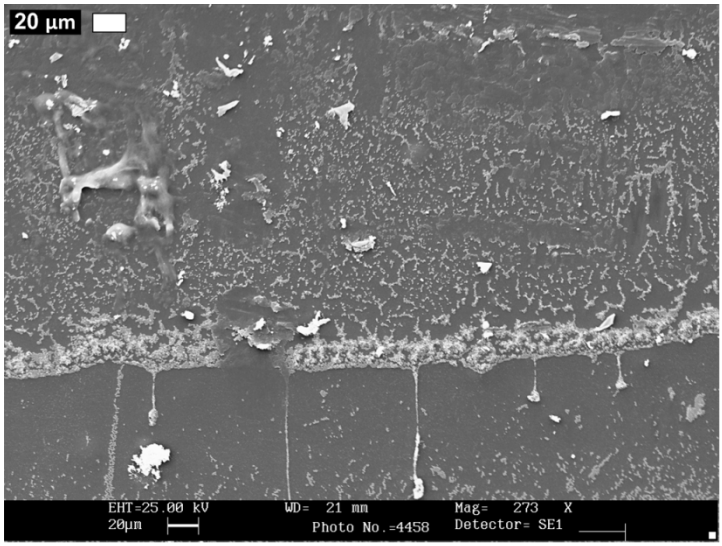

Figure 30. Non-uniformity in Coating on Cationic Cellulose Film. Ridges created during deposition of 0.5 μm PS spheres on cationic cellulose film.

3.6.4. SEM Analysis of Effect of Particle Size on Coverage on Fabric

The SEM analysis was performed to assess the uniformity of the coating on the fibers. From the analysis of the films, the smaller particles provided a more uniform coating; a similar evaluation by particle size will be presented herein.

3.6.4.1. SEM of 0.2 μm PS Sphere Coated Fabrics

Fabrics coated with 0.2 μm PS spheres were typically well coated over all the fibers, as shown in Figure 31. The particles were densely packed on the fibers. Some areas of the fibers were more densely coated than others. As shown in Figure 31b, the fiber in the far right corner is more densely coated than the other fibers. Also, the nylon-cotton fabric, shown in Figure 31f, was highly coated throughout and had some formations off of the fibers due to the high density of the coating. Furthermore, the 0.2 μm spheres coat the cationic cotton fibers well as seen in Figure 31g and Figure 31h. As with the cationic films, the 0.2 μm spheres do form multilayer structures in some cases on both the nylon-cotton and the cationic cotton fabrics, as seen in Figure 31e, Figure 31f and Figure 31h .

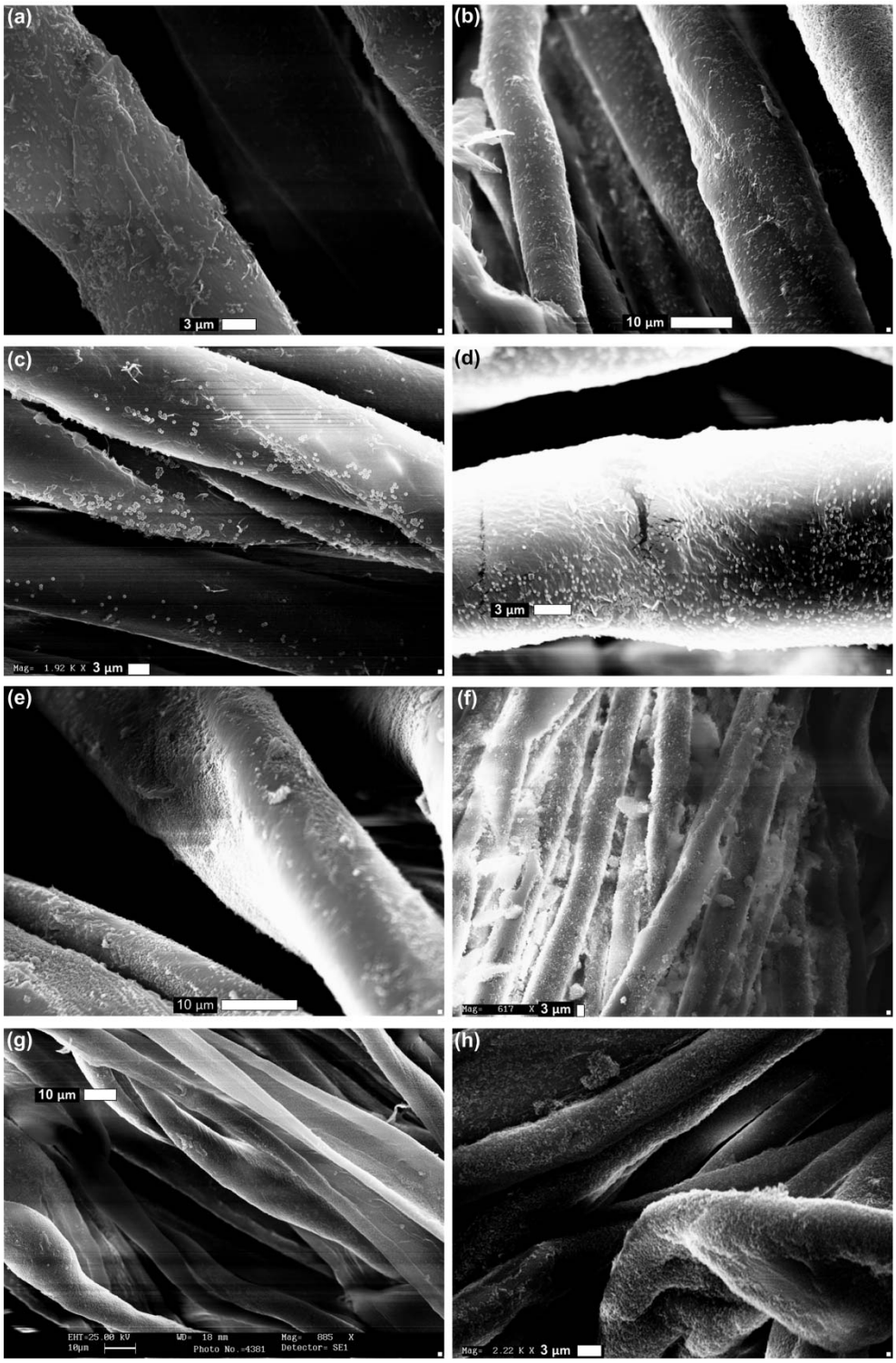

Figure 31. SEM Micrographs of 0.2 µm PS Sphere Coated Nylon-Cotton and Cationic Cotton Fabric. (a), (b), (c), (d), (e), and (f) are fibers from nylon-cotton camouflage fabrics; and (g) and (h) are from cationic cotton fabric coated with 0.2 µm PS spheres.

3.6.4.2. SEM of 0.5 µm PS Sphere Coated Fabrics

Fabrics coated with 0.5 µm PS spheres were well covered, as seen in Figure 32. Most areas contained single layer coverage of particles rather than multilayers.

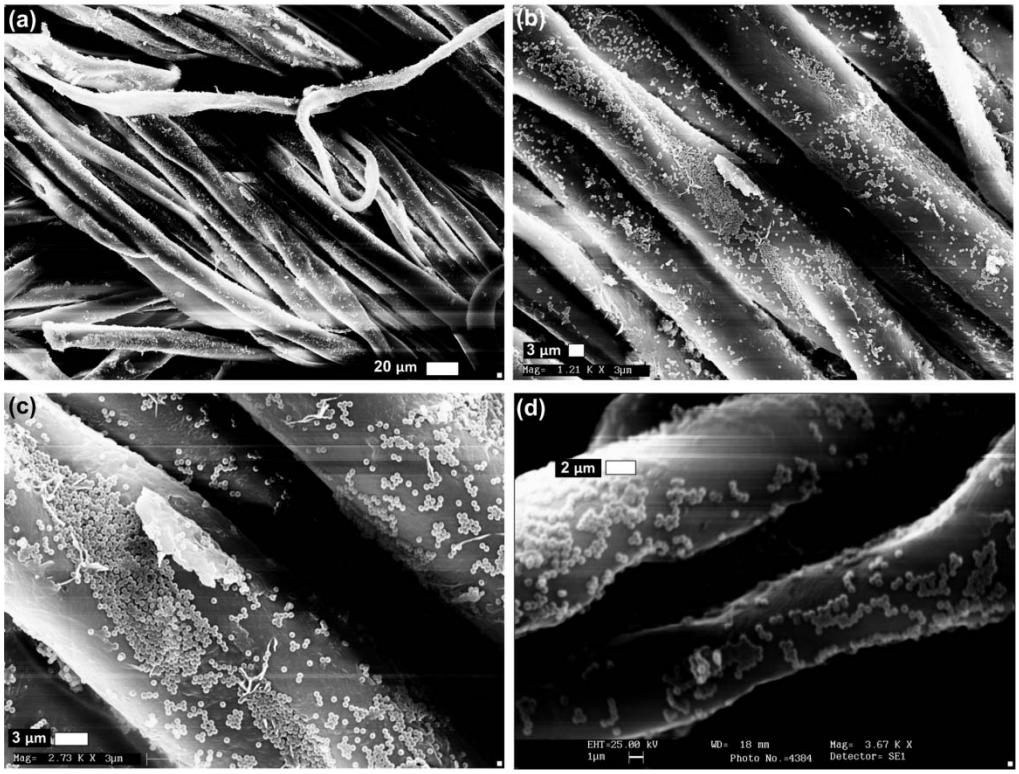

Figure 32. SEM Micrographs of 0.5 µm PS Sphere Coated Nylon-Cotton and Cationic Cotton Fabric. (a), (b), and (c) are fibers from nylon-cotton camouflage fabrics; and (d) has fibers from cationic cotton fabric coated with 0.5 µm PS spheres.

3.6.4.3. SEM of 1.0 µm PS Sphere Coated Fabrics

Fabrics coated with 1.0 µm PS particles were well coated, but there were agglomerates of particles present on some of the samples, shown in Figure 33. There are single layer of particles shown on nylon-cotton shown in Figure 33a-d. Good single layer coverage of 1.0 µm spheres on cationic cotton can be seen in Figure 33a. There is single layer coverage in Figure 33e; however,

there is some agglomeration of particles also present. This is similar to the behavior found when cellulosic films were coated with the same particles.

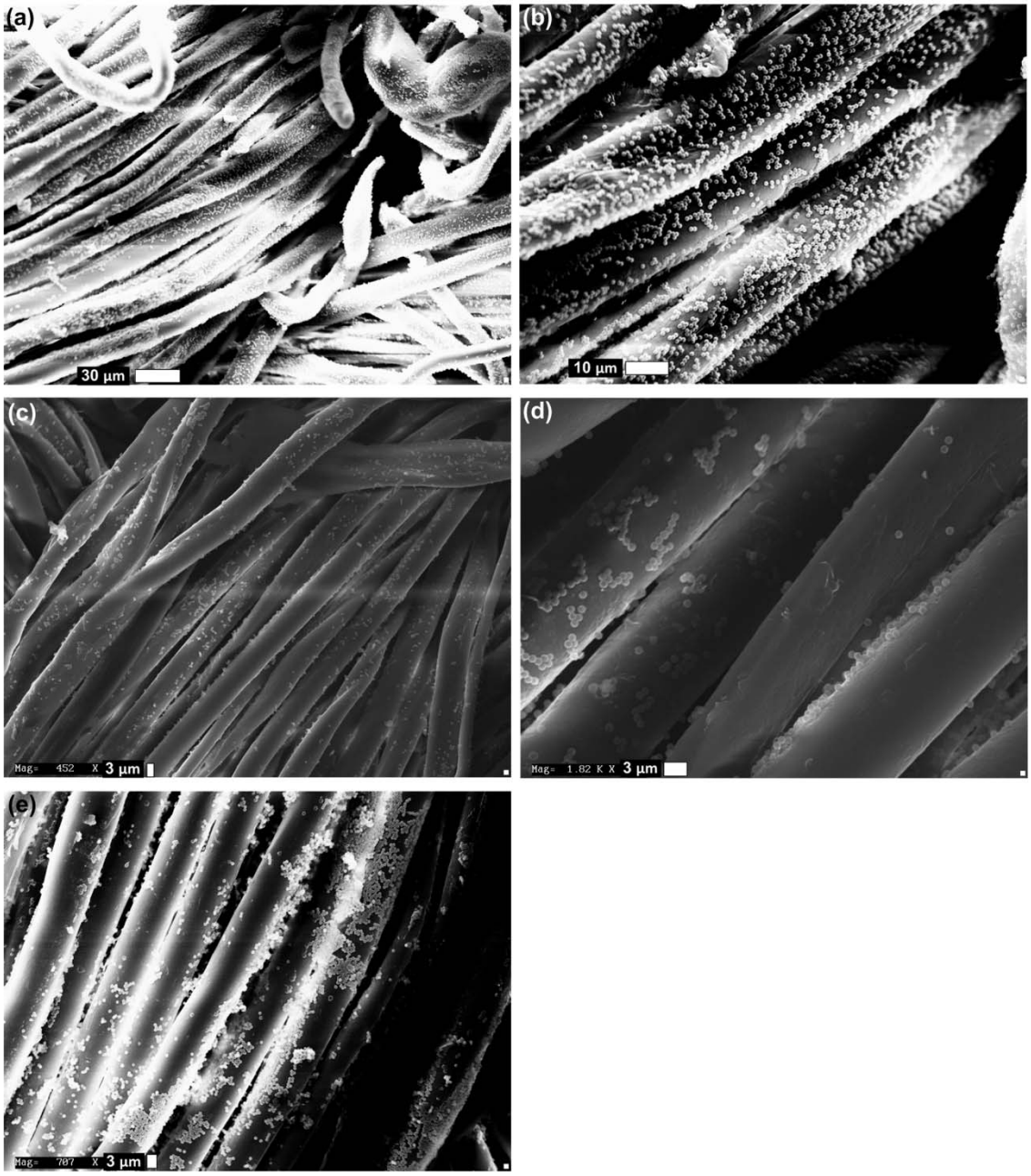

Figure 33. SEM Micrographs of 1.0 µm PS Sphere Coated Nylon-Cotton Fabric. (a), (b), (c), (d), and (e) are fibers from nylon-cotton camouflage fabrics coated with 1.0 µm PS spheres.

3.6.4.4. SEM of 1.2 µm PS Mushroom Cap Coated Fabrics

Fabric with 1.2 mushroom cap coating had varying degrees of coating, as shown in Figure 34. The mushroom caps had single layer coatings on the cationic cotton as seen in Figure 34a and Figure 34b. While there is single layer coverage on the nylon-cotton fabric; there are agglomerates of particles present in Figure 34e. These coverage trends are similar to that exhibited by the cationic film.

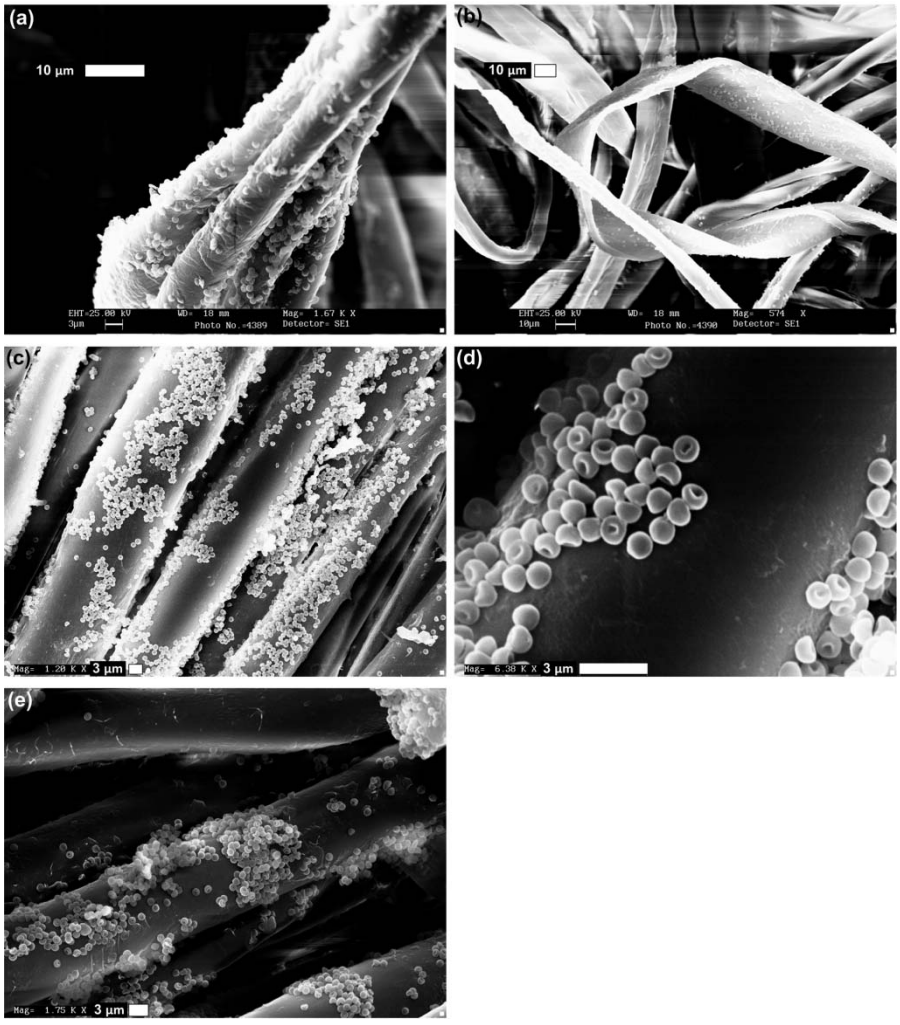

Figure 34. SEM Micrographs of 1.2 µm PS Mushroom Cap Coated Nylon-Cotton and Cationic Cotton Fabrics. (a) and (b) are from cotton and (c), (d), and (e) are fibers from nylon-cotton camouflage fabrics coated with 1.2 µm PS mushroom cap particles.

3.6.4.5. Comparison of Particle Coverage of Fabrics

The particle coverage on the nylon-cotton and cationic cotton fabric is similar to that on the films based on particle size. The smaller particles, 0.2 and 0.5 μm spheres, have longer range single layer coverage of the fibers. As with the films, the 0.2 μm spheres form multilayer structures. These structures are expected due to the size limitation of the meniscus which prevents larger particles from depositing in multilayers. The larger particles, 1.0 μm spheres and the 1.2 μm mushroom caps, deposit as single layers on the fibers but not in as long range order as the smaller particles. Also, the large particles are prone to agglomerate on the fiber surface.

3.7. Summary

In this chapter, sulfate functionalized polystyrene (PS) submicron and single micron sized particles were deposited on positively charged cotton and nylon-cotton fabric substrates. Spherical particles of 0.2, 0.5, and 1.0 μm were used. A non-spherical, 1.2 μm mushroom cap particle was also used. The deposition method utilized electrostatic and convective forces for self-assembly of PS particle from aqueous solutions. The particle coverage on the substrates was evaluated using SEM.

The 3-D nature of the substrate did not present a limitation for the deposition technique. The particles, both spherical and non-spherical, were able to conformally coat the bends and twists of the fibers. The particles, also, coated both surface layer fibers and subsurface layers of fibers.

The effect of particle size on coating was evaluated using SEM. For this analysis, a cellulosic film substrate was used for comparison. Both the fabrics and film showed similar characteristics for size effects. The smaller particles, 0.2 and 0.5 μm spheres, have long range, single layer coverage of fibers. The

0.2 μm sphere coated substrates had ordered, multilayer formations. This behavior is consistent with size limitation of the meniscus which prevents larger particles from depositing in multilayers [11]. The larger particles, 1.0 μm spheres and the 1.2 μm mushroom caps, deposited in single layers on the fibers, but not with long range order as the smaller particles. The large particles were prone to agglomerate on the fiber surface.

Chapter 4. NIR Reflectance

In this chapter the effect of PS particle coating on the NIR reflectance of textile substrates is discussed. The effect of particle size and substrate type on reflectance properties of the modified fabrics was also analyzed. A comparison of average reflectance by particle size within each substrate type was performed as well as a comparison of changes in percent reflectance and standard deviation within each substrate group. The reflectance of the different substrates was compared using principal component analysis (PCA) due to complexity of the data set. From the PCA results, we evaluated the ability of colloidal particles to significantly modify the NIR reflectance of fabrics. We also investigated if the non-spherical particles behave similarly to spherical particles of similar diameter. Finally, we also evaluated what influence the dye on the fabric have on the NIR reflectance signature of the fabrics.

4.1. NIR Reflectance Analysis

The reflectance data was analyzed in terms of variation within group, i.e. same substrate and same particle coating; variation within substrates, i.e. same substrate but different particle coating; variation between particles, and variation between substrates. In the first analysis method, the data was assessed using the average spectra. The average spectrum for a given substrate s with particle coating p was found by averaging the reflectance value r at each wavelength λ for all the samples i with sp substrate-particle combination. Each sample spectrum is represented by the series of coordinates:

$$\left(\lambda_{n_i}, r_{n_i}\right)_{(s,p)_i}$$

where n has integer values from 400 to 1500, s has 5 substrate types, and p has 4 particle types. The resulting average spectrum is represented by the series of coordinates:

$$(\lambda_n, \bar{r}_n)_{s,p}$$

To evaluate the variation in reflectance of coated fabrics, the standard deviation from the mean reflectance was calculated. The graphs of these spectra were used to evaluate whether trends in reflectance behavior were due to the influence of the particle and/or substrate type.

The area between the upper and lower limit of the 95% confidence interval (CI) was used to compare different sample types and determine if there is significant difference in the spectra according to a method proposed by Knüttel and Fiedler [70]. The 95% CI was determined using $\bar{y} \pm 1.96\sigma_{\bar{y}}$, where $\sigma_{\bar{y}} = \frac{\sigma}{\sqrt{n}}$ and $\bar{y}$ is the mean reflectance at a given wavelength *λ* of incident light, *σ* is standard deviation from the mean at *λ*, and *n* is the sample size. By combining the values from the 95% CI calculations the upper and lower limit spectrum were created for each substrate and coating type.

Principal component analysis (PCA) was used to assess the reflectance data. PCA is a tool which can reduce the number of variables needed to explain data. The new variables, called components, replace each of the original observations; however, most of the variation can be explained by a few components and thus the number of variables can be greatly reduced. A principal component is “a linear combination of optimally weighted observed variables.” The weights are determined by computing eigenvalues. The set of weights are computed such that they account for the maximum amount of variation in the data. [71]

In this work PCA was used to reduce the number of wavelength variables to three principle components. With PCA, the reflectance data was assessed.

4.2. Reflectance Measurements with Integrating Sphere

The percent reflectance of the coated and uncoated samples was measured with a Shimadzu UV-3101PC UV-Vis-NIR Scanning Spectrophotometer using an integrating sphere, see Figure 35 .

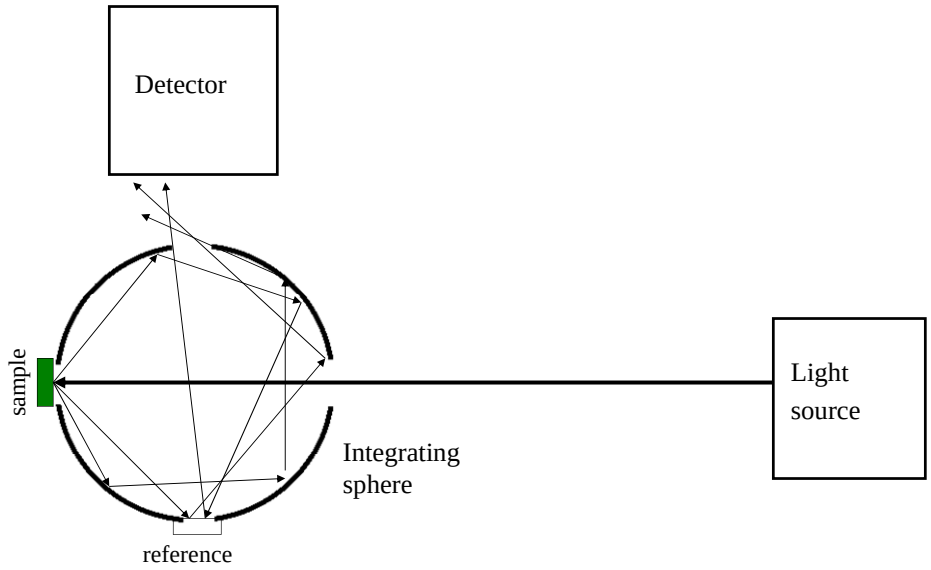

Figure 35. Integrating Sphere schematic. Incident light from light source is diffusely reflected light from sample and reflected within integrating sphere until it passes through opening toward detector.

Spectra data was acquired and processed using Shimadzu UVProbe version 2.20 software. Incident light was normal to sample. Barium sulfate was used as a reference as specified in military standard MIL-DTL-44436A [13]. A baseline scan was performed with the reference placed both in the reference and sample position of the integrating sphere; this ensured the samples were compared to 100% reflectance standard. Scans were run from 1500 to 400 nm, with a detector change at 896 nm. The percent reflectance as compared

to the reference was collected at each wavelength. The detector shift at 896 nm created noise in the measurements from 860 to 900 nm.

4.3. NIR Reflectance of Nylon-Cotton Camouflage Fabric Substrates

This section addresses the reflectance of the nylon-cotton fabric as three different substrates according to the ACU camouflage fabric colors: desert sand, urban gray and foliage green. The analysis is done using average reflectance spectra of the samples by substrate type and particle size. The section covers variation within group, i.e. same substrate and same particle size coating, and variation within substrates, i.e. same substrate but different particle size. The analysis also covers comparison of average reflectance, change in average reflectance, standard deviation, and 95% confidence interval upper and lower limits. The change in % reflectance was calculated by subtracting the average % reflectance of the uncoated fabric from the average % reflectance from the PS particle coated fabric.

4.3.1. Desert Sand Nylon-Cotton Camouflage Fabric

The averaged spectra for the desert sand fabrics from 400 to 1500 nm are shown in Figure 36. The fabrics coated with PS particles still had the same characteristic peaks as the uncoated desert sand camouflage fabric. In order to assess the trends, the reflectance in the shorter wavelength region, 400 to 860 nm, and the longer wavelength region, 900 to 1500 nm were analyzed separately due to the detector change at 896 nm.

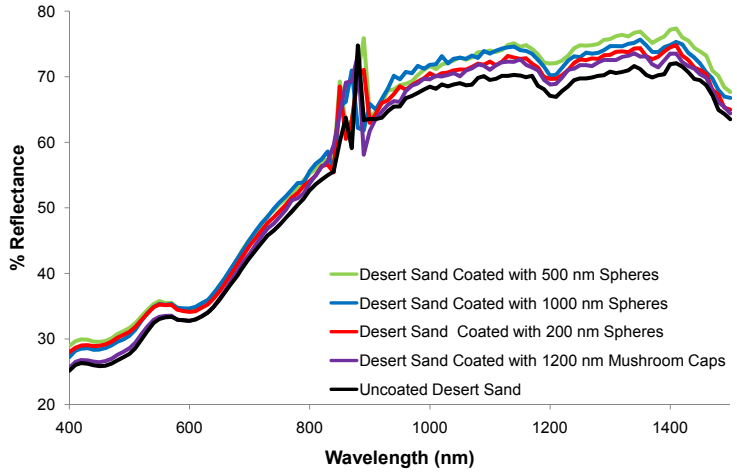

Figure 36. Average % Reflectance Values for Desert Sand Nylon/Cotton Camouflage Fabric from 400 to 1500 nm

From 400 to 860 nm, shown in Figure 37, all of the coated fabrics have higher reflectance than the uncoated desert sand fabric. From 400 to 550 nm, the % reflectance trends for the coated fabrics do not linearly correspond to the increasing size of the coating particles.

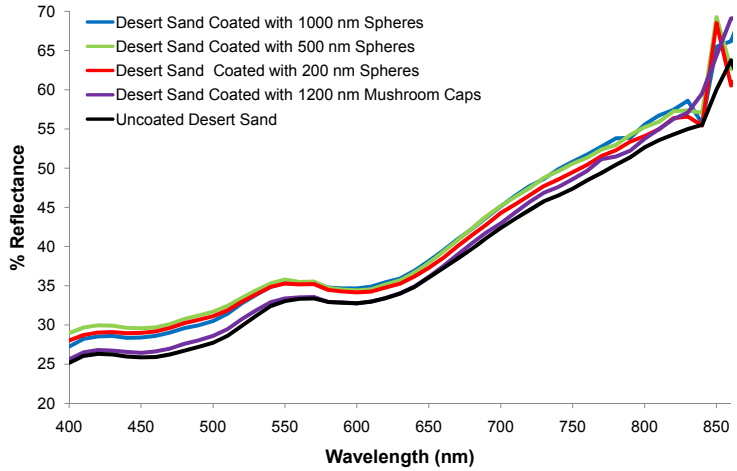

Figure 37. Average % Reflectance Values for Desert Sand Nylon/Cotton Camouflage Fabric from 400 to 860 nm

The desert sand fabric coated with the 1200 nm PS mushroom caps has little to no change in % reflectance in the 400 to 800 nm wavelength range,

while small change in the spherical particle coated fabric, as seen in Figure 38. From about 550 to 840 nm the increase in reflectivity trend linearly follows the increasing size of the sphere diameter with the 200 nm PS sphere coated desert sand fabric having the lowest reflectance.

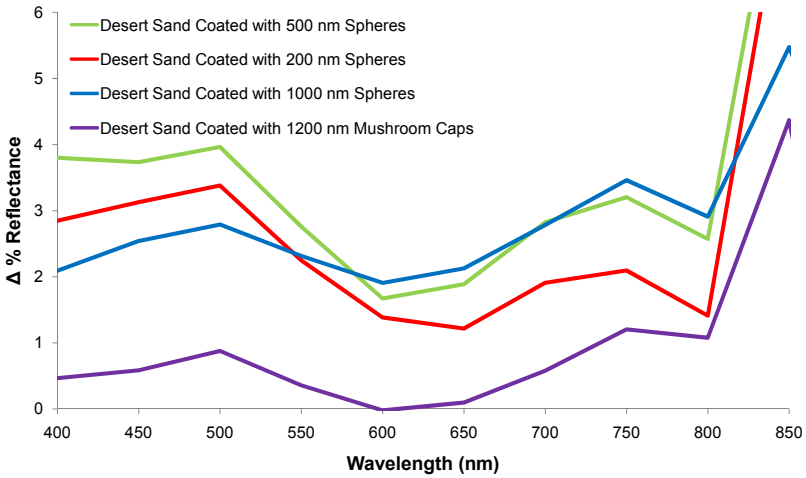

Figure 38. Average Change in % Reflectance of Coated Desert Sand Fabrics from 400 to 850 nm

The trend of increasing reflectance with increasing particle diameter continues from 900 to about 1050 nm, as seen in Figure 39. After 1050 nm the reflectance of the 1000 nm PS sphere particle coated fabric drops below the 500 nm PS sphere coated fabric.

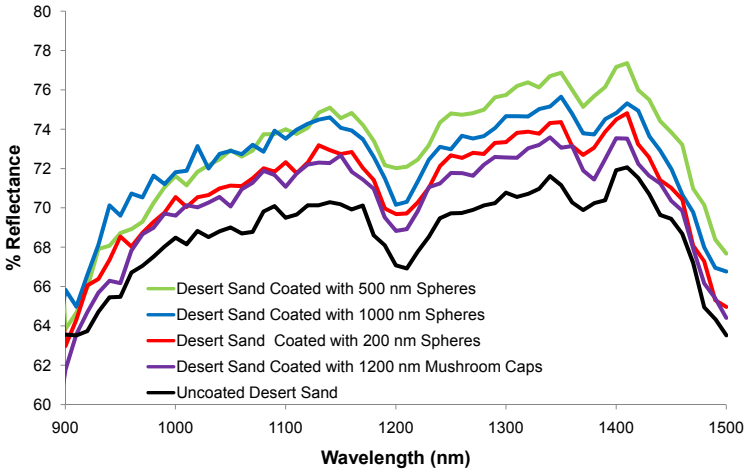

Figure 39. Average % Reflectance Values for Desert Sand Nylon/Cotton Camouflage Fabric from 900 to 1500 nm

In the longer wavelengths there is greater change in reflectance over a longer range than in the shorter wavelengths. The mushroom cap coating had a greater modifying effect at the higher wavelengths than the lower wavelengths, but remained lower than other coatings over the tested range, as seen in Figure 40.

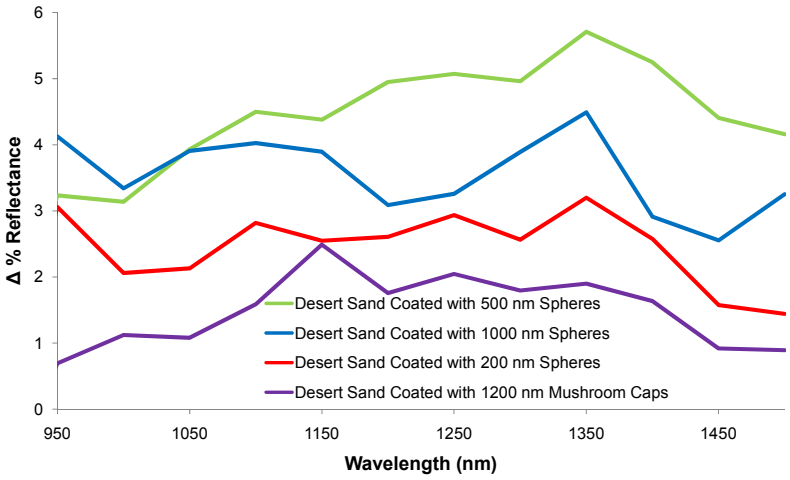

Figure 40. Average Change in % Reflectance of Coated Desert Sand Fabrics from 950 to 1500 nm

The variability of the coatings over the wavelength range tested differs by coating particle size as seen in Figure 41 and Figure 42. The untreated desert sand fabric has the least amount of variation in % reflectance throughout the wavelength range tested. The 500 nm PS sphere coated fabric has the greatest variation throughout the range tested.

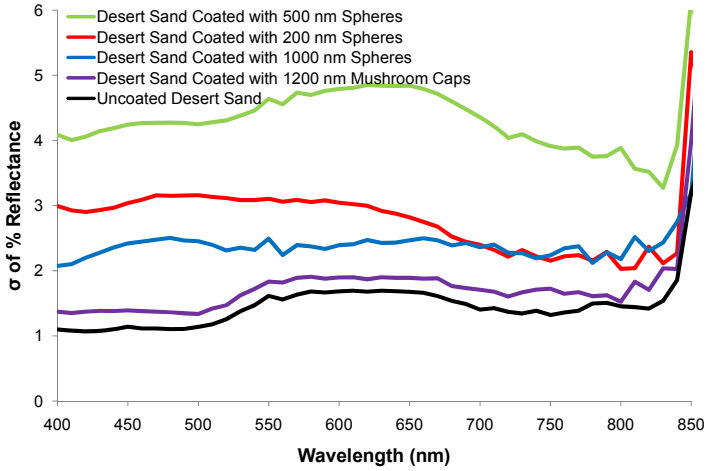

Figure 41. Standard Deviation of % Reflectance for Desert Sand from 400 to 860 nm

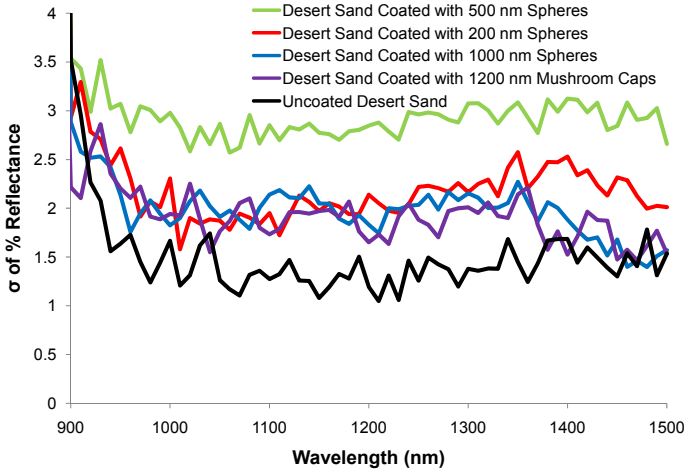

Figure 42. Standard Deviation of % Reflectance for Desert Sand from 900 to 1500 nm

Since there is variation in the reflectance, it is of interest to examine the 95% confidence interval for mean reflectance spectra to compare the coated fabrics to the uncoated fabrics, shown in Figure 43 and Figure 44. The overlap of region between the upper and lower limit 95% CI spectra for the desert sand fabrics indicate that some of the coated fabrics have lower reflectance than some of the uncoated fabrics. The mushroom cap particles have reflectance below the upper 95% CI limit of the uncoated desert sand from 400 to 725 nm and from 900 to about 1000 nm. Also, the 200 and 500 nm sphere coated desert sand fabric 95% CI reflectance area falls below the upper limit of the uncoated desert sand reflectance.

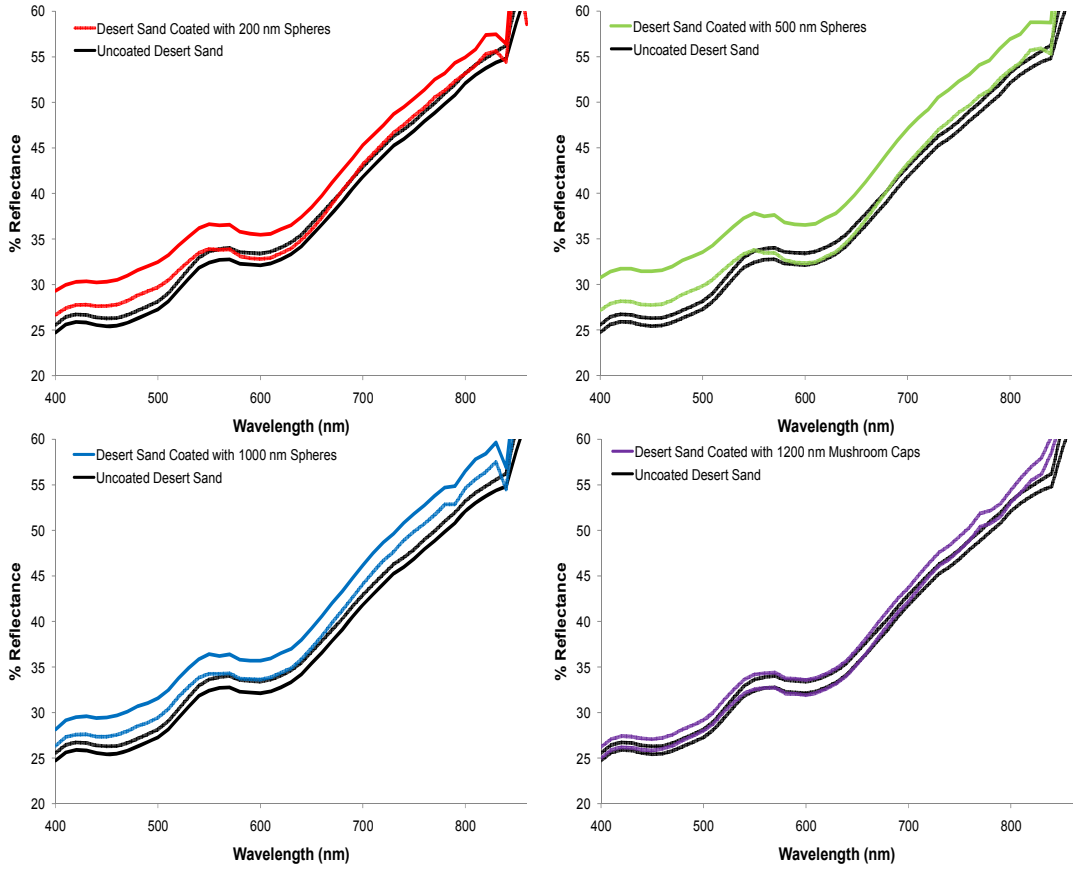

Figure 43. 95% Confidence Interval of Average % Reflectance Spectra of Desert Sand Camouflage Fabric from 400 to 860 nm

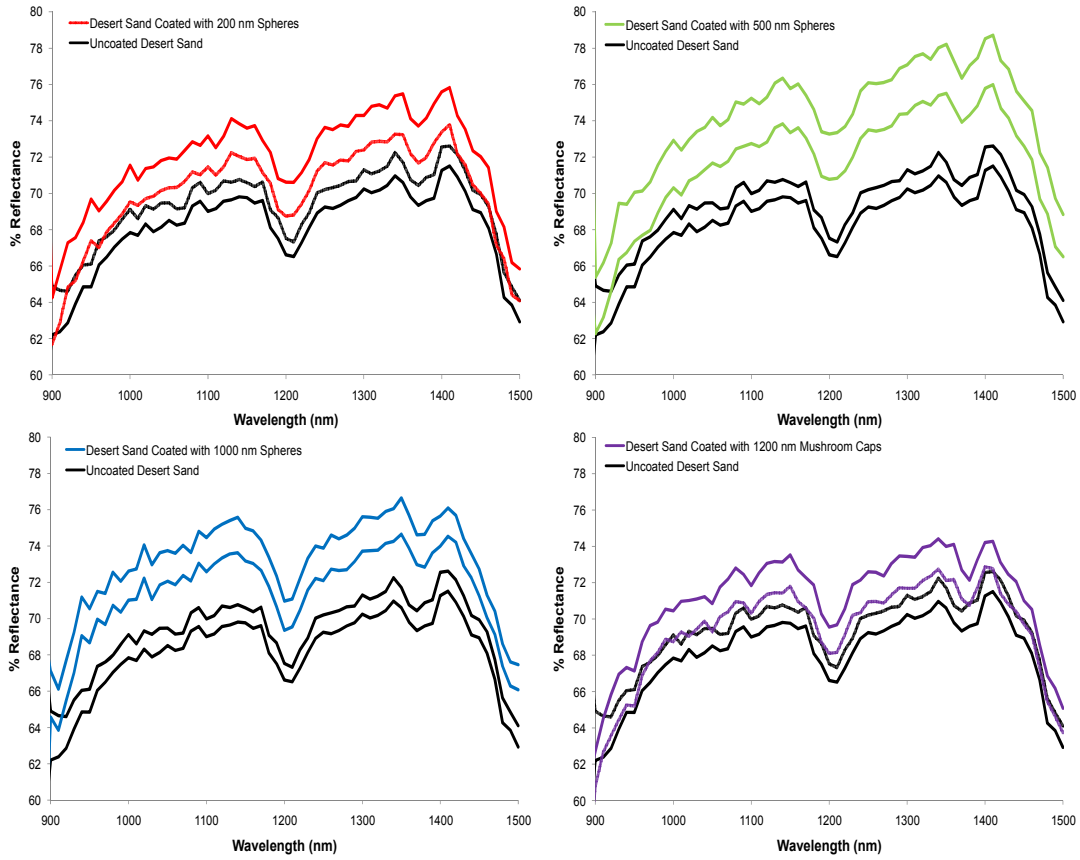

Figure 44. 95% Confidence Interval of Average % Reflectance Spectra of Desert Sand Camouflage Fabric from 900 to 1500 nm

4.3.2. Urban Gray Nylon-Cotton Camouflage Fabric

The average reflectance spectra of the urban gray nylon-cotton camouflage fabric samples are shown in Figure 45. All of the urban gray coated fabric samples have similar characteristic peaks as the uncoated urban gray fabric. The general shape of the spectra is similar to that of the desert sand but the reflectance in the 400 to 860 nm range is lower than that of the desert sand due to the effects of the dye in the visible range.

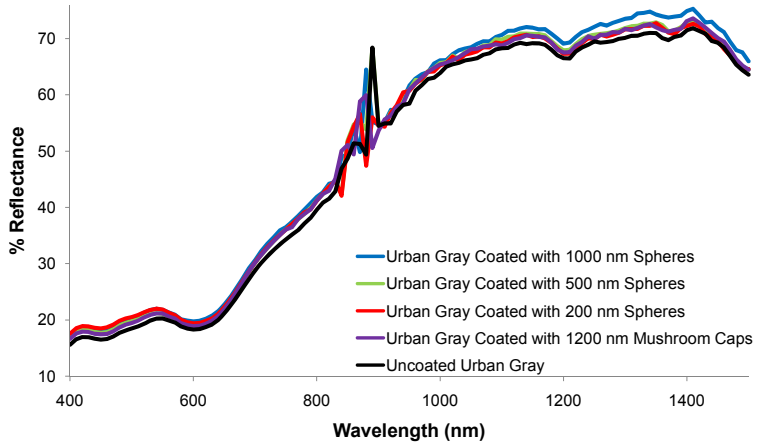

Figure 45. Average % Reflectance Values for Urban Gray Nylon/Cotton Camouflage Fabric from 400 to 1500 nm

In the lower wavelength range, the order of the average reflectance spectra do not increase with particle coating size, seen in Figure 46. There are two areas where the spectra intersect. The 200 and 500 nm reflectance spectra change position in the trend around 550 nm, this could be attributed to the closeness in the size dimension to the incident wavelength of light. From 650 to 800 nm the average reflectance of the 500 nm PS sphere coated fabric and mushroom cap coated fabric are nearly identical.

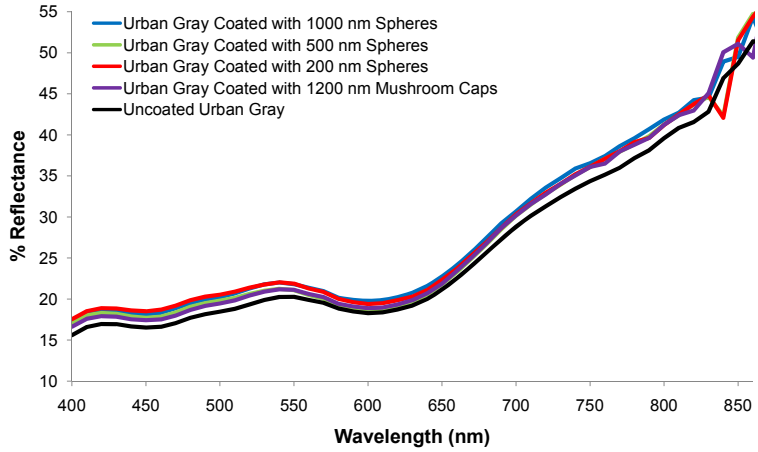

Figure 46. Average % Reflectance Values for Urban Gray Nylon/Cotton Camouflage Fabric from 400 to 860 nm

The difference in the change in % reflectance between the particle coating types on the urban gray, shown in Figure 47, is not as large as on the desert sand in the shorter wavelength ranges. In the 550 to 750 nm range, the 1000 nm PS sphere coated fabric has the highest reflectance, shown in Figure 47.

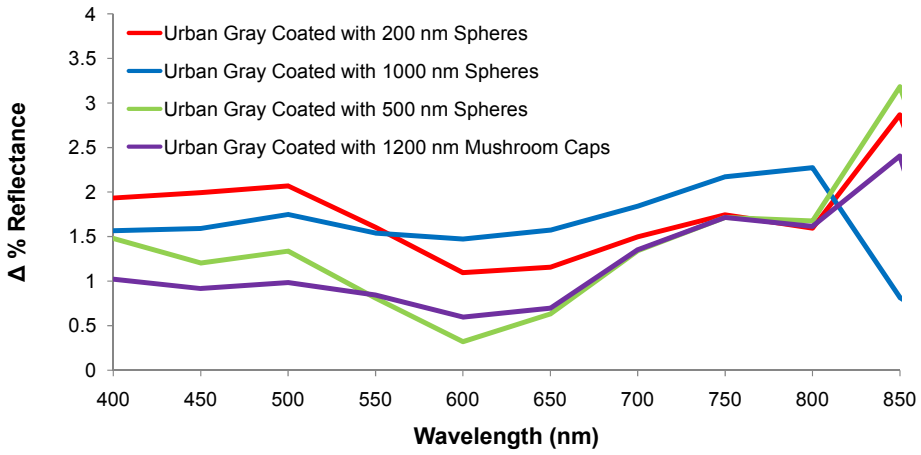

Figure 47. Average Change in % Reflectance of Coated Urban Gray Fabrics from 400 to 850 nm

In the longer wavelength range of 900 to 1500 nm, the mushroom caps and two smaller spherical particle coatings have similar change in % reflectance and average % reflectance spectra, shown in Figure 48 and Figure 49, respectively. The 1000 nm PS sphere coated fabric has the highest reflectance. In this range there is not a clear trend among the other three sample types; the average change in % reflectance for these sample types range is less than the 1000 nm coated fabric.

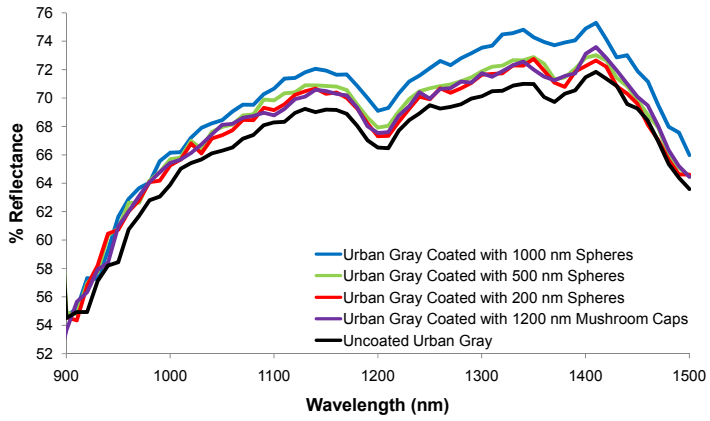

Figure 48. Average % Reflectance Values for Urban Gray Nylon/Cotton Camouflage Fabric from 900 to 1500 nm

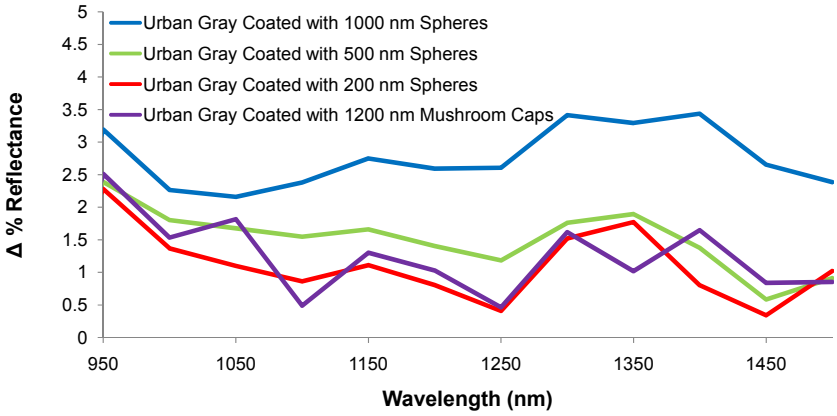

Figure 49. Average Change in % Reflectance of Coated Urban Gray Fabrics from 950 to 1500 nm

The amount of variation in the % reflectance between urban gray fabric samples varies by particle coating size and by wavelength of incident light as seen in Figure 50 and Figure 51. In the visible range the uncoated urban gray samples have the least variation in reflectance; however, in the 900 to 1500 nm wavelength range the 500 and 1000 nm PS sphere coated fabrics have less variability in reflectance than the uncoated fabric. In the 400 to 860 nm wavelength range the 500 and 1000 nm sphere coated fabrics have greater standard deviation than in the higher wavelengths of incident light. The larger

variation may be due to more interaction effects at higher incident wavelengths because the light and particles are similar in size. In contrast to the larger spherical particle coatings, the 200 nm sphere coated urban gray fabric has lower variation across 400 to 860 mm wavelength range and higher variation in the longer wavelengths of incident light tested, with the variation beginning to drop off around 1400 nm. The mushroom cap coated fabric has a relatively constant variation throughout the 400 to 860 nm range and variation similar to the uncoated fabric, in the 900 to 1500 nm range.

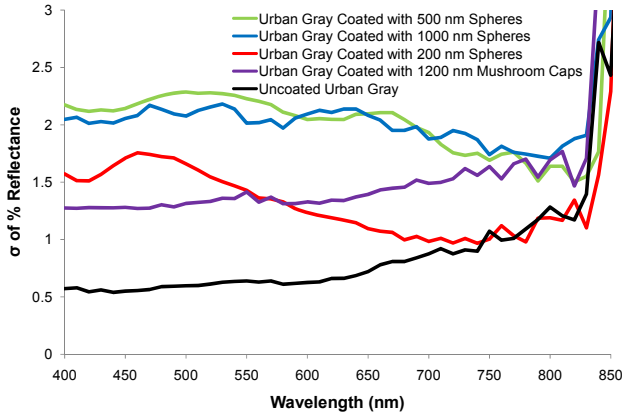

Figure 50. Standard Deviation of % Reflectance for Urban Gray from 400 to 860 nm

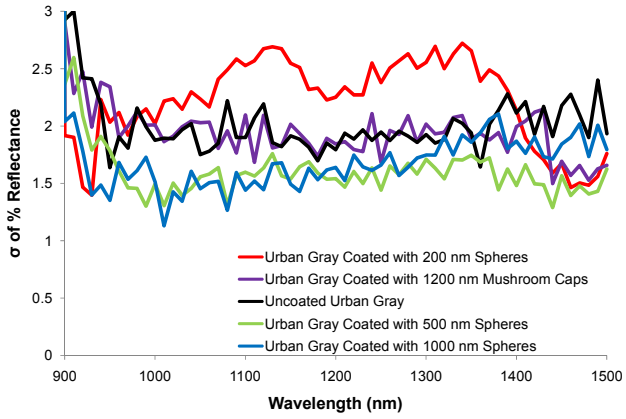

Figure 51. Standard Deviation of % Reflectance for Urban Gray from 900 to 1500 nm

The 95% CI upper and lower limit reflectance spectra for the urban gray fabrics can be used to illustrate that the coated fabric can statistically have a lower reflectance than the uncoated one at particular incident light wavelengths. As shown in Figure 52, the 500 nm sphere coated urban gray fabric has reflectance below that that of the upper 95% CI limit of the uncoated urban gray from 525 to 700 nm and reflectance below the lower limit of uncoated urban gray from 550 to 650 nm. In these regions, the 500 nm coated fabric statistically has lower reflectance than uncoated fabric. The mushroom cap coated fabric has reflectance range that falls below that of the uncoated fabric between 550 and 650 nm.

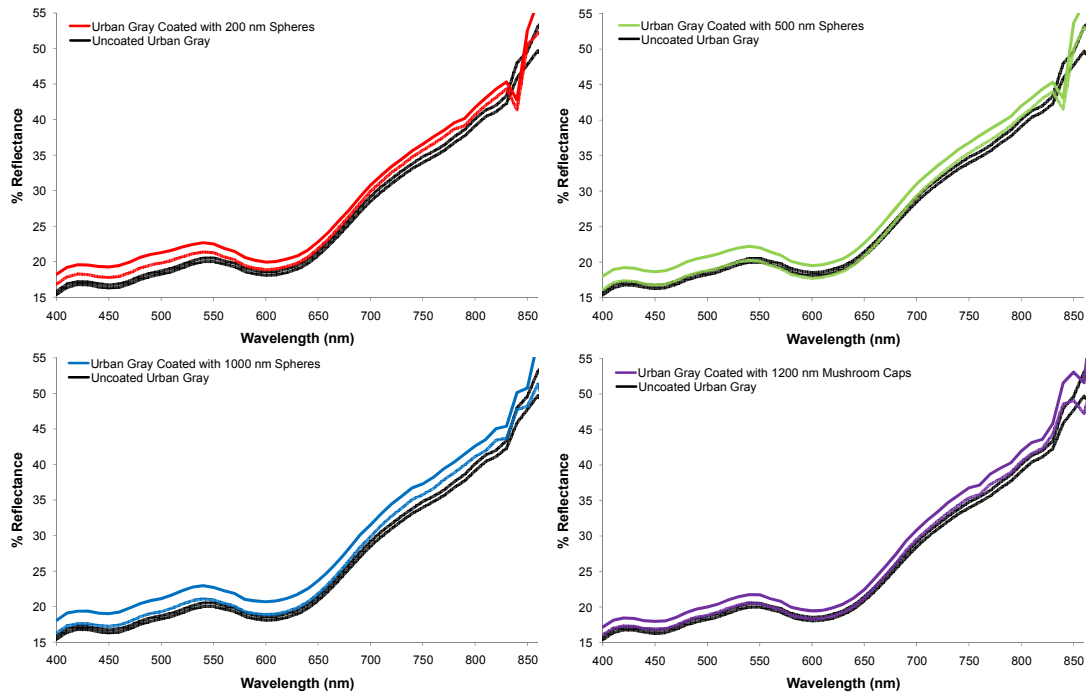

Figure 52. 95% Confidence Interval of Average % Reflectance Spectra of Urban Gray Camouflage Fabric from 400 to 860 nm

In the longer wavelengths of incident light, the 200 nm spheres and the mushroom cap reflectance range overlaps that of the uncoated fabric from 900

to 1500 nm, shown in (Figure 53); while the 500 and 1000 nm spheres 95% CI spectra area overlaps the uncoated area only between 900 and 1000 nm wavelengths.

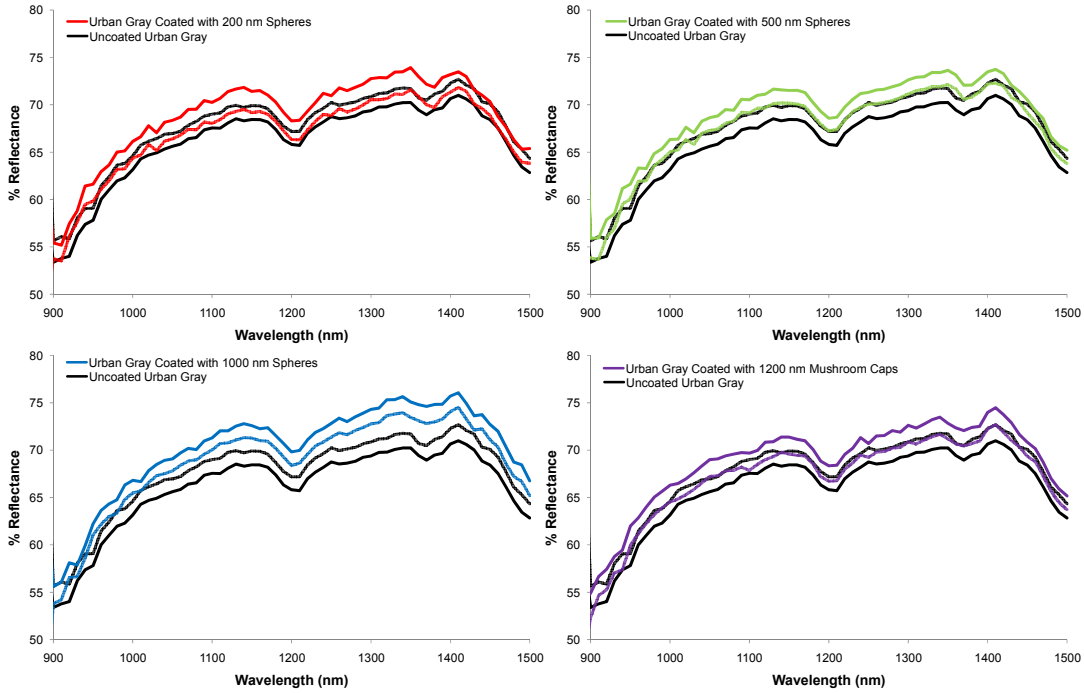

Figure 53. 95% Confidence Interval of Average % Reflectance Spectra of Urban Gray Camouflage Fabric from 900 to 1500 nm

4.3.3. Foliage Green Nylon-Cotton Camouflage Fabric

By selection of dyes, the foliage green has the lowest reflectance of the three colors found in the Army universal camouflage design; the average reflectance spectra for the particle coated and uncoated fabric over the 400 to 1500 nm wavelength range are shown in Figure 54. The average spectra for the coated foliage green have the same characteristic peaks and shape as the uncoated fabric sample.

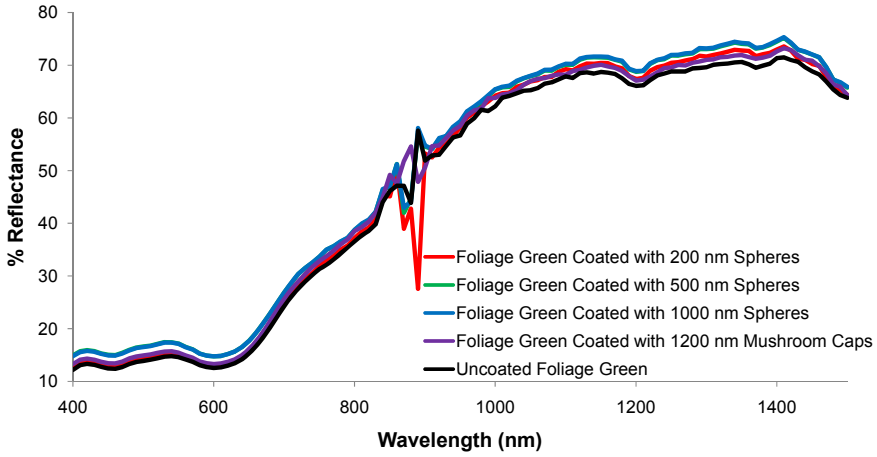

Figure 54. Average % Reflectance Values for Foliage Green Nylon/Cotton Camouflage Fabric from 400 to 1500 nm

For the foliage green samples, all of the coated samples have higher reflectance than the uncoated fabric with the exception of the 200 nm PS spherical particle coated sample in the 825 to 850 nm range. This reduction in reflectance is not definitively due to the coating since it is close to the wavelength range where the detector change occurs. Throughout most of the 400 to 860 nm wavelength range, the 200 nm PS spherical particle coated foliage green fabric has the lowest average reflectance of the coated fabric samples, see Figure 55. The 200 nm PS sphere coated fabric has a minimal increase % reflectance over the range 400 to 800 nm and from 800 to 850 nm the change in % reflectance drops and becomes a reduction in reflection, see Figure 56. The 500 and 1000 nm spherical PS coated foliage green fabrics have very similar average reflectance spectra over the range tested and are difficult to distinguish from each other in Figure 54; however, in Figure 55 the greatest difference in the two averaged spectra can be seen between 400 and 600 nm. The 500 and 1000 nm coatings have a more substantial change in % reflectance than other two particle coatings.

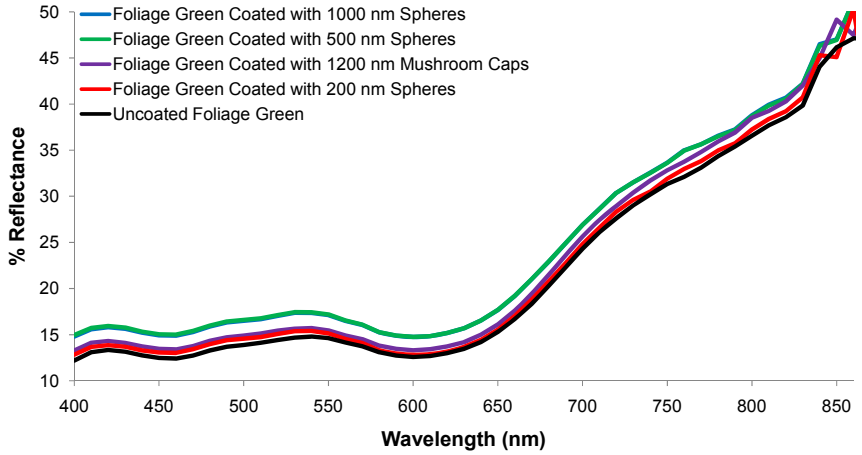

Figure 55. Average % Reflectance Values for Foliage Green Nylon/Cotton Camouflage Fabric from 400 to 860 nm

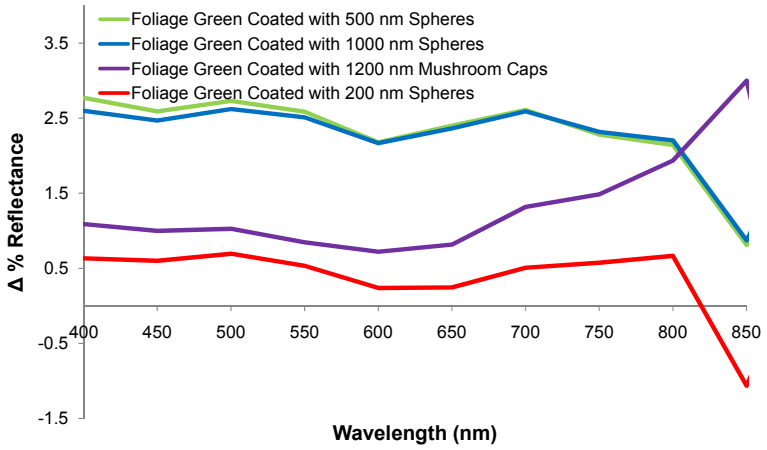

Figure 56. Average Change in % Reflectance of Coated Foliage Green Fabrics from 400 to 850 nm

In the longer wavelength range, the similar reflectance behavior of the 500 and 1000 nm PS sphere coated fabric continues; while the order for increasing reflectance for the mushroom cap and 200 nm sphere coated fabrics changes, shown in Figure 57. The difference in the two average spectra for the 500 and 1000 nm coated fabrics is sustained over the entire longer wavelength range, as shown in Figure 58, unlike for the shorter wavelength range, shown in

Figure 55. For the longer wavelengths, there is a greater modification of the % reflectance for the spherical particle coated fabrics.

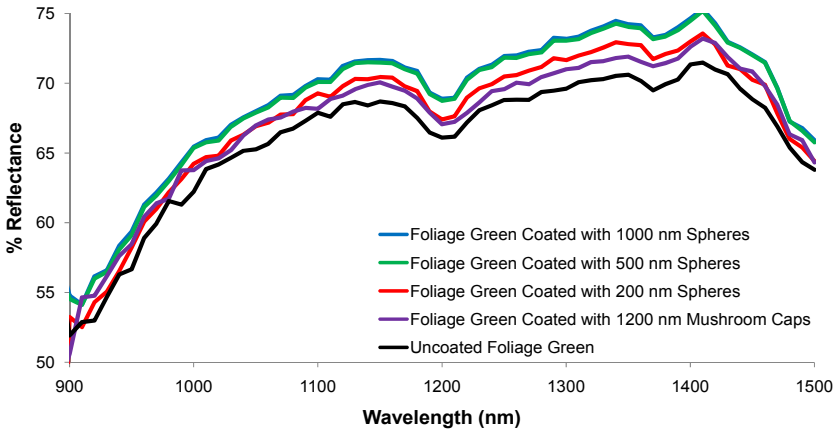

Figure 57. Average % Reflectance Values for Foliage Green Nylon/Cotton Camouflage Fabric from 900 to 1500 nm

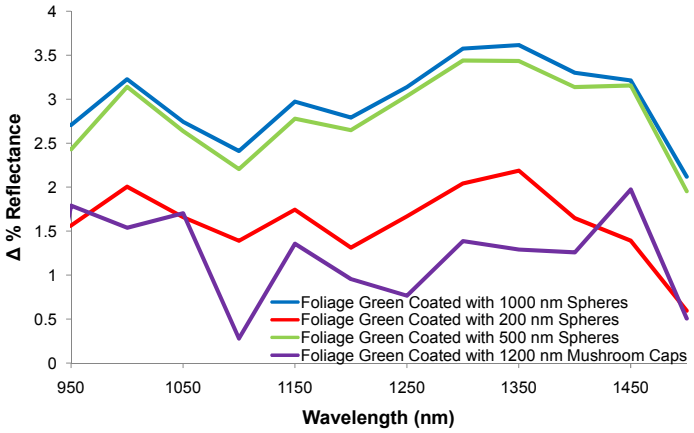

Figure 58. Average Change in % Reflectance of Coated Foliage Green Fabrics from 950 to 1500 nm

The variation between samples for the foliage green coated fabrics differ by coating size and wavelength of incident light as seen in Figure 59 and Figure 60. In the 400 to 860 nm wavelength range, the uncoated foliage green fabric has the least amount of between sample variations. The 200 nm spheres and 1200 nm mushroom cap coatings have larger amounts of variation and are

relatively constant across the 400 to 860 nm range at about 0.9 and 1.25 units, respectively. The 500 and 1000 nm sphere coated fabrics exhibit the greatest amount of variation in the shorter wavelength range. In the 900 to 1500 nm region, all of the fabrics have variation of between 1.5 and 2.5 units. The 200 and 1000 sphere coated and mushroom cap coated fabrics have slightly lower variation in reflectance in the longer wavelength range than the uncoated fabric.

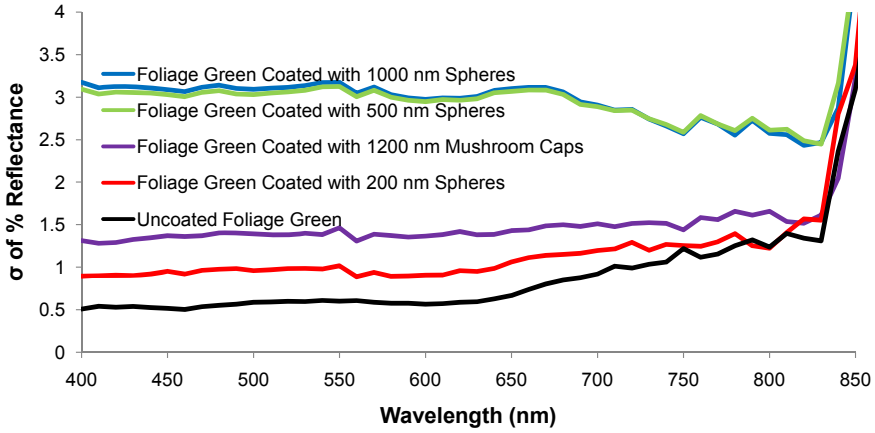

Figure 59. Standard Deviation of % Reflectance for Foliage Green from 400 to 860 nm

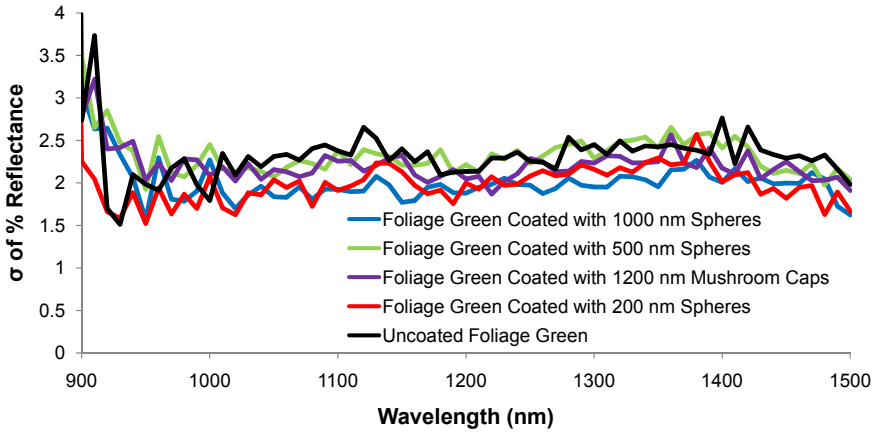

Figure 60. Standard Deviation of % Reflectance for Foliage Green from 900 to 1500 nm

The 95% CI upper and lower limit spectra for the foliage green fabric reveal that some of the coated fabrics have reflectance below that of the uncoated samples. The 200 nm sphere coated fabric has reflectance that lies below the upper limit and overlaps the lower limit spectra line for the 400 to 860 wavelength range, as seen in Figure 61. A portion of the mushroom cap coated fabric 95% CI area falls below the upper limit of the uncoated foliage green 95% CI spectra between 550 and 675 nm. For the longer wavelengths of incident light, both the 200 nm sphere coated and mushroom cap coated fabric 95% CI areas over lap that of the uncoated fabric from 900 to 1500 nm, shown in Figure 62.

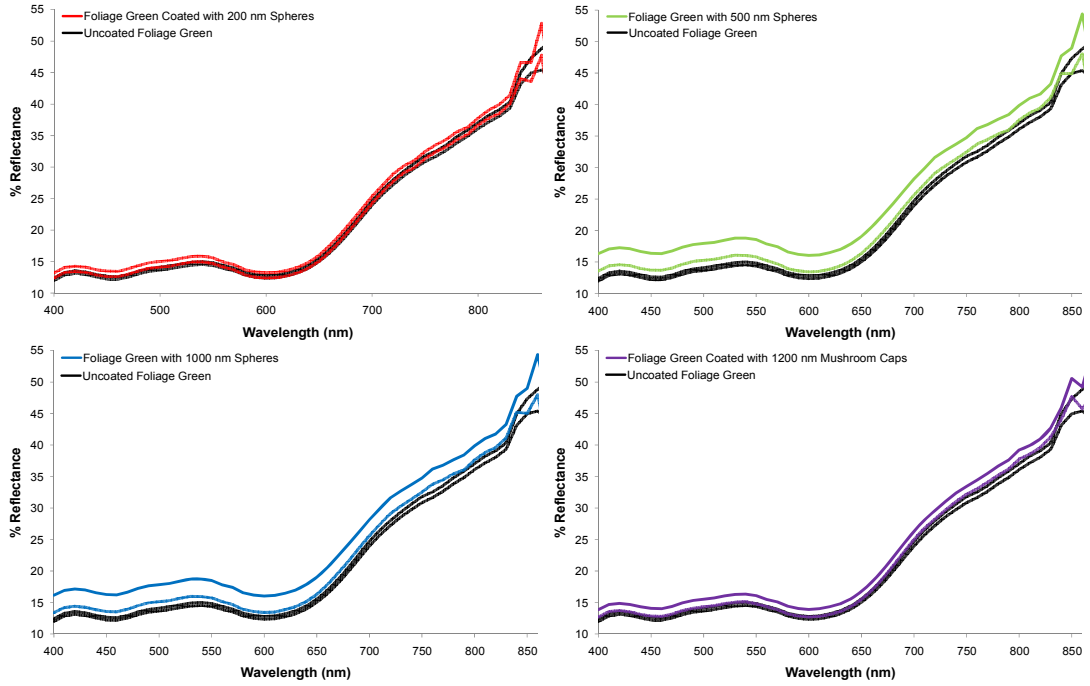

Figure 61. 95% Confidence Interval of Average % Reflectance Spectra of Foliage Green Camouflage Fabric from 400 to 860 nm

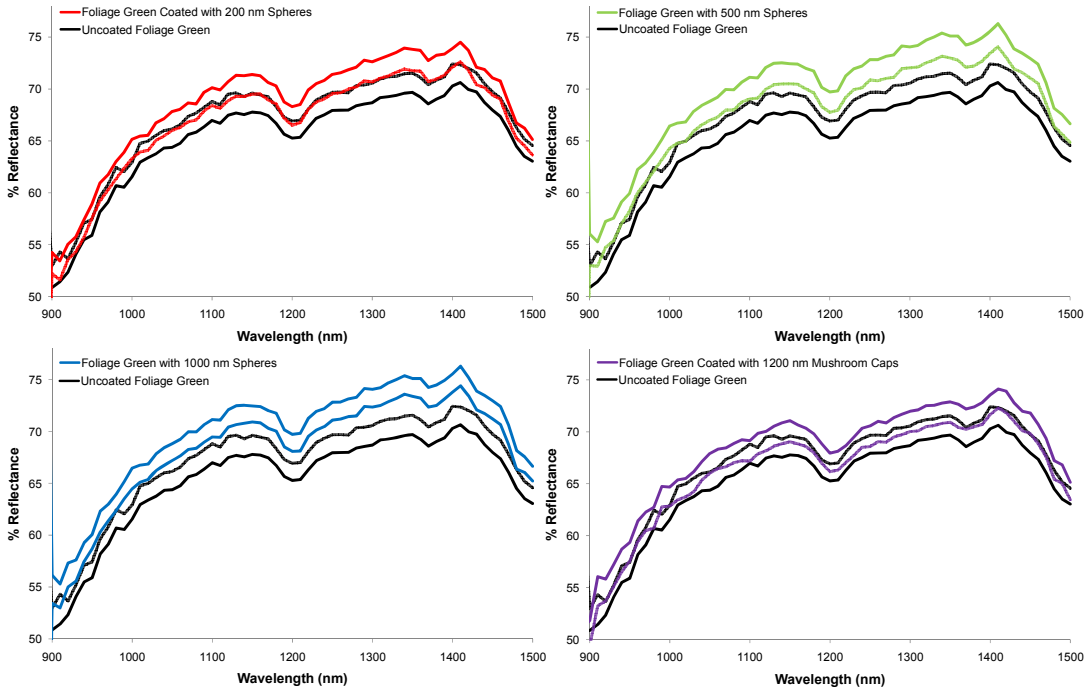

Figure 62. 95% Confidence Interval of Average % Reflectance Spectra of Foliage Green Camouflage Fabric from 900 to 1500 nm

4.4. NIR Spectroscopy Analysis of Cellulosic Substrates

This section addresses the reflectance of the two cellulosic substrates: cationic cotton and cationic cellulosic film. The analysis is done using average reflectance spectra of the samples by substrate type and particle size. As with the nylon-cotton substrates, an analysis of within group variation, i.e. same substrate and same particle size coating, and variation within substrates, i.e. same substrate but different particle size, is done. The analysis covers a comparison of average reflectance, change in average reflectance, standard deviation, and 95% confidence interval upper and lower limits.

4.4.1. Cationic Cotton Fabric

The cationic cotton has higher reflectance than the nylon-cotton across the wavelengths tested due to the fact that it is not dyed and the inherent high reflectance of the cotton, the % reflectance ranges from 60 to about 90, as

shown in Figure 63. The coated cationic cotton samples have similar peaks and shape as the uncoated cationic cotton fabric; however, the uncoated has a much smoother average reflectance spectrum. The appearance of additional peaks and roughness in the reflectance spectra of the coated cotton samples is an indication of that the original cotton has been modified. Small peaks are present in visible range at 600 nm in the coated samples as well as additional peaks in the NIR range.

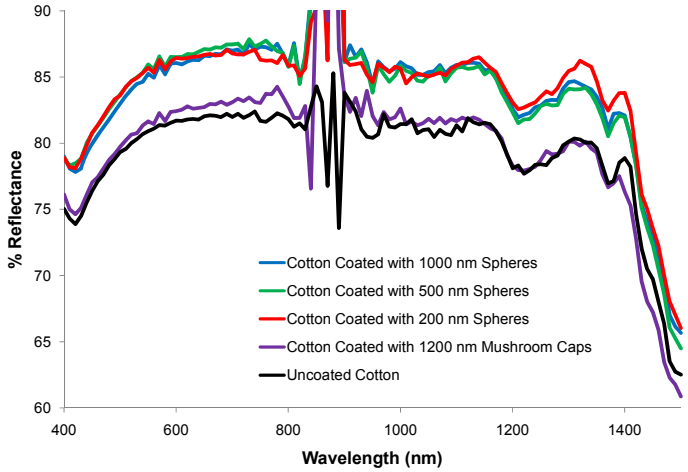

Figure 63. Average % Reflectance Values for Cationic Cotton Fabric from 400 to 1500 nm

The uncoated cationic cotton has lower average reflectance than the particle coated cotton average spectra from 400 to about 840 nm, shown in Figure 64. The mushroom cap coated cotton fabric has the lowest average reflectance of the coated cotton fabrics and has minimal change in % reflectance in the 400 to 800 nm range, shown in Figure 65. From 400 to about 650 nm the order of the remaining spectra in increasing reflectance are 1000 nm, 200 nm, and 500 nm sphere coated. After 650 nm the reflectance of the 200 nm sphere coated fabric drops below the 1000 nm coated fabric.

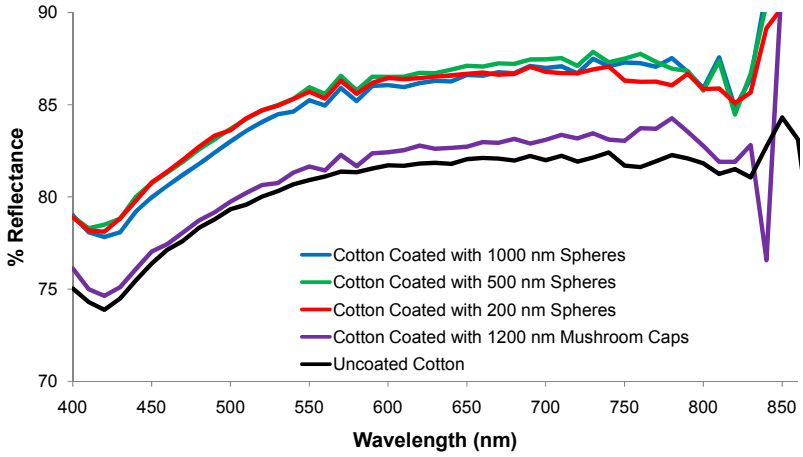

Figure 64. Average % Reflectance Values for Cationic Cotton Fabric from 400 to 860 nm

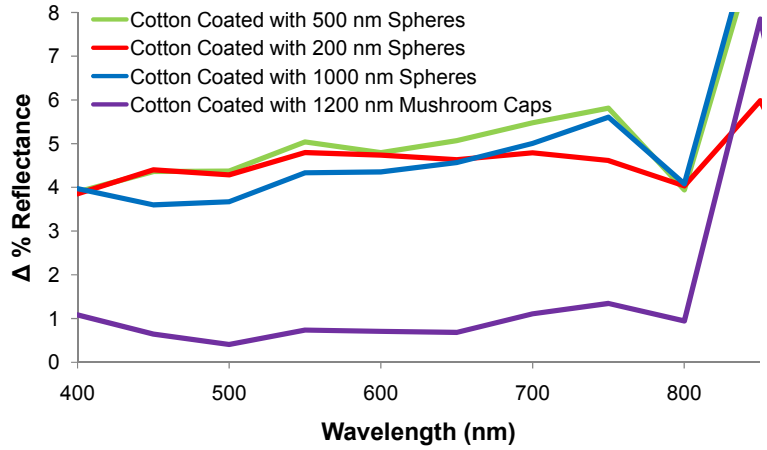

Figure 65. Average Change in % Reflectance of Coated Cationic Cotton Fabrics from 400 to 850 nm

At longer wavelengths of incident light the mushroom cap coated cotton fabrics' average reflectance drops below that of the uncoated cotton, as seen in Figure 66. The mushroom cap coated cotton change in reflectance drops below that of the uncoated cotton from 1375 to 1500 nm, see Figure 67. The sphere coated cotton fabrics have higher reflectance than the mushroom cap coated fabrics and similar average reflectance spectra. The 200 nm sphere

coated fabric has the greatest change in reflectance in the longer wavelength range.

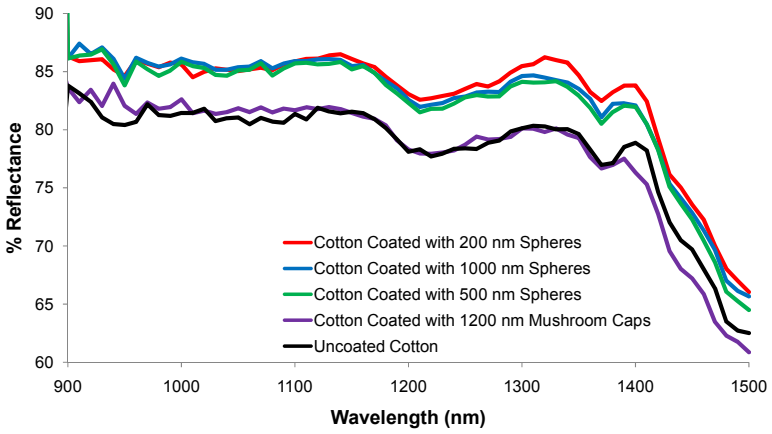

Figure 66. Average % Reflectance Values for Cationic Cotton Fabric from 900 to 1500 nm

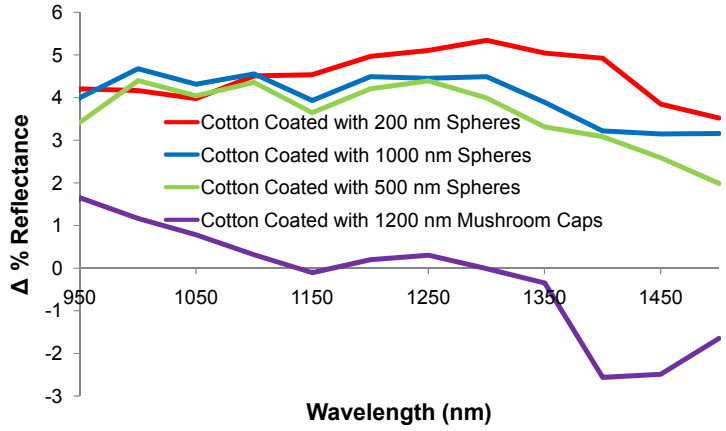

Figure 67. Average Change in % Reflectance of Coated Cationic Cotton Fabrics from 950 to 1500 nm

The variation in the amount of change in % reflection in relation to the uncoated cationic cotton might suggest great *within group* variability; however, this is not the case with most of the coated samples. The uncoated cotton has the least amount of variation throughout the majority of the wavelengths of incident light test, Figure 68 and Figure 69. While the mushroom cap coated

cotton has the lowest average reflectance of the coated cotton fabrics, it has the highest amount of variation throughout the range and the most fluctuation in standard deviation across the spectrum. The 500 and 1000 nm coated cotton had relatively uniform variation throughout the range tested. The 200 nm sphere coated cotton had greater variation at the longer wavelengths of incident light.

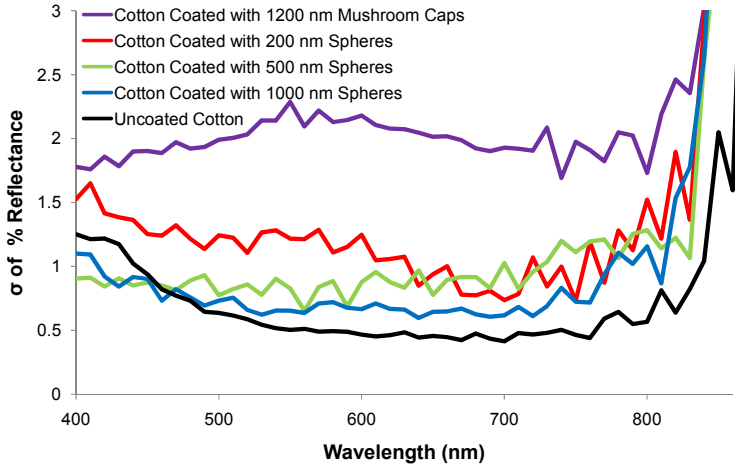

Figure 68. Standard Deviation of % Reflectance for Cationic Cotton Fabric from 400 to 860 nm

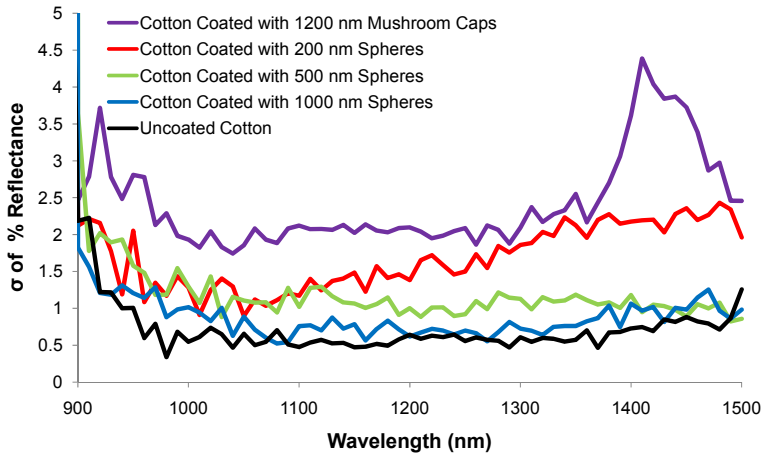

Figure 69. Standard Deviation of % Reflectance for Cationic Cotton Fabric from 900 to 1500 nm

The 95% CI upper and lower limit reveal some information regarding the cationic cotton samples. For the spherical coated samples, the limited overlap of the areas of the 500 and 1000 nm coated fabric in the 450 to 700 nm range indicates significant difference in the particle coating, shown in Figure 70. Also, the 95% CI range for the mushroom cap coated cotton fabric overlaps that of the uncoated cotton meaning that some of the coated fabric has lower reflectance than some of the uncoated. From 450 to 600 nm the mushroom cap coated lower CI limit falls below that of the uncoated.

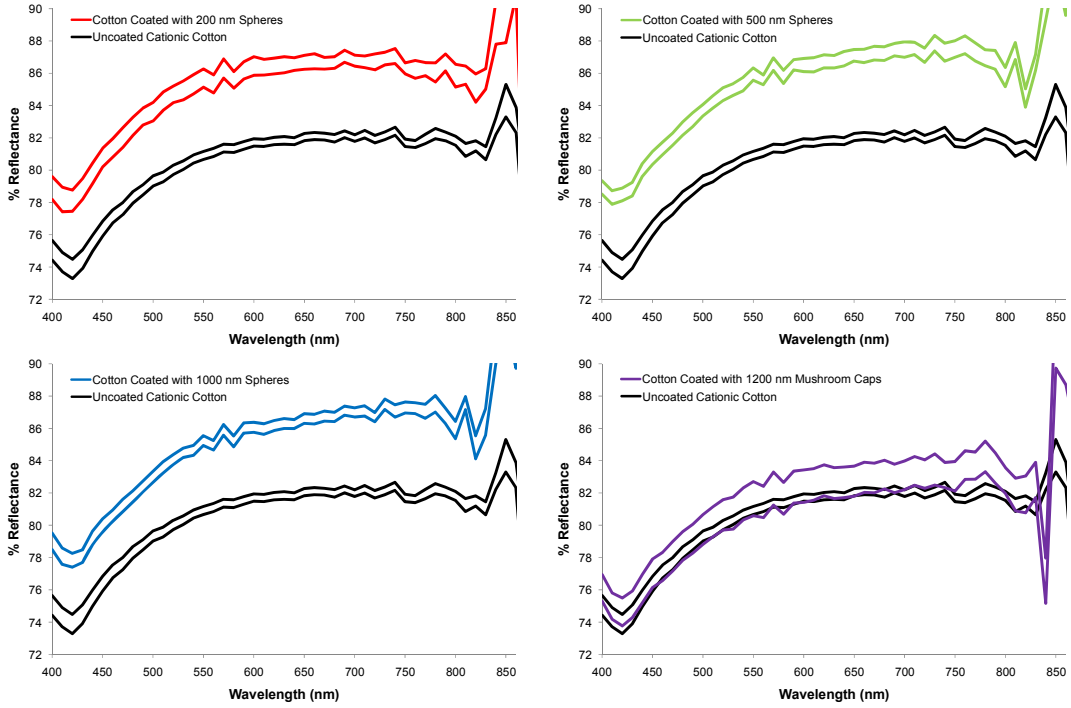

Figure 70. 95% Confidence Interval of Average % Reflectance Spectra of Cationic Cotton Fabric from 400 to 860 nm

For the longer wavelengths of incident light, the mushroom cap coated fabric 95% CI range overlaps the uncoated from 900 to 1400 nm and the CI range falls below the uncoated CI range from 1400 to 1500 nm, as seen in

Figure 71. In these ranges it is statistically possible to have mushroom cap coated fabrics with lower reflectance than uncoated fabrics.

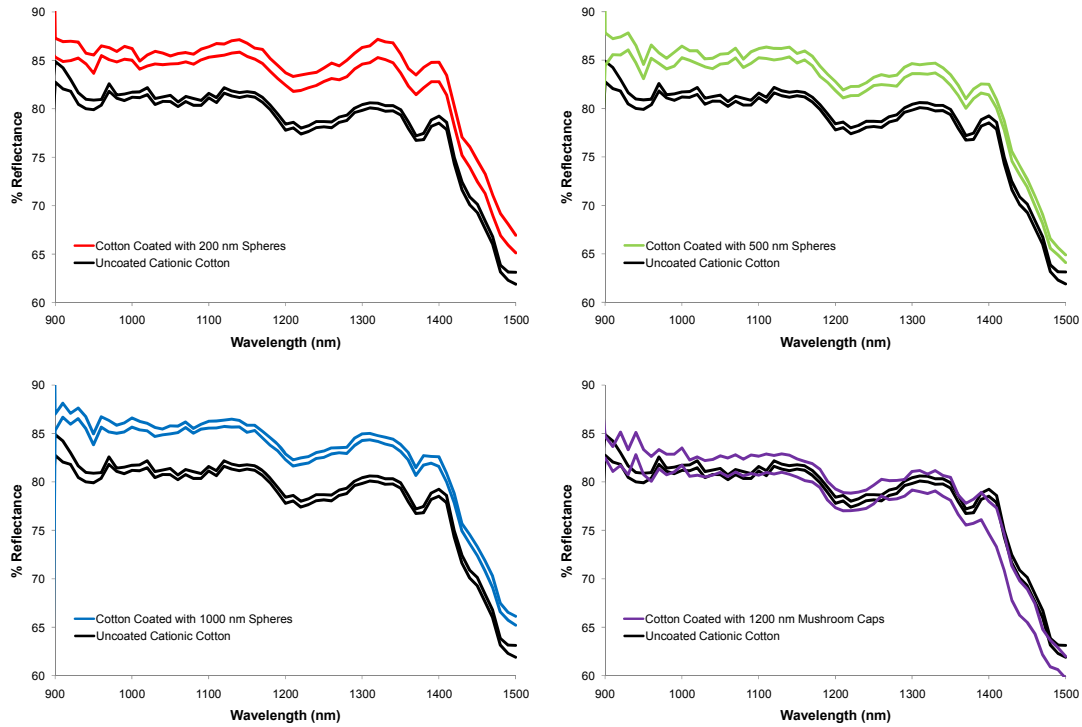

Figure 71. 95% Confidence Interval of Average % Reflectance Spectra of Cationic Cotton Fabric from 900 to 1500 nm

4.4.2. Cationic Cellulosic Film

The uncoated cationic cellulose film has low reflectance due to its transparent nature. The uncoated cationic film has relatively constant % reflectance values throughout the wavelengths of incident light tested, while the coated samples have decreasing % reflectance with increasing wavelength, see Figure 72.

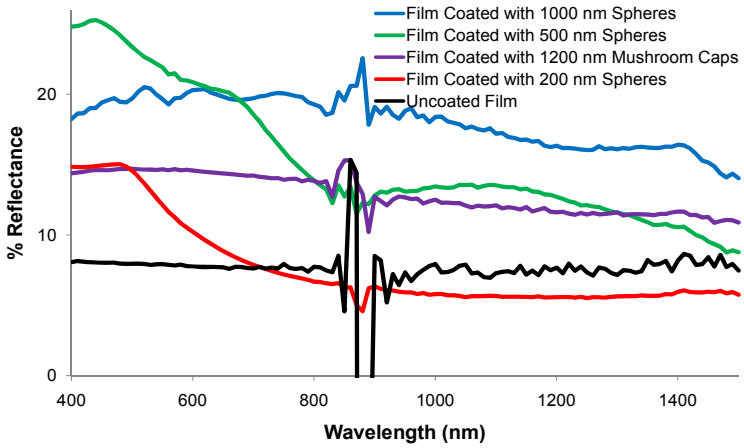

Figure 72. Average % Reflectance Values for Cationic Cellulose Film from 400 to 1500 nm

The mushroom cap and 1000 nm sphere coated films have a uniform reflectance profile from 400 to 825 nm, shown in Figure 73. The 200 nm and 500 nm sphere coated film average reflectance spectra begin with a relatively constant reflectance and then the reflectance decreases in until 860 nm. The 200 nm sphere coated film has lower reflectance than the average uncoated film from about 725 to 825 nm, shown in Figure 74. The difference in behavior of the larger and smaller particles may be due to greater interaction of light with smaller particles with the shorter wavelengths of light, which are more similar in size to those particles.

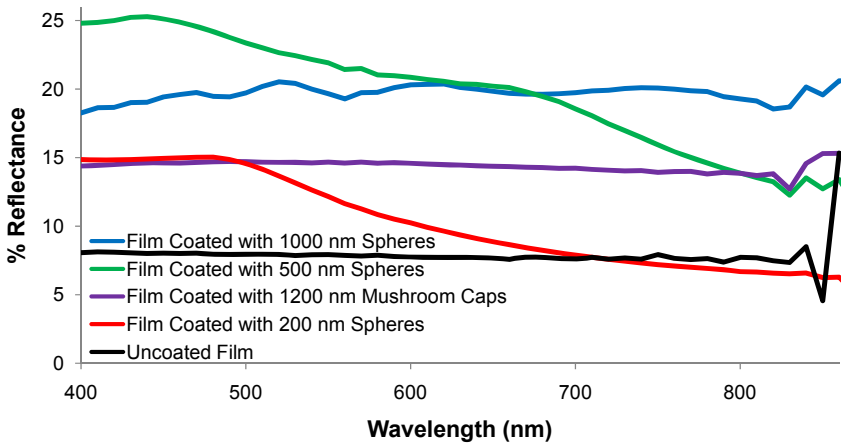

Figure 73. Average % Reflectance Values for Cationic Cellulose Film from 400 to 860 nm

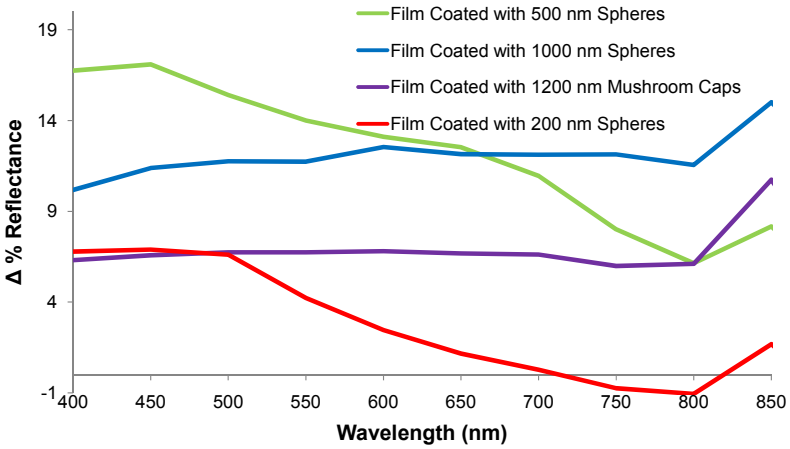

Figure 74. Average Change in % Reflectance of Coated Cationic Cellulose Film from 400 to 850 nm

In the longer wavelengths of incident light, the uncoated, 200 nm sphere coated, and mushroom cap coated films have relatively constant reflectance spectra while the two larger spherical particle coated films have a drop in reflectance as the wavelength of light increases, shown in Figure 75. The 200 nm sphere coated has a % reflectance less than the reflectance of the uncoated film, as seen in Figure 76. The reflectance of the 500 nm sphere coated film begins decreasing around 1100 nm, which is about double the

diameter of the particle. The reflectance of the 1000 nm sphere coated film gradually decreases. The 1000 nm sphere coated film has the greatest change in reflectance for the longer wavelengths of incident light on the cationic film.

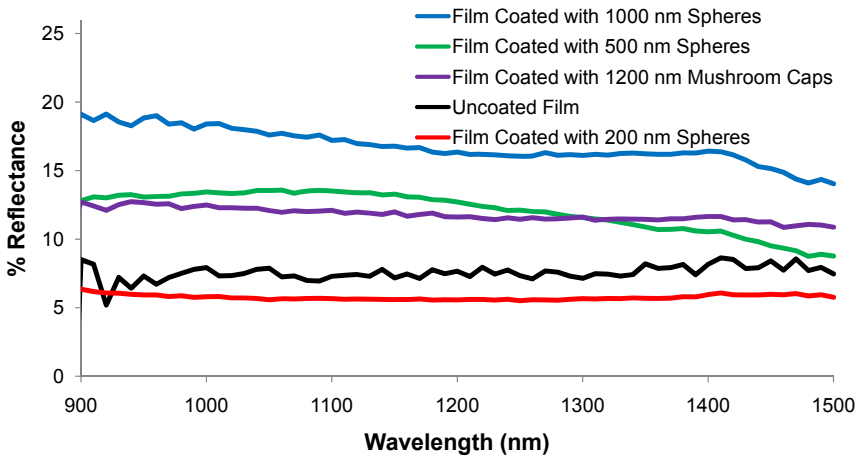

Figure 75. Average % Reflectance Values for Cationic Cellulose Film from 900 to 1500 nm

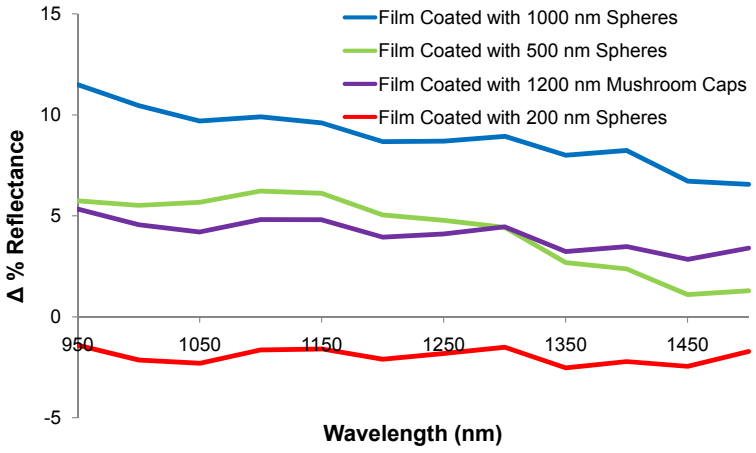

Figure 76. Average Change in % Reflectance of Coated Cationic Cellulose Film from 950 to 1500 nm

The variation in the reflectance of the coated film changes with the wavelength of incident light and with particle size of the coating. The standard

deviation from the average spectra for the 200 and 500 nm sphere coated film share a similar shape as the average spectra, see Figure 77. The 500 nm sphere coated film has the greatest standard deviation in the lower wavelength range.

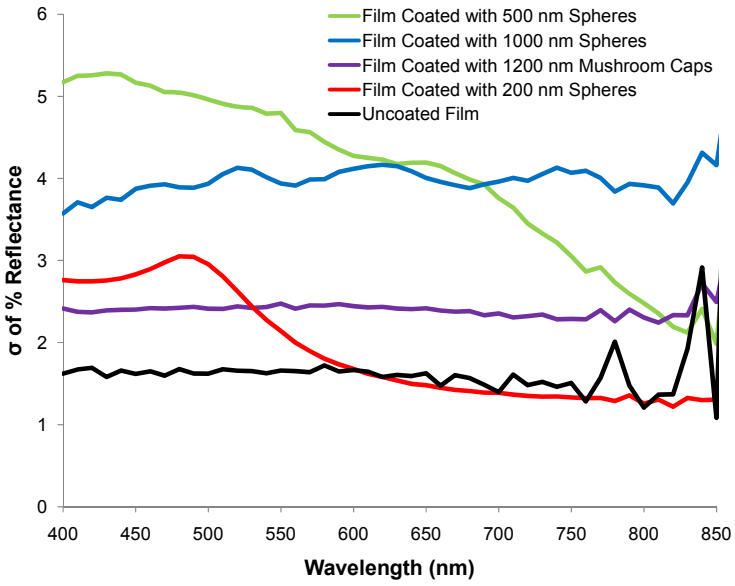

Figure 77. Standard Deviation of % Reflectance for Cationic Cellulose Film from 400 to 860 nm

In the longer wavelengths of incident light, the amount of variation increases with particle coating size for the spherical coatings with the mushroom cap coated film having standard deviation values between that of the 500 and 1000 nm sphere coated films, as seen in Figure 78. The standard deviation spectra between 900 and 1500 nm are relatively constant with values.

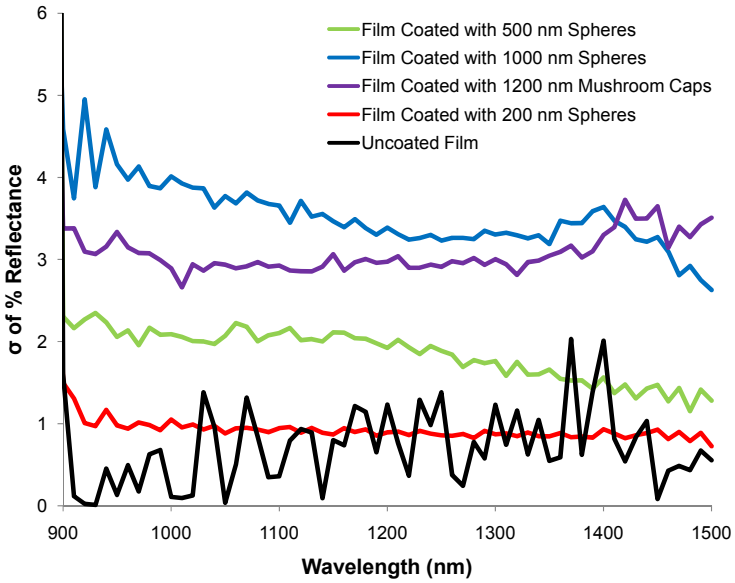

Figure 78. Standard Deviation of % Reflectance for Cationic Cellulose Film from 900 to 1500 nm

Due to the large amounts of change in reflectance from the uncoated samples, the 95% CI upper and lower range area graph reveal only a small amount of information. The 95% CI spectra confirms with the spectra in Figure 73 and Figure 75 that the 200 nm coated film has lower reflectance that the uncoated film from both 600 to 860 nm and from 900 to 1500 nm, shown in Figure 79 and Figure 80, respectively. The 95% CI area spectra reveals also that the 500 nm sphere coated film has potential for lower reflectance than uncoated film at incident light wavelengths greater than 1450 nm.

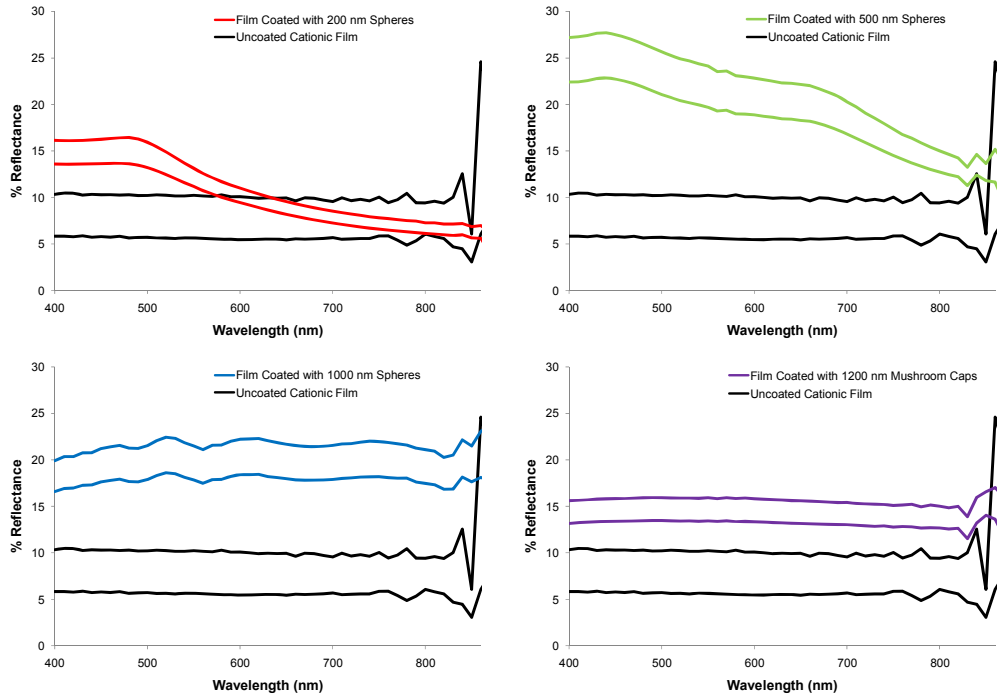

Figure 79. 95% Confidence Interval of Average % Reflectance Spectra of Cationic Cellulose Film from 400 to 860 nm

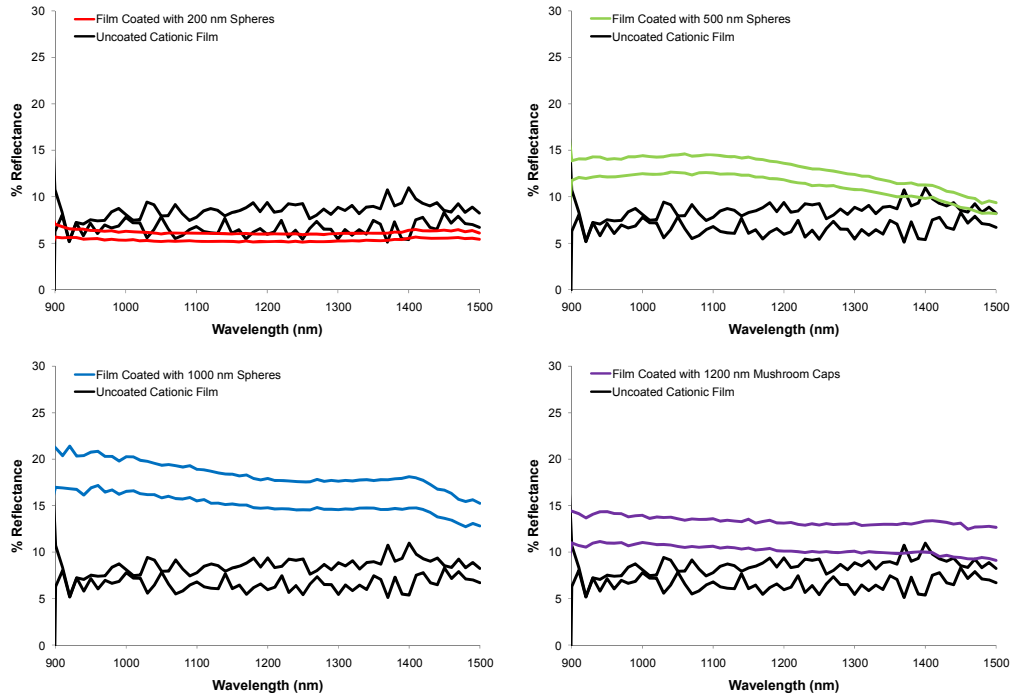

Figure 80. 95% Confidence Interval of Average % Reflectance Spectra of Cationic Cellulose Film from 900 to 1500 nm

4.5. Between Substrate Comparison of NIR Reflectance

This section compares the reflectance of different substrates. A comparison of the variation in reflectance of the three nylon-cotton substrates is presented. Also a comparison of average change in reflectance of all five substrates is presented.

4.5.1. Variation in Reflectance between Nylon-Cotton Substrates

The spectra analysis tried to determine if there were trends in the modified reflectance by particle size. The analysis revealed that the while trends existed over certain wavelengths, they were not consistent over the entire wavelength range tested and did not apply for all the nylon-cotton substrate colors. The absence of a uniform trend is proposed to have several sources including the nature of the coated fabric structure and the dye on the fabric. The fabrics consist of multiple layers of twisted fibers. Many of these subsurface layers contain particles from the deposition process. Due to the complex nature of the composite fabric created by depositing particles onto the fabric, multiple light interaction opportunities were created. Fabrics themselves are not completely uniform due to variation in fibers and yarns introducing variation into the reflectance. Furthermore, the dye on the fabric is expected to influence the reflectance of the fabric. This is explored further in section 4.8.4. Due to the complexity of the coated fabric system, extending the infinitely long cylindrical reflectance model is insufficient even if coupled with a model for reflection of spherical particles because the yarns in the fabric are bundles of fiber.

A comparison of the variance of the spectra samples reveals several effects about the uncoated nylon-cotton fabric. There was greater variation in the uncoated urban gray and foliage green fabrics at wavelengths beyond the US

Army's current reflectance specification than below them. Researchers from the US Army at Natick Soldier Center were not willing to comment on the sources of this additional variation, since it lies above its current specification limits; however they stated there is current ongoing research [37]. Also, at wavelengths above 900 nm, many of the coated fabrics had less variation between samples than the uncoated, thus the particle coatings reduced the *within group* reflectance variation in the NIR range.

4.6. Principal Component Analysis

Principal component analysis (PCA) with SAS JMP 7 software was performed on the reflectance measurements for all five substrates. The initial reflectance variables were from reflectance value at every 10 nm from 400 to 1500 nm. The number of variables was reduced by computing principal components (PC), five of which cumulatively explain 99.690 % of the variation between the samples. The percent of variation explained by new principal components variables is shown in Table 2 . The majority of the variation, 77.8%, is explained by principal component 1 (PC1); 20.1% is explained by PC2; and 0.8% by PC3. The first three principal components explain almost 98.8% of the variation and will be used in the analysis.

Table 2. Principal Components Analysis for All Substrates - Explanation of Variation on Correlations

Principal Component Number	Eigenvalue	Percent Variation Explained	Cumulative Percent
PC1	86.4079	77.845	77.845
PC2	22.3655	20.149	97.994
PC3	0.9161	0.825	98.819
PC4	0.6228	0.561	99.381
PC5	0.3437	0.310	99.690

The principal components can be plotted in 3-D spin plots using JMP software as well as in 2-D using scatter plots. The PCs were used in addition to fit model to evaluate and compare the reflectance of the coated samples. The 3-D spin plots are shown in various orientations in order to view the relation between the variables and the substrates.

4.7. Analysis of Principal Components

The plots of principal components for the reflectance data for all the substrates reveal some initial information into the meaning of the principal components and their relation to various factors, which will be further evaluated using the standard least squares fit model on the PC1 and PC2. The spin plots show that PC1 is closely related to substrate type and color as seen in Figure 81.

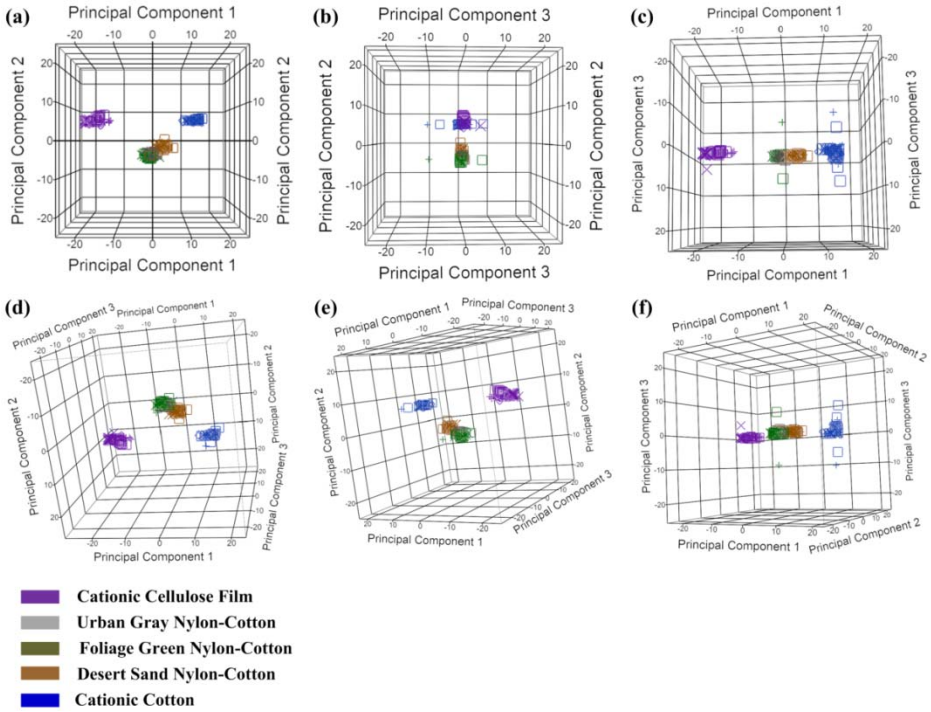

Figure 81. Three-Dimensional Spin Plots of Principal Components for % Reflectance Grouped by Substrate Type. Most variation exists in principal component one less variation is explained by principal components two and three.

The relationship between PC1 and substrate type and color can be further seen in the 2-D graphs of the principal components by the spread of the data points of each substrate in the PC1 axis direction Figure 82. The % reflectance values increase with PC1, as the film had the lowest reflectance values followed by foliage green nylon-cotton, urban gray, desert sand. The cationic cotton has the highest reflectance which corresponds to the horizontal position of the data points in along the PC1 axis in Figure 82. As shown in Table 2, PC1 explains the 77.8% of the variation in the reflectance between the samples and it is reasonable that the majority of the variation is due to substrate type and color. The nylon-cotton fabric PC1 values are nearer to each other as compared to the film and the cationic cotton, lying closer to the cotton than the film; and are closely grouped together in the horizontal direction as seen in plots in Figure 82. The less variation in these samples is because the base fabric is the same nylon-cotton composition and the closeness to the cotton is because the substrate is more similar to the cotton fabric than the cellulose film in macroscopic structural formation. The inset of Figure 82 shows the variation in the PC1 values of the nylon-cotton substrates, which shows boundaries between the data points for the three nylon-cotton substrates.

Principal component 2 explains less of the variation in the reflectance and has less range in its values. From the spin plots Figure 81, PC2 appears to be related to the composition of the substrate based on the PC2 values for the substrates of similar composition. The values for PC2 are similar for the Cellulosic materials and the nylon-cotton fabric have very similar PC2 values.

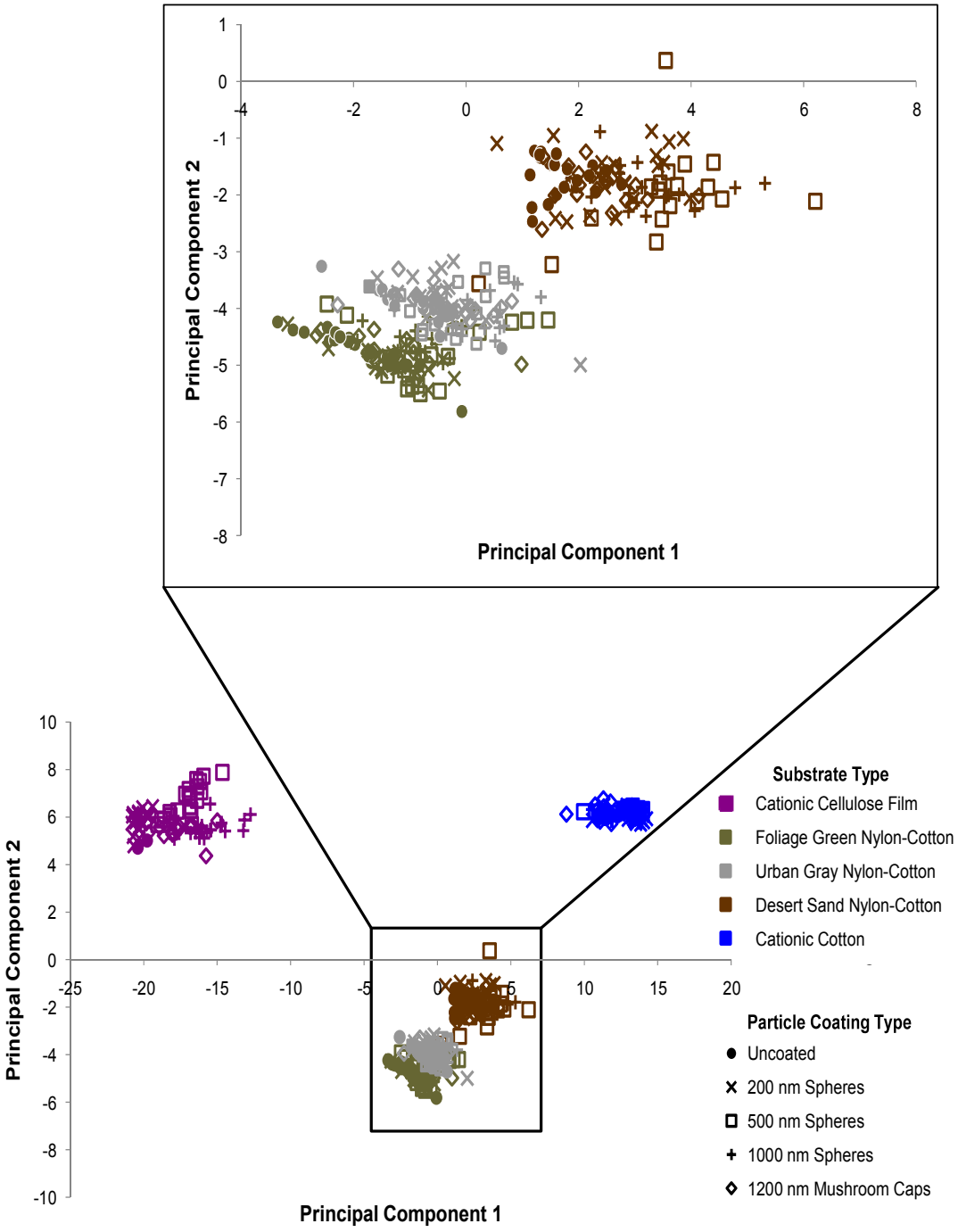

Figure 82. Principal Component 1 vs Principal Component 2 for all samples. Inset shows expanded view of nylon-cotton samples.

This composition and PC2 relationship can be seen in the 2-D cuts of the spin-plots, Figure 82 and Figure 83, in which the PC2 values of the cotton and film are the same value and the nylon-cotton fabrics have similar values for PC2. Furthermore, since all five substrates contain some cellulosic material, the small range in PC2 values is reasonable. The separation in PC2 values between the camouflage fabric and cellulosic substrates is due to the presence of nylon in the material. The separation in the PC2 values between the camouflage fabrics, which can be seen in the insets of Figure 82 and Figure 83, is due to the different dyes on their surfaces.

Principal component 3 explains less than 1% of the variation in the reflectance data. The variation in the PC3 values is not visibly detectable in the spin plots; however, it is shown in the 2-D plots in Figure 83 and Figure 84. The variation in PC3 may be attributed to particle coating size as the data points for particular substrate*particle size combinations are grouped in a similar order in the PC3 axis direction. The small amount of change in % reflectance and the small amount of variation of in reflectance explained by PC3 is fitting. However, due to the small variation in PC3 and the small about of variation in reflectance explained by PC3, the conclusion about the factors which influence PC3 cannot be made. Also, due to the small amount of variation explained by PC3 and that PC1 and PC2 explain 98% of the variation in the reflectance data, only PC1 and PC2 will be used in the fit model analysis.

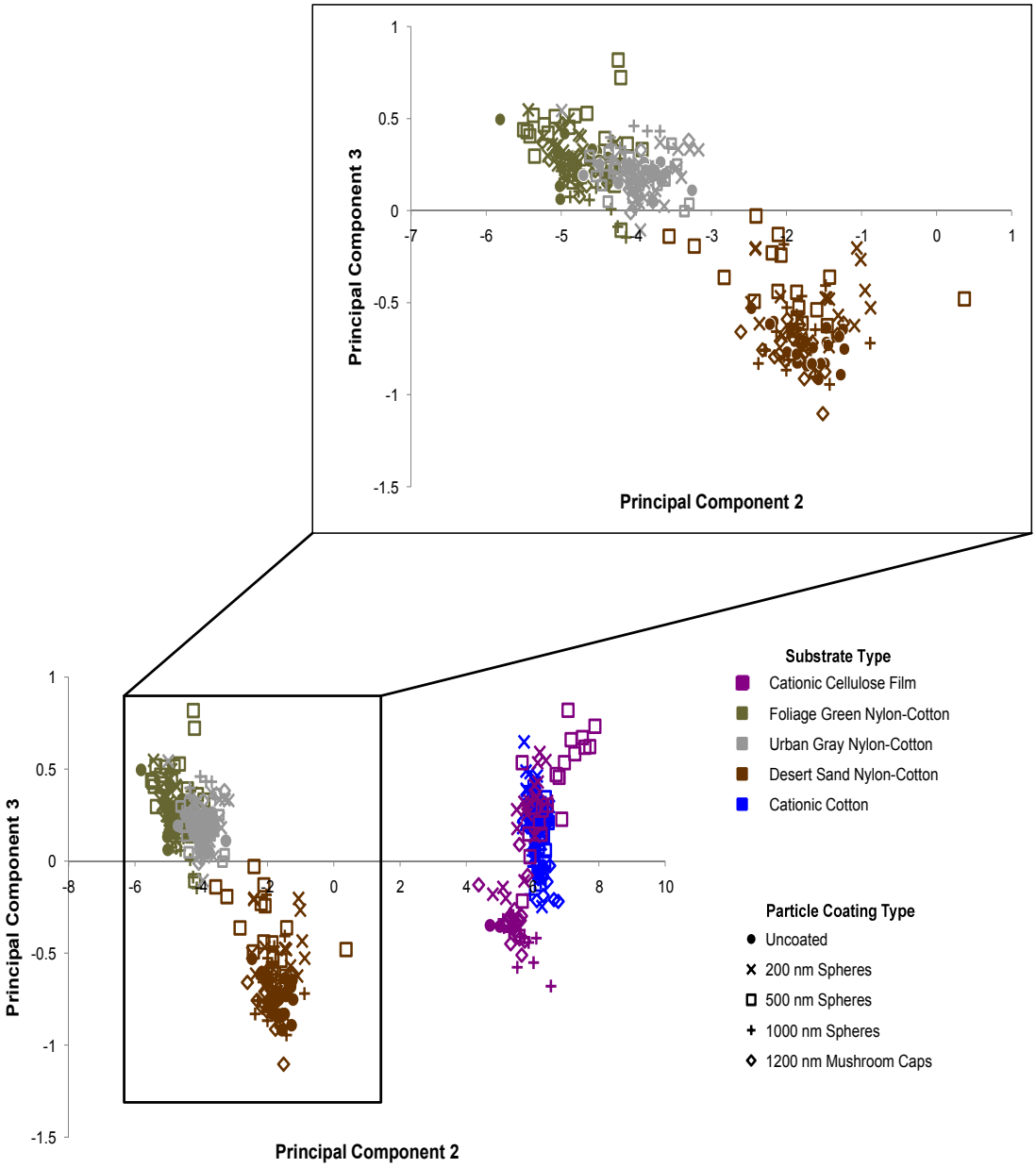

Figure 83. Principal Component 2 vs Principal Component 3 for all samples. Inset shows expanded view of nylon-cotton samples.

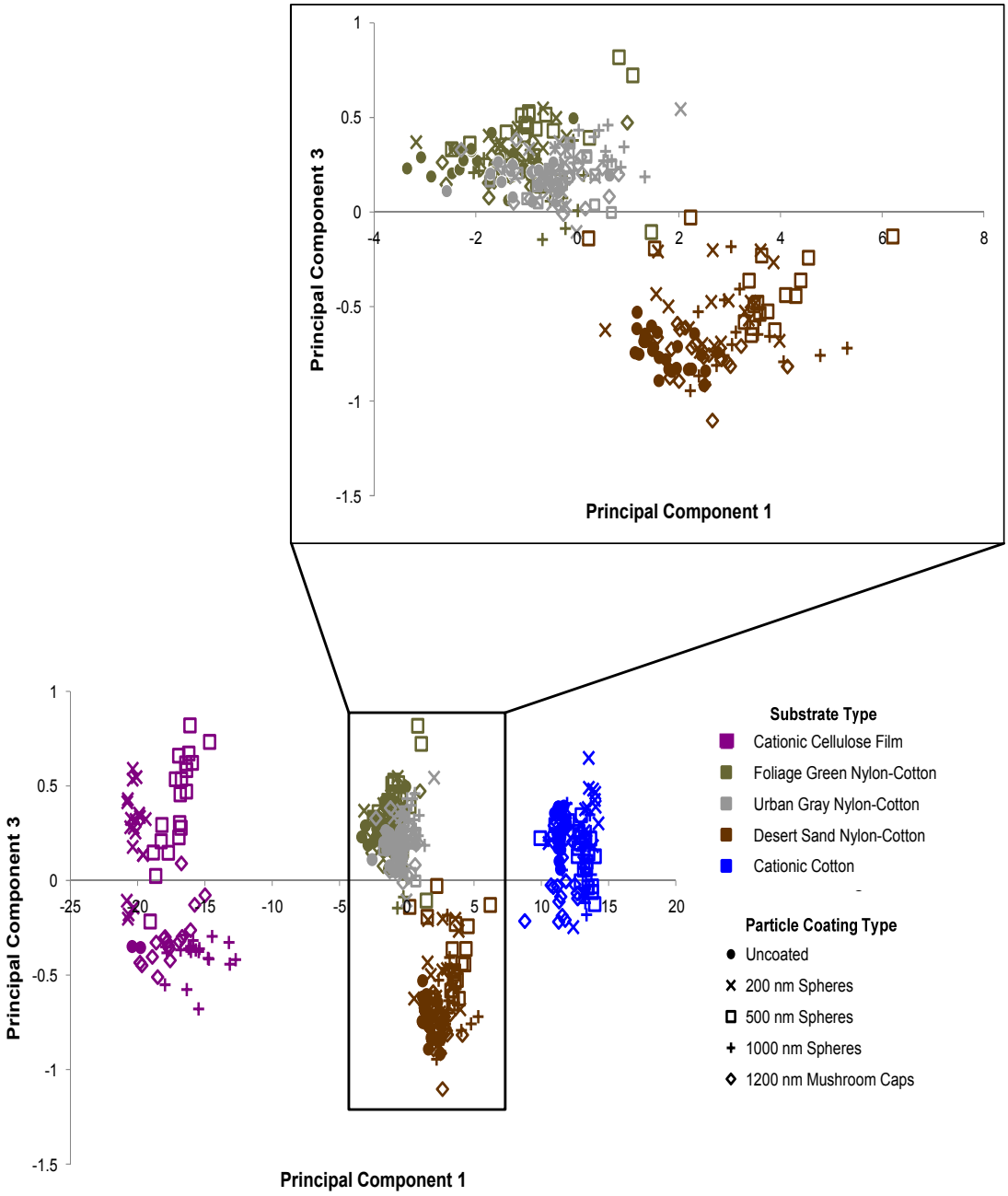

Figure 84. Principal Component 1 vs Principal Component 3 for all samples. Inset shows expanded view of nylon-cotton samples.

4.8. Fit Model for Principal Components PC1 and PC2 for Reflectance Data

A fit model was used with the principal component variables in order to address the hypotheses posed at the beginning of this project. With JMP, fit model was performed using standard least squares method with y variables of PC1 and PC2 and model effects of substrate, particle size, and the interaction term substrate*particle size. The first task was to determine if these effects were significant; if so, their F-value would be less than 0.05. The results from the effects tests for PC1 and PC2 are shown in Table 3 and Table 4, respectively. From the effects test, we conclude that the substrate, particle size, and the interaction term are significant effects in the model since their F values are much less than 0.05. The substrate has the greatest effect on reflectance from the effect tests results.

Table 3. Fit Model Effect Test for Principal Component 1 for Reflectance Data of All Substrates

Source	Number of Parameters	Degrees of Freedom	Sum of Squares	F Ratio	Prob > F
Substrate	4	4	26903.7	8933.4	0.0000
Particle Size	4	4	153.0	50.8	<.0001
Substrate*Particle Size	16	16	190.7	15.8	<.0001

Table 4. Fit Model Effect Test for Principal Component 2 for Reflectance Data of All Substrates

Source	Number of Parameters	Degrees of Freedom	Sum of Squares	F Ratio	Prob > F
Substrate	4	4	9144.1	15145.6	0.0000
Particle Size	4	4	3.9	6.4	<.0001
Substrate*Particle Size	16	16	24.3	10.1	<.0001

4.8.1. Modification of NIR Reflectance by Colloidal Particles

Hypothesis 1 is “the NIR reflectance of fabrics can be significantly modified by coating them with colloidal particles”. To address hypothesis 1, a least square means differences Tukey Honestly Significant Difference (HSD) test was performed using JMP with the fit model analysis of PC1 and PC2. Hypothesis 1 is supported by the Tukey test as shown in (Table 5) because all of the coating types have different letters values from the uncoated type calculated by the Tukey test meaning they are significantly different from the uncoated fabric. From the fit model of the principal component data, it can be conclude that the colloidal particle coatings can significantly change the reflectance of the fabrics in the NIR range.

Table 5. Least Square Means Tukey HSD Test for Principal Component 1 - Particle Coating Comparison to Uncoated

Particle Size / Coating Type	Level				Least Sq. Mean
1000 nm Spheres	A				-0.031735
500 nm Spheres		B			-0.374135
1200 nm Mushroom Caps			C		-1.088113
200 nm Spheres			C		-1.239552
Uncoated				D	-1.931383

4.8.2. Particle Size of Coating Effects on Reflectance

Hypothesis 2 is “the size of the particle used for coating the fabric has a significant impact on the reflectance of the modified fabrics”. The principal component analysis supports that for some cases the particle size of coatings significantly affects the reflectance. From Table 5 using PC1, the 0.2, 0.5, and

1.0 μm PS sphere coatings are significantly different from each other. However, the 0.2 μm PS sphere coating is not significantly different from the 1.2 μm mushroom cap PS particles. For PC2 and PC3, the spherical particle coatings are not all significantly different from each other as determined by the Tukey test. For PC2 and PC3, there is significant difference between the 0.5 and 1.0 μm sphere coatings from the levels of the Tukey test, A and B, respectively, shown in Table 6 and Table 7. For PC 3, there is also significant difference between there 0.2 and 1.0 μm sphere coatings and between the 0.2 μm sphere and 1.2μm mushroom cap coatings from the Tukey test shown in Table 7 whose levels are different.

Table 6. Least Square Means Tukey HSD Test for Principal Component 2 - Particle Coating Size Comparison

Particle Size / Coating Type	Level		Least Sq. Mean
500 nm Spheres	A		0.42645
200 nm Spheres	A	B	0.29368
1000 nm Spheres		B	0.22979
1200 nm Mushroom Caps		B	0.21823
Uncoated		B	0.11155

Table 7. Least Square Means Tukey HSD Test for Principal Component 3 - Particle Coating Size Comparison

Particle Size / Coating Type	Level		Least Sq. Mean
500 nm Spheres	A		0.15050
200 nm Spheres	A		0.11260
Uncoated		B	-0.07826
1000 nm Spheres		B	-0.10653
1200 nm Mushroom Caps		B	-0.12644

While three of the principal components were used to evaluate the hypotheses, since 77.8% of the variation of reflectance data is explained by PC1, the result of the Tukey test on PC1 holds more weight than that of PC2 and PC3 on drawing conclusion towards hypothesis 2. From PC1, the reflectance resulting from spherical particle coatings are significantly different from each other.

4.8.3. Non-Spherical Particle vs. Spherical Particles of Similar Diameter

Hypothesis 3 states “the reflectance of fabric coated with non-spherical particles will be significantly different from spherical particles of similar diameter”. The truth of this hypothesis is conclusive if only PC1 is examined. From Table 5 the Tukey test for particle size on PC 1, the 1.0 μm sphere coated samples are significantly different than the 1.2 μm mushroom cap particle coated samples, as the level for the two are A and C, respectively. From PC1 in Table 5, the 1.2 μm mushroom cap coating is more similar to the 0.2 μm spheres, as they are both given level C and thus not significantly different. However, in Table 6 and Table 7 for PC2 and PC3, which explain less of the variation than PC1, the two particle coatings are not significantly different.

The difference in the reflectance behavior of the mushroom cap and spherical particle is proposed to be a function of the curvature and the introduction of additional interfaces. At these interfaces refraction and reflection occur as well as additional changes in media happen, thus altering the refractive index through which the light must pass. The shape of the mushroom cap particle introduces more surfaces at shorter distances of travel that light can interact with, as shown in Figure 85. The shell thickness in some areas is as short as 200 to 400 nm which is half that of the diameter of the

1000 nm sphere, thus giving more surfaces where light can be internally reflected, shown in Figure 16, as compared to the sphere, shown in Figure 14. Furthermore, the mushroom cap particle coating has additional media interfaces as compared to the spheres. The light ray may travel from air through the particle through air and then to the fiber and then back out or be reflected back at some point in between. The light has the potential to change media and thus be altered by the refractive indices three times in each direction. The incident light into spherical particles typically encounters only two changes in media. These changes in media alter the amount of light reflected back and thus make a difference in reflectance behavior between the mushroom cap and 1000 nm spherical particles, even though they have similar diameters.

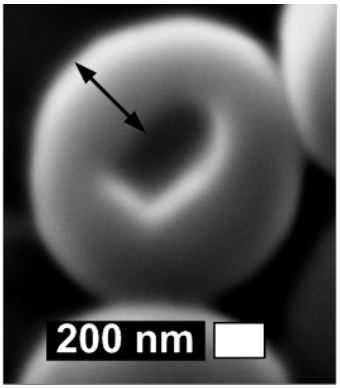

Figure 85. SEM Micrograph of Mushroom Cap Particle with Dimensions Enhanced. Length from outer shell to inner shell of mushroom cap on bottom is about 200 to 400 nm depending on location.

4.8.4. Dye on the Fabric Effect on the NIR Reflectance Signature

Hypothesis 4 states that the dye on the fabric influences the NIR reflectance signature. The results from the Tukey test on the substrate types support the hypothesis, shown in Table 8 and Table 9. Each of the substrates, including the three different colors of the camouflage nylon-cotton fabric, has

different levels for the Tukey test for both PC1 and PC2. The different levels support that the coated substrates are significantly different from each other. Since the three different nylon-cotton substrates are significantly different, it can be concluded that the dyes on the fabrics influence the NIR reflectance of the fabrics. Also, the reflectance of the dyed nylon-cotton is significantly different from the undyed cationic cotton thus further supporting the influencing the impact of the dye on the NIR signature.

Table 8. Least Square Means Tukey HSD Test for Principal Component 1 - Substrate Comparison

Substrate	Level					Least Sq. Mean
Cationic Cotton Fabric	A					12.36785
Desert Sand Nylon-Cotton Fabric		B				2.64405
Urban Gray Nylon-Cotton Fabric			C			-0.36463
Foliage Green Nylon-Cotton Fabric				D		-1.18643
Cationic Cellulose Film					E	-18.12575

Table 9. Least Square Means Tukey HSD Test for Principal Component 2 - Substrate Comparison

Substrate	Level					Least Sq. Mean
Cationic Cotton Fabric	A					6.13152
Cationic Cellulose Film		B				5.68513
Desert Sand Nylon-Cotton Fabric			C			-1.81904
Urban Gray Nylon-Cotton Fabric				D		-3.94595
Foliage Green Nylon-Cotton Fabric					E	-4.77197

4.9. Conclusions

This project explored the feasibility of using colloidal particles to manipulate the near-infrared signature of a textile. Unlike previous work and published theories, the particles used to coat the fabric were similar in size to the wavelength of incident light. A combination of electrostatic and convective self-assembly methods were used to successfully deposit submicron and micron sized polystyrene spherical and non-spherical particles onto nylon and cotton fabrics, as well as a flat cellulosic film. The particles were capable of conforming to the bends and twists of the textile fibers and coating the surface and subsurface fibers. The smaller particles, 200 and 500 nm spheres, achieved the best long range single layer coverage of the fabrics and film substrates tested. The larger particles, 1000 nm spheres and 1200 nm mushroom caps, formed single layer coverage, but the particles were prone to form agglomerates.

Analysis of the Vis-NIR reflectance spectra was used to calculate the average change in the % reflectance of the fabrics as a result of the particle coatings. The average change in % reflectance for desert sand nylon-cotton ranged from 0 to 6 units, with the 500 nm sphere coated having the highest change. The urban gray had a range in change in % reflectance of 0.5 to 3.5, with the 1000 nm sphere coated having the highest change. The foliage green nylon-cotton change in % reflectance ranged from -1 to 3.5, with the 200 nm coated fabric having a reduction in reflectance and the 1000 nm having the highest change in reflectance.

The cationic cotton had a range of change in % reflectance of -3 to 6, with the mushroom caps having the greatest reduction in reflectance of all the substrates and the 500 nm spheres most change in reflectance on the cotton.

The cationic cellulosic film had the widest range of change in reflectance from -2 to 17, with a reduction in reflectance by the 200 nm spheres and the greatest increase in reflectance by the 500 nm spheres.

For most cases there was an increase in reflectance based on the average reflectance spectra. However, by using the areas bounded by the upper and lower 95% confidence intervals of the average spectra and the standard deviation, overlaps of the particle coated region and the uncoated region indicate that the particle coated samples statistically can have lower reflectance than the uncoated. Based on this analysis, there were several particle coatings which in some portion of the region tested, had reflectance lower than the upper 95% confidence interval of the corresponding uncoated substrate. For some the reflectance fell below the lower 95% CI for the uncoated substrate. For the desert sand nylon-cotton, the 200 nm spheres, 500 nm spheres, and 1200 nm mushroom caps had portions of their 95% CI areas overlapping the uncoated, meaning their reflectance can be reduced. For urban gray nylon-cotton, all of the coatings tested overlapped the uncoated 95% CI area at some point during the tested wavelength range. The 200 nm spheres and the mushroom caps have potential for reducing reflectance of the foliage green nylon-cotton based on the overlap of the uncoated 95% CI range. The mushroom caps were the only coating that showed reduction on cotton. For the cellulosic film, the 200 and 500 nm spheres on the film showed reduction based on the 95% CI analysis. These results indicate that a reduction in reflectance and tailor-ability can be achieved in military camouflage.

Principal component analysis was performed on the experimental data using SAS JMP software. The number of variables was reduced from 111,

which is one % reflectance value taken at every 10 nm from 400 to 1500 nm, to three principal components. PC1 explains 77.8% of the variation in the data and it is closely related to substrate type and color. PC2 explains 20.1% of the variation and is proposed to be related the composition of the substrate. PC3 explains 0.8% of the variation in the reflectance. Using the new variables, a fit model was constructed and Tukey tests used to evaluate the hypotheses of the project. Hypothesis 1—the near-infrared reflectance of fabrics can be significantly modified by coating them with colloidal particles—was supported by least square means Tukey test of PC1 for particle size. Hypothesis 2—the size of the particle used for coating the fabric has a significant impact on the resulting modified reflectance of fabrics—was supported in some cases depending on particle size. Hypothesis 3—the reflectance of fabric coated with non-spherical particles will be significantly different from spherical particles of similar diameter—was true if only PC1 is examined, but inconclusive if PC2 and PC3 were taken into account. Hypothesis 4—the dye on the fabric influences the NIR signature of the particle coated fabrics—was supported by least square means Tukey test for substrates.

The project was successful in presenting a novel method of modifying the reflectance of textile fabrics and validating three of the four hypotheses of the project. Additional work is proposed to further modify reflectance and to use particles to both modify reflectance and impart color.

Chapter 5. Future Work

5.1. Modification of Particles

In order to further improve the tailor-ability of the reflectance, modifications to the particles and particle composition can be made. Smaller sized particles can be used. Also, coated particles can be used as well. Ung et al. have used silica coated gold nanoparticles to create film coatings on glass, these coatings vary in perceived color based on the thickness of the silica coating [72]. This process can be modified to coat PS, silica, or metallic particles with polyelectrolyte or nanoparticle multilayers as described by Caruso et al [73]. Using multilayer particles introduces additional interfaces into the material which will further alter the interaction of the light with the material. Also, the use of metallic particles can impart color which can offer new means of coloration on fabric.

5.2. Durability of Particles

Additional testing of the particle coated fabrics needs to be completed. Durability to laundering needs to be tested using the standards outlined by the US Army. Also, mechanical properties of the coated versus uncoated fabrics need to be compared.

5.3. Improvement of NIR Absorbing Dyes for Textile Materials

Addition research should be done on the NIR absorbing dyes [28-30, 33] explored in non-textile industries for application on textile materials. The wash fastness of color of these dyes needs to be tested, since textile apparel must sustain repeated launderings. Also, the materials must be studied over time to see if there are any changes in the reflectance properties due to laundering or exposure to other agents such as UV.

5.4. Development of Metamaterial Coated Fabrics

As found in this project, the majority of the coatings increased the reflectance of the uncoated materials. It would be useful to coat a textile fabric with a negative refractive index metamaterial in order to reduce the reflectance of the system. This application may not be as useful for uniforms and apparel applications due to the various bends and conformations to the body, as most of the present metamaterials are made of rigid materials [56, 57, 59]. Nonetheless, metamaterials could be useful in coverings for machinery and tents since there are made of stiffer fabric. For development of this application it will be most useful to use multilayered metallic based particles, as discussed in section 5.1, as silver has been used in NIR and optical metamaterials [57, 59].

REFERENCES

1. Yablonovitch, E., *Inhibited Spontaneous Emission in Solid-State Physics and Electronics.* Physical Review Letters, 1987. **58**(20): p. 2059 - 2062.

2. John, S., *Strong Localization of Photons in Certain Disordered Dielectric Superlattices.* Physical Review Letters, 1987. **58**(23): p. 2486 - 2489.

3. Gould, P., *Photonics: Practically There?* Materials Today, 2002: p. 32 - 37.

4. Krauss, T.F., R.M.D.L. Rue, and S. Brand, *Two-Dimensional Photonic-Bandgap Structures Operating at Near-Infrared Wavelengths.* Nature, 1996. **383**: p. 699 - 702.

5. Joannopoulos, J.D., P.R. Villeneuve, and S. Fan, *Photonic Crystals: Putting a New Twist on Light.* Nature, 1997. **386**: p. 143 - 149.

6. Grüning, U., et al., *Macroporous Silicon with a Complete Two-Dimensional Photonic Band Gap Centered at 5 μm.* Appl. Phys. Lett., 1996. **68**(6): p. 747 - 749.

7. Hosein, I.D. and C.M. Liddell, *Homogeneous Core-Shell, and Hollow-Shell ZnS Colloid-Based Photonic Crystals.* Langmuir, 2007. **23**: p. 2892 - 2897.

8. Hosein, I.D. and C.M. Liddell, *Convectively Assembled Nonspherical Mushroom Cap-Based Colloidal Crystals.* Langmuir, 2007. **23**: p. 8810 - 8814.

9. Martinez, F. *Developing Near Infrared Spectral Reflectance Requirements for Military Textiles*. in *Expo HighTex*. 2006. Montreal, Ontario, Canada.

10. Felicetti, G., *The Limits of Training in Iraqi Force Development.* Parameters, US Army War College Quarterly, 2006 - 2007(Winter): p. 71 - 81.

11. Hosein, I.D. and C.M. Liddell, *Convectively Assembled Asymmetric Dimer-Based Colloidal Crystals.* Langmuir, 2007. **23**: p. 10479 - 10485.

12. Zhang, J., et al., *Template-Directed Convective Assembly of Three-Dimensional Face-Centered-Cubic Colloidal Crystals.* Applied Physics Letters, 2002. **81**(17): p. 3176 - 3178.

13. *Detail Specification: Cloth, Camouflage Pattern, Wind Resistant Poplin, Nylon/Cotton Blend*, in *MIL-DTL-44436A*. 2005.

14. Kennedy, S.J., *Cotton and Ideal Military Textiles.* Textile Research Journal, 1954: p. 572 - 577.

15. Schutz, H.G., A.V. Cardello, and C. Winterhalter, *Perceptions of Fiber and Fabric Uses and the Factors Contributing to Military Clothing Comfort and Satisfaction.* Textile Research Journal, 2005. **75**(3): p. 223 - 232.

16. Kiserow, D. and J. Joannopoulos, *The Institute for Soldier Nanotechnologies -- Developing Revolutionary Survivability Technologies for Soldiers.* Army Acquisition, Logistics, and Technology Magazine, 2007. **2007**(October - December): p. 28 - 31.

17. Roddin, M.I. and M.J. Varhola, *Fielding the Best Equipment to the Best Army in the World.* Army Acquisition, Logistics, and Technology Magazine, 2006(April - June): p. 40 - 47.

18. Vanderbilt, T., *The U. S. Army's New Clothes: Why has the Army redesigned its uniforms?*, in *Slate*. 2004, Washington Post Newsweek Interactive.

19. Biberdorf, C., *Facility Sifts out Camouflage Design Duds.* Army Acquisition, Logistics, and Technology Online, 2005(January - February).

20. Perepelkin, K.E., *Chemistry and Technology of Chemical Fibres: Principles and Methods of Modification of Fibres and Fiber Materials. A Review.* Fibre Chemistry, 2005. **37**(2): p. 123-140.

21. Güneşoğlu, C., D. Kut, and M. Orhan, *Effect of the Particle Size of Finishing Chemicals on the Color Assessment of Treated Cotton Fabrics.* Journal of Applied Polymer Science, 2006. **194**: p. 2587 - 2594.

22. Lau, L., et al., *Effects of Repeated Laundering on the Performance of Garments with Wrinkle-Free Treatment.* Textile Research Journal, 2002. **72**(10): p. 931 - 937.

23. Lee, H.J., S.Y. Yeo, and S.H. Jeong, *Antibacterial Effect of Nanosized Silver Colloidal Solution on Textile Fabrics.* Journal of Materials Science, 2003. **38**(10): p. 2199 - 2204.

24. Zhang, H., W. Gao, and H. Qiu, *Retro-Reflection of Round Fibers.* Textile Research Journal, 2003. **73**(11): p. 965-970.

25. Hyde, K., M. Rusa, and J. Hinestroza, *Layer-by-layer deposition of polyelectrolyte nanolayers on natural fibres: cotton.* Nanotechnology, 2005. **16**: p. S422 - S428.

26. Dubas, S.T., P. Kumlangdudsana, and P. Potiyaraj, *Layer-by-layer deposition of antimicrobial silver nanoparticles on textile fibers.* Colloids and Surfaces A: Physicochemical and Engineering Aspects, 2006. **289**(1-3): p. 105 - 109.

27. Decher, G., *Fuzzy Nanoassemblies: Toward Layered Polymeric Multicomposites.* Science, 1997. **277**(5330): p. 1232 - 1237.

28. Langhals, H., *Au Unexpectedly Simple NIR Dye for 1.1 µm with a Central Mesoionic Structure.* Angew. Chem. Int. Ed., 2003. **42**: p. 4286-4288.

29. Kubo, Y., et al., *Experimental and Theoretical Study of Near-Infrared Absorbing Naphthoquinone Methide Dyes with a Nonplanar Geometry.* J. Am. Chem. Soc., 1991. **113**: p. 2868-2873.

30. Zhao, W. and E.M. Carreira, *Conformationally Restricted Aza-Bodipy: A Highly Fluorescent, Stable, Near-Infrared-Absorbing Dye.* Angew. Chem. Int. Ed., 2005. **44**: p. 1677-1678.

31. Eldo, J. and A. Ajayaghosh, *New Low Band Gap Polymers: Control of Optical and Electronic Properties in Near Infrared Absorbing π-Conjugated Polysquaraines.* Chem. Mater., 2002. **14**: p. 410-418.

32. Adachi, M. and Y. Nagao, *Design of Near-Infrared Dyes Based on π-Conjugation System Extension 2. Theoretical Elucidation of Framework Extended Derivatives of Perylene Chromophore.* Chem. Mater., 2001. **13**: p. 662-669.

33. Avlasevich, Y. and K. Müllen, *Dibenzopentarylenebis(dicarboximide)s: Novel Near-Infrared Absorbing Dyes.* Chem. Commun., 2006: p. 4440-4442.

34. Gobin, A.M., et al., *Near Infrared Laser-Tissue Welding Using Nanoshells as an Exogenous Absorber.* Lasers in Surgery and Medicine, 2005. **37**: p. 123-129.

35. Yu, J., et al., *Synthesis of Near-Infrared-Absorbing Nanoparticle-Assembled Capsules.* Chem. Mater., 2007. **19**: p. 1277-1284.

36. Wang, Z.Y., et al., *Near-Infrared Absorbing Organic Materials.* Pure Appl. Chem., 2004. **76**(7-8): p. 1435-1443.

37. Martinez, F. and R. Cowan, *US Army Camouflage Dyes and Modification of NIR Signal of Textiles - Personal Communication*. 2008.

38. Kerker, M., *The Scattering of Light: and Other Electromagnetic Radiation*. Physical Chemistry: A Series of Monographs, ed. E.M. Loebl. 1969, New York: Academic Press. 666.

39. Papini, M., *Analysis of the Reflectance of Polymers in the Near- and Mid-Infrared Regions.* J. Quant. Spectrosc. Radiat. Transfer, 1997. **57**(2): p. 265-274.

40. Jasper, W.J. and E.T. Kovacs, *Using Neural Networks NIR Spectrophotometry to Identify Fibers.* Textile Research Journal, 1994. **64**(8): p. 444-448.

41. Yamada, J., *Radiative Properties of Fibers with Non-Circular Cross Sectional Shapes.* Journal of Quantitative Spectroscopy & Radiative Transfer, 2002. **73**: p. 261-272.

42. Yamada, J. and Y. Kurosaki, *Radiative Characteristics of Fibers with a Large Size Parameter.* International Journal of Heat and Mass Transfer, 2000. **43**: p. 981-991.

43. Makino, T. and J.-i. Horiba, *Scattering of Radiation by a Fiber with a Rough Surface.* Heat Transfer--Asian Research, 1999. **28**(4): p. 322-335.

44. Chan, C.K. and C.L. Tien, *Radiative Transfer in Packed Spheres.* Journal of Heat Transfer, 1974. **96**: p. 52-58.

45. Papini, M., *Study of the Relationship Between Particle Shzes of Polymer Powders and their Radmative Properties.* Infrared Phys., 1993. **34**(6): p. 607-619.

46. Modest, M.F., *Radiative Heat Transfer*. McGraw-Hill Series in Mechanical Engineering, ed. J.P. Holman and J.R. Lloyd. 1993, New York: McGraw-Hill. 832.

47. Wilhelm, R.H. and J.B. Smith, *Transmittance, Reflectance, and Absorptance of Near Infrared Radiation in Textile Materials.* Textile Research Journal, 1949. **19**(2): p. 72-88.

48. Greenler, H.F. and F.J. O'Neil, *Radiantenergy Reflectance of Men's-Wear Colors.* Textile Research Journal, 1947. **17**: p. 63-68.

49. Fourt, L., et al., *Improvement of Luster of Cotton: Part V: Fiber Shape in Relation to Luster.* Textile Research Journal, 1954: p. 156 - 163.

50. Lynch, L.J. and N. Thomas, *Optical Diffraction Profiles of Single Fibers.* Textile Research Journal, 1971. **41**: p. 568-572.

51. Swathi, P.S. and T.W. Tong, *A New Algorithm for Computing the Scattering Coefficients of Highly Absorbing Cylinders.* J. Quant. Spectrosc. Radiat. Transfer, 1988. **40**(4): p. 525 - 530.

52. Ventura, C. and M. Papini, *Diffuse Reflection Spectroscopy Suudy of Granular Materials and their Mixtures in the Mid-Infrared Spectral Range.* Vibrational Spectroscopy, 1999. **r1**: p. 17-36.

53. Tong, T.W., P.S. Swathi, and J. G. R. Cunnington, *Examination of the Radiative Properties of Coated Silica Fibers.* Journal of Building Physics, 1987. **11**: p. 7 - 31.

54. Fan, T.-H. and A.G. Fedorov, *Radiative Transfer in a Semitransparent Hemispherical Shell.* Journal of Quantitative Spectroscopy & Radiative Transfer, 2002. **73**: p. 285 - 296.

55. Smith, D.R., J.B. Pendry, and M.C.K. Wiltshire, *Metamaterials and Negative Refractive Index.* Science, 2004. **305**: p. 788 - 792.

56. Quan, B., et al., *Microfabrication and Properties of the Meta-Materials.* Microelectronic Engineering, 2006. **83**: p. 1364 - 1367.

57. Lezec, H.J., J.A. Dionne, and H.A. Atwater, *Negative Refraction at Visible Frequencies.* Science, 2007. **316**: p. 430 - 432.

58. Shelby, R.A., D.R. Smith, and S. Schultz, *Experimental Verification of a Negative Index of Refraction.* Science, 2001. **292**: p. 77-79.

59. Xia, X., et al., *Fabrication of Near-Infrared and Optical Meta-Materials on Insulating Substrates by Lift-off Using PMMA/Al Stack.* Microelectronic Engineering, 2007. **84**: p. 1144 - 1147.

60. Vukusic, P. and J.R. Sambles, *Photonic Structures in Biology.* Nature, 2003. **424**: p. 852 - 855.

61. Hart, S.D., et al., *External Reflection from Omnidirectional Dielectric Mirror Fibers.* Science, 2002. **296**: p. 510 - 513.

62. Jiang, P., et al., *Single-Crystal Colloidal Multilayers of Controlled Thickness.* Chem. Mater., 1999. **11**: p. 2132 - 2140.

63. Liang, Z., A.S. Susha, and F. Caruso, *Metallodielectric Opals of Layer-by-Layer Processed Coated Colloids.* Advanced Materials, 2002. **14**(16): p. 1160 - 1164.

64. Liang, Z., A. Susha, and F. Caruso, *Gold Nanoparticle-Based Core-Shell and Hollow Spheres and Ordered Assemblies Thereof.* Chem. Mater., 2003. **15**: p. 3176 - 3183.

65. Han, S., X. Shi, and F. Zhou, *Polyelectrolyte Hollow Sphere Lithographic Patterning of Surfaces: Construction of 2-Dimensional Well-Ordered Metal Arrays.* Nano Letters, 2002. **2**(2): p. 97 - 100.

66. Schroden, R.C., M. Al-Daous, and A. Stein, *Self-Modification of Spontaneous Emission by Inverse Opal Silica Photonic Crystals.* Chem. Mater., 2001. **13**: p. 2945 - 2950.

67. Liddell, C.M. and C.J. Summers, *Monodispersed ZnS Dimers, Trimers, and Tetramers for Lower Symmetry Photonic Crystal Lattices.* Advanced Materials, 2003. **15**(20): p. 1715 - 1719.

68. Hauser, P.J. and A.H. Tabba, *Improving the Environmental and Economic Aspects of Cotton Dyeing Using a Cationised Cotton.* Coloration Technology, 2001. **117**: p. 282 - 288.

69. Navarro, F. and M. Roman. *Ink-jet Printing of Cellulose Nanocrystal Suspensions*. in *223rd American Chemical Society National Meeting*. 2007. Chicago, IL.

70. Knüttel, H. and K. Fiedler, *Host-Plant-Derived Variation in Ultraviolet Wing Patterns Influences Mate Selection by Male Butterflies.* Journal of Experimental Biology, 2001. **204**: p. 2447-2459.

71. Lehman, A., et al., *Principal Component Analysis*, in *JMP for Basic Univariate and Multivariate Statistics: A Step-by-Step Guide*. 2005, SAS Press.

72. Ung, T., L.M. Liz-Marzan, and P. Mulvaney, *Optical Properties of Thin Films of Au@SiO_2 Particles.* J. Phys. Chem. B., 2001. **105**: p. 3441-3452.

73. Caruso, F. and H. Mohwald, *Preparation and Characterization of Ordered Nanoparticle and Polymer Composite Multilayers on Colloids.* Langmuir, 1999. **15**: p. 8276-8284.